DEVELOPMENT OF ENVIRONMENTAL AND OCEANOGRAPHIC REAL-TIME ASSESSMENT SYSTEM FOR THE NEAR-SHORE ENVIRONMENT

A Dissertation

by

TEMITOPE O. OJO

Submitted to the Office of Graduate Studies of
Texas A&M University
in partial fulfillment of the requirements for the degree of

DOCTOR OF PHILOSOPHY

May 2005

Major Subject: Civil Engineering

DEVELOPMENT OF ENVIRONMENTAL AND OCEANOGRAPHIC REAL-TIME ASSESSMENT SYSTEM FOR THE NEAR-SHORE ENVIRONMENT

A Dissertation

by

TEMITOPE O. OJO

Submitted to Texas A&M University
in partial fulfillment of the requirements
for the degree of

DOCTOR OF PHILOSOPHY

Approved as to style and content by:

James S. Bonner (Chair of Committee)	Billy L. Edge (Member)
Bruce Herbert (Member)	Ralph Wurbs (Member)

David Rosowsky
(Head of Department)

May 2005

Major Subject: Civil Engineering

ABSTRACT

Development of Environmental and Oceanographic Real-time Assessment System for the Near-shore Environment. (May 2005)

Temitope O. Ojo, B.Sc., University of Ife;

M.Eng., Texas A&M University

Chair of Advisory Committee: Dr. James S. Bonner

The coupling of real-time measurements and numerical models will be important in overcoming the challenges in environmental and oceanographic assessments in surface waters. Continuous monitoring will take advantage of current state-of-the-art in sensor development, remote sensing technology. The numerical modeling tools available exist in many different forms and varying levels of complexity from depth integrated one-dimensional (1-D) models to full three-dimensional (3-D) models. Common to all are the constraints and forcing required in driving the models. These include hydrodynamic and barometric information, which are relatively difficult to obtain given the time scale of the bio-chemical and physical processes governing the fate and transport of the constituents of interest.

This study is focused on the development of a framework that couples real-time measurements and numerical simulation for tracking constituents in surface waters. The parameterization of the mixing and turbulent diffusion impacts the formulation of the constituent-transport governing equations to the extent that the numerical model is

being driven by near real-time observations of hydrodynamic data and the consequent evaluation of model coefficients. The effects of shear-augmented diffusion processes in shallow embayment and near-shore waters are investigated in order to develop algorithms for obtaining a *shear diffusion coefficient*, K_e from shear-current measurements and *turbulent diffusion-coefficient*, K_z measured by the auto-correlation function, R_τ of the velocity time-series.

Typically, the diffusion coefficients are measured through tracer experiments as determined by the time rate of change of the variance of a growing patch ($K = ½\ d\sigma^2 /dt$), which introduces the concept of diffusion length-scale (or time-scale). In this study, the dye-tracer experiment was used, not so much in the context of evaluation of a diffusion coefficient, but within a modeling framework to validate a numerical scheme driven by real-time hydrodynamic observations. Overall, the effect of shear-currents in shallow wind-driven estuaries is studied using a prototype bay typical of the Texas Gulf-coast. A numerical model was developed and used in testing these hypotheses through a series of dye-tracer experiments under varying meteorological conditions.

DEDICATION

In memory of Daniel Funmilayo "Ojo-Ugbole" Ojo, Ph.D., OON.

To God Almighty, the source of all inspiration and without whom none of this would have been possible.

To the two most important women in my life, Esther O. Ojo and Phoebean O. Ojo.

ACKNOWLEDGMENTS

This project could not have been embarked upon let alone completed without the support of individuals and groups of people. I want to thank my committee chair, Dr. James Bonner for providing an environment in which the seeds of intellectual pursuits are planted and nurtured and for dedication of time and effort to this project. I thank members of my advisory committee, Dr. Bruce Herbert, Dr. Billy Edge, and Dr. Ralph Wurbs for their encouragement and dedication.

Dr. Autenrieth, Ms. Jan Rinehart, Dr. Cheryl Page, Dr. George Krise and Mrs. (Late) Trudie Krise, Mr. and Mrs. Adeyi, Anthony and Vicki Deanes. You stood by us and provided immeasurable support and encouragement.

I want to thank the Pastor, staff and members of First Baptist Church College Station, most especially Dr. and Mrs. Malcolm Bane, Dr. and Mrs. Rodney McGlothlin and The Good News Class under the leadership of Dr. Mark English for your labor of love.

To my colleagues at work for all your contributions to the success of this project; Michele Carter, Donnie Golden, Isabel Flores, Chris Fuller, Terry Riggs, Kinjal Shah, Dixie Smith, staff of Conrad Blucher Institute at Texas A&M University, Corpus Christi as well as fellow workers, former and current students of Environmental Engineering at Texas A&M University, College Station.

To friends and relatives at home and abroad. Your patience and understanding is commendable.

To my mother, Phoebean Obagbolaro Ojo. You taught me all about discipline and patience.

Finally, I want to express heartfelt gratitude to my family; Olubunmi, Kanyinsola, Folakemi and Tolulope Ojo. You sacrificed a lot for this and I don't know how I could have pulled this through without your emotional support and your love.

TABLE OF CONTENTS

Page

ABSTRACT iii

DEDICATION v

ACKNOWLEDGMENTS vi

TABLE OF CONTENTS viii

LIST OF FIGURES xii

LIST OF TABLES xviii

CHAPTER

I INTRODUCTION 1

Statement of Purpose 1
Background 2
Research Objectives 5
Methods and Materials 8
Determination of Transport Model Coefficients from Direct Observations 8
Diffusion Coefficients in Surface Waters 10
Transport Model Development and Algorithm Selection 14
Tracer-study for System Evaluation and Model Validation 15
Modeling Framework and System Block Diagram 16
Trajectory Tracking and Vessel Guidance System 17
Integrated Sensor Interface, Data Acquisition and Computing Network 17
Site Description 18
Meteorological and Experimental Conditions 20

II A RAPID DEPLOYMENT INTEGRATED ENVIRONMENTAL AND OCEANOGRAPHIC ASSESSMENT SYSTEM (IEOAS) FOR COASTAL WATERS: DESIGN CONCEPTS AND FIELD IMPLEMENTATION 22

Overview 22

CHAPTER Page

Introduction 23
Background 24
Near Term Objectives and Project Scope 26
Design Concept 27
Environmental Monitoring in Surface Waters 29
System Description 35
Integrated Data Acquisition Communications and Control (IDACC) Unit....35
Submersible Multi-Port Instrument Interface 38
The Multi-Parameter Instrument Array and Control System: MPIACS 39
Ship-to-Shore Wireless Telemetry 42
Implementation....46
Data Acquisition Module 46
Instrument Control Module....47
Data Post-Processing Module 47
Data Visualization Module....49
Data Archiving Module....49
Results 50
Operational Tests....50
Bench Tests 51
Field Test....54
Field Deployment....55
Discussion 57

III STUDIES ON TURBULENT DIFFUSION PROCESSES AND EVALUATION OF DIFFUSIVITY VALUES FROM HYDRODYNAMIC OBSERVATIONS IN CORPUS CHRISTI BAY 60

Overview 60
Introduction 61
Turbulent Diffusivity....63
Methods and Materials 70
Review of Analytical Models of Velocity Autocorrelation Function, ACF 71
Time Series Generation from Spatial Series of Velocities Taken from a Moving Platform....73
Instrumentation and Data Acquisition....77
Data Analysis 78
Site Description 79
Results 80

CHAPTER Page

Velocity Time Series from a Moving Platform – Error Analysis 80
Autocorrelation Function 89
Scale of Turbulent Diffusion 90
Turbulent Diffusivity 90
Discussion 92
Conclusion 94

IV OBSERVATIONS OF SHEAR-AUGMENTED DIFFUSION PROCESSES AND EVALUATION OF EFFECTIVE DIFFUSIVITY FROM CURRENT MEASUREMENTS IN CORPUS CHRISTI BAY 96

Overview 96
Introduction 97
Background Theory 101
Shear-Augmented Diffusion and Effective Diffusivity 101
Method 109
Site Description 110
Instrumentation 111
Data Analysis 112
Results 116
Characteristic Velocity Distribution, Dimensionless Integral and Initialization Time 116
Shear Diffusivity 123
Discussion 126
Future Work 129

V DIFFUSION AND MIXING EXPERIMENTS IN CORPUS CHRISTI BAY, TX: DYE-TRACER STUDY TO DETERMINE DIFFUSIVITY VALUES 130

Overview 130
Introduction 131
Methods and Materials 132
Study Site 133
Instrumentation 134
Data Acquisition 135
Data Analyses 136
Method A 137
Method B 141
Results 144
Discussion 152

CHAPTER Page

Future Work 157

VI SIMULATION OF CONSTITUENT TRANSPORT USING A REDUCED 3D CONSTITUENT TRANSPORT MODEL (CTM) DRIVEN BY HF RADAR: MODEL APPLICATION AND ERROR ANALYSIS 159

Overview 159
Introduction 160
Background Theory 163
Model Coefficients for Simplified CTM 165
Model Error Analysis 167
Methods and Materials 170
Surface Current Measurements and Vertical Velocity Profile 171
Turbulent Diffusivity 172
Modeling Framework 173
Model Error Analysis 176
Results 177
Turbulent Diffusivity 181
Error Analyses 186
Model Results 189
Discussion 196
Future Work 198
Conclusion 199

VII SUMMARY AND CONCLUSION 200

Algorithms and Software Modules Developed 202
Future Work 202

REFERENCES 204

VITA 214

LIST OF FIGURES

FIGURE Page

1.1. System block diagram. 17

1.2. Top; map of Corpus Christi Bay in the Texas Gulf of Mexico. Approximate location for each study is indicated (■ – Study 0828_1 and 1007; ◘ -- Study 0820_2). Bottom; bathymetry of the study area. 19

1.3. Wind speed measurements over a 24 hour period taken during the experiments. Top panel; experiment 0828_2. Bottom panel; experiment 1007. Wind strength is comparable during the two experiments reported but conditions during experiment 1007 is highly variable. 21

1.4. Water level (height above MLLW (─ solid line) and surface current measurements (-. dashed line) covering the duration of the experiments. 21

2.1. DCE architecture (Brando, 1995). 26

2.2. Representation of data flow for real-time data acquisition and visualization. 32

2.3. System block diagram for IEOAS. 33

2.4. Schematic diagram of IDACC and submersible multi-port instrument interface. 34

2.5. Top, inset; submersible multi-port device server. Bottom; IDACC comprising GPS unit, industrial computer in NEMA 4X enclosure, NEMA keyboard, power distribution and 4-port network interface. The main unit, which houses the electronics tilts up into operating position, supported by gas springs. 36

2.6. IDACC and tow-body with instrumentation and submersible multi-port device server undergoing bench tests. 38

2.7. The MPIACS software interface. Lower right panel is a zoomed in portion of one of the 6 data visualization panes from the main instrument panel. 41

FIGURE Page

2.8. Map of coverage area. 45

2.9. Data acquisition module with slider controls for setting instrument levels and drop down menu for selecting study area. 48

2.10. Typical output from IEOAS; contaminant plume trajectory simulation with current vectors overlay, concentration profile, and concentration-time plot. 56

3.1. Analytical forms of $R_i(\tau)$ proposed by several researchers for $T_c = 10$ (upper panel) and $T_c = 100$ (lower panel) . —●— T; —*— F1; —■— F2; —◊— ATG. 73

3.2. Illustration of sampling scheme and spatial series of current measurements generated from ADCP mounted on a moving platform. 74

3.3. Horizontal velocity gradients from surface current mapping of the study area at the instant when gradients were at a maximum. The shear structure was determined from HF radar surface current mapping. Approximate location of the 2 study sites is indicated. These sites are in the region marked by very weak horizontal shear. 81

3.4. Errors resulting from velocity time series generated from spatial series evaluated against number of samples in series. The error increases as the square of number of samples for monotically increasing transect design while the relationship is linear based on a running average of the transect set. 81

3.5. Top panel; distribution of sampling points in relative coordinates in both east-west (blue) and north south (red) directions. Bottom; normal probability plot. Left is for east-west and right is for the north-south distribution of (relative coordinates) of the sampling points plotted in blue. The red line is the straight-line plot from the ideal normal distribution. 83

3.6. Top, typical time series of velocity fluctuations along *x, y, z* coordinate axes respectively; middle, corresponding depth profile of average velocity variance; bottom, corresponding velocity distribution function. 85

FIGURE Page

3.7. From top to bottom, Lagrangian (scaled) velocity autocorrelation function derived from velocity time series along *x, y,* coordinate axes respectively (similar for the *z*-axes).....86

3.8. From top to bottom; depth profile of turbulent diffusivity for each of the three studies. Top, study 0828_1; middle, study 0828_2; bottom, study 1007. Open circle (—○—), *x*-coordinate; diamond (----◊---), *y*-coordinate; open squares (---□---), *z*-coordinate. 87

3.9. Typical frequency spectrum of velocity time series up to the Nyquist frequency. Identified ~3 s period events (corresponding to ~ 10 ensembles) used in sizing low-pass filter for noise and error reduction. 88

3.10. Observed dye patch from study 0828_2, 6202 s after instantaneous release. Outlined (- - -) is the 68% numerical estimate of spread within 2σ based on computed turbulent parameters (K_x = 1.03 x 10^4, K_y = 0.33 x 10^4).....88

4.1. This is a depiction of the effect of a vertical shear current on a line source leading up to shear diffusion. 1. The line source is introduced. 2. The line source is displaced under the influence of the velocity (linear) profile, shifting the center of mass. 3. Next, vertical (turbulent) mixing redistributes the constituent as shown. 4. The overall effect is the apparent diffusion of a line source into a plane under the combined effect of a vertical shear current and vertical mixing. 99

4.2. Illustration of fluid element under the influence of vertical current shear. 114

4.3. Study 0828_1. Top-left panel -- E-W shear current profile at 0.3 m depth intervals; top right panel – N-S shear current profile at 0.3 m depth intervals; bottom panel – compass plot of velocity vectors. 117

4.4. Study 0828_2. Top-left panel -- E-W shear current profile at 0.3 m depth intervals; top right panel – N-S shear current profile at 0.3 m depth intervals; bottom panel – compass plot of velocity vectors. 118

4.5. Study 1007. Top-left panel -- E-W shear current profile at 0.3 m depth intervals; top right panel – N-S shear current profile at 0.3 m depth intervals; bottom panel – compass plot of velocity vectors. 119

FIGURE Page

4.6. Statistical summary of characteristic velocities. Top -- study 0828_1; middle -- study 0828_2; bottom -- study 1007. Open circle, --o-- outliers within dataset.....120

4.7. Density distribution function of characteristic velocity computed from shear-current. Top – study 0828_1; middle – study 0828_2; bottom – study 1007 (-○- east-west; -◊- north-south). 121

4.8. Top; observed dye patch, 5557 s after instantaneous release. Outlined (- - -) is the 68% numerical estimate of spread with 2σ based on shear (K_x = 2.09 x 10^5, K_y = 0.43 x 10^5). Bottom; same dye patch outlined open circles (-o-) is the 68% numerical estimate of spread with 2σ based on turbulence and open squares, the 99% numerical estimate also based on turbulence (K_x = 1.69 x 10^4, K_y = 0.30 x 10^4). The estimates based on turbulence presents an underestimation of the concentration distribution.....125

5.1. Time series of concentration. Solid line (-); observed concentration; dashed line (--) exponential fit to observed data; open circle (o) peak concentration (approx. center of mass). Top, study 0828_2; bottom, study 1007.....145

5.2. Time series of fluorescence values from tracer experiments. Temporally localized peaks show the declining maximum concentration values during each leg of the several crossing made through the dye patch. 2nd order exponential (--*--) curve-fit through the localized peaks.....146

5.3. Contour plots of reconstructed dye concentration profile at successive time intervals from study 0828_2. The current structure from ADCP measurements is shown upper left. 147

5.4. Top panel; centerline concentration distribution from study 0828_2. Bottom; variance time plots from concentration profile (S^2_x – east-west, S^2_y – north-south). Regression line fitted to observed data with r^2 = 0.94 and 0.87 respectively.....148

5.5. Contour plots of reconstructed dye concentration profile at successive time intervals from study 1007. The current structure from ADCP measurements is shown upper left. 149

FIGURE Page

5.6. Top panel; centerline concentration distribution from study 1007. Bottom; variance time plots from concentration profile (S^2_x – east-west, S^2_y – north-south). Regression line fitted to observed data with r^2 = 0.97 and 0.94 respectively.....150

5.7. Comparison between results of experiments conducted in Corpus Christi Bay and those obtained by Murthy in Lake Ontario and Elliot from coastal waters around Ireland. Okubo's data were from numerous studies conducted from around the world. Fickian diffusion is also presented for comparison. 154

6.1. Top panel; finite difference computational grid. Bottom pane; bathymetry of the study area, relatively shallow and flat at ~4 m.....174

6.2. Framework for data driven transport model.....175

6.3. Typical velocity time series from surface current measurements at one location in the computational grid, shown as a time series (solid line) and the de-tided signal (dotted line) for east-west (top panel) and north-south (lower panel) coordinate axes. 182

6.4. From top left to bottom right, the spatial distribution of current vector, colored arrows scaled by current magnitude (cm/s) at successive times: time t = 60, 120, 180 and 240 hrs.....183

6.5. Distribution density for turbulent diffusivity along the coordinate axes.....184

6.6. Spatial distribution of turbulent diffusivity; top panel, diffusivity K_x in x-direction (modal value = 2.1 x 10^4 cm^2/s; bottom panel, diffusivity K_y in y-direction (modal value = 4.0 x 10^4 cm^2/s).....185

6.7. Normalized error from model simulation for spatial location of plume with varying Re; -●-, constant diffusivity, varying velocity; -■-, varying diffusivity, constant velocity. 187

6.8. Normalized error from model simulation for variance of concentration distribution with varying Re; -●-, constant diffusivity, varying velocity; -■-, varying diffusivity, constant velocity. 187

FIGURE Page

6.9. Plot of peak concentration against time; top panel, $K_x = 1 \times 10^4$, $K_y = 1 \times 10^5$; bottom panel, $K_x = 1 \times 10^5$, $K_y = 1 \times 10^6$. Solid line, exact solution, open circle, results from model simulation. 188

6.10. Plot of variance of concentration for pulse discharge initialized at two different locations within the computational domain. The difference in variance attributable to the difference in diffusivity values dependent on spatial location.....190

6.11. Top panel; peak concentration vs. time for scenario 1 (-●-) and scenario 2 (-■-). Bottom left panel; vertical profile from run #1. Bottom right panel; vertical profile from run #2. 191

6.12. Evolution of diffusing conservative material over three tidal cycles; run #1. The arrows representing the current vectors are colored for relative strength from blue to red on a scale of 0-150 cm/s. 194

6.13. Evolution of diffusing conservative material over three tidal cycles; run #2. The arrows representing the current vectors are colored for relative strength from blue to red on a scale of 0-150 cm/s. 195

LIST OF TABLES

TABLE Page

1.1 Mathematical expressions for longitudinal dispersion coefficients 10

1.2 Summary of experimental and meteorological conditions.....20

2.1 Services implemented for IEOAS bench test.....52

3.1 Various models proposed for the analytical evaluation of R_L. T -- Taylor (1921); F1 and F2 -- Frenkiel (1953); ATG -- Altinsoy and Tuğrul (2002). 72

3.2 Summary of turbulent diffusivity results for all three studies conducted. 91

4.1 Typical values proposed for the value of dimensionless time, Ψ based on different shear current 107

4.2 Summary of shear diffusivity results for all three studies conducted. Mean and maximum values of the dimensionless integral, initialization time and shear diffusivity are given for each of the coordinate axes, *x, y*. 122

5.1 Experimental and meteorological conditions for dye diffusion experiment. 134

5.2 Diffusion models prescribed on the basis of parameter *m*. 139

5.3 Summary of dye patch characteristics.....151

6.1 Variance and spatial location estimates of a dye patch from an instantaneous point discharge for different values of Re (constant velocities) 178

6.2 Variance and spatial location estimates of a dye patch from an instantaneous point discharge for different values of Re (constant diffusivities) 179

6.3 Normalized error from numerical estimates of variance and spatial location in comparison with exact solution for different values of Re 180

TABLE Page

6.4 Peak concentration at successive time intervals for modeled scenarios 193

6.5 Variance-time summary for modeled scenarios.....193

7.1 Listing of routines developed and their respective applications. 202

CHAPTER I

INTRODUCTION

Statement of Purpose

For emergency response in situations involving oil or contaminant spill in surface waters, one of the tools that can be used for monitoring and tracking constituent trajectory and spatial extent is a constituent transport model. These modeling tools exist in many different forms and varying levels of complexity but even the simplest models still require a certain skill level usually beyond that of the first responder. Most operational models require input for forcing information, which, generally will not be available given the small window of opportunity and the time scale of the physical-chemical processes governing the fate and transport of the constituents of interest.

Another challenge when it comes to monitoring of water quality parameters and environmental indicators in surface waters has to do with the spatial extent and dynamics involved. Continuous monitoring from fixed platforms provides high temporal but low spatial resolution while mobile platforms on the other side of the spectrum provide medium to high spatial and relatively low temporal resolution. There being a practical limit to the number of such units that can be deployed to improve on resolution, satellite based monitoring can be used to provide medium to high temporal and spatial resolution but suffers limitation in terms of sensors that can potentially be deployed. As we attempt to draw inference over the spatial extent for the domain of interest from information

---

This dissertation follows the style and format of *Estuarine, Coastal and Shelf Science*.

available from a finite number of fixed sampling stations, we fall back on spatial smoothing techniques such as Kriging, Objective Analysis, and Delaunay Tesselation among others.

Alternatively, the coupling of real-time measurements and numerical models will be important in overcoming these challenges in environmental and oceanographic assessments in surface waters. Model output in terms of trajectory and spatial distribution of the constituents of interest (temperature, salinity, fluorescence etc.) take into account the dynamics involved being forced or constrained by the surface current data, leading to a reduced transport model with an extremely simplified input requirement. Output was presented as animated sequences and viewable over the Internet through the implementation of a webserver. Instrumentation design and development, data telemetry and other special hardware and software tools required for performing field experiments that ultimately form parts of this decision support tool are described.

Background

The coastal zone as defined by the International Geosphere Biosphere Program (IGBP) in its Land Ocean Interactions in the Costal Zone (LOICZ) initiative encompasses the entire region from the 200 m bathymetric seaward contour and 200 m elevation inland contour. This would include all estuaries and bays, a very important part of the marine ecosystem, which also supports human activities such as recreation, transportation and industry. Some of these different structures being juxtaposed, there is

a resultant increase in demand being placed on this major socioeconomic structure. Going by the above definition, the coastal zone occupies 18% of the global surface, and is inhabited by 60% of the human population, supplying 90% of the world's fishery, an area that accounts for 8% of the ocean surface, and acts as a sink for 75-90% of suspended river load and associated pollutants (Cracknell, 1999).

The rate of anthropogenic driven change is much higher in the coastal zone with 90% of land-based pollution (including sewage, nutrients and toxic pollutants) remaining in the coastal zone (Pernetta and Milliman, 1995). Against this backdrop, protecting and sustaining this delicate balance is imperative leading to the development of a number of water quality and contaminant transport models for monitoring and management. Water quality models are important in carrying out environmental and oceanographic assessments in bays and estuaries going by the spatial extent of this water bodies. Direct monitoring of water quality parameters over the observational domain is constrained in terms of spatial resolution by the number of sampling points from finite set of fixed stations. Mobile sensing platforms on the other hand provide better spatial resolution but limited coverage requiring *a priori* knowledge of the gradients. One strategy for overcoming these limitations would involve using a combination of fixed and mobile observational platforms coupled with numerical modeling as implemented in a constituent transport model forming an adaptive sampling framework.

Transport and water quality models are often based on coupled sets of Navier-Stokes and advection-diffusion equations. Numerical solution of the Navier-Stokes equations, which provide the hydrodynamic information within this modeling

framework, is generally the most intensive in terms of computation and data required for model input. The characterization of the turbulent flow field is predicated on a number of turbulent closure schemes used in some ocean and general circulation models (Mellor and Yamada, 1982). Whereas, many water quality models exist and several operational ocean circulation models that have been developed, these schemes are difficult to implement. If we factor in the variability and uncertainties inherent in the boundary and initial conditions, these coupled models suffer serious limitations for rapid, real-time field deployments as required for instance, during emergency response efforts. Furthermore, accuracy in model predictions depend on how well the overall scheme has been calibrated an exercise that is expensive, time consuming and depends on availability of field data for validation.

This study seeks to address the issue of model complexity through a modified modeling framework resulting in a simplified constituent transport model. Through this research, a system was developed that employs direct observations of hydrodynamic data (currents in two spatial dimensions) to drive a constituent transport model. Effectively decoupling the hydrodynamic module from the advection-diffusion module, it would serve to increase model accuracy as well as capture most of the information that attends the variability encountered in the environment. Algorithms were developed that allow real-time calibration of the resulting albeit simplified, constituent transport and water quality model using direct observations of hydrodynamic data. Inputs into the resulting transport model were surface current measurements and should enhance field deployments for near real-time constituent tracking and water quality monitoring.

Furthermore, it will become possible to characterize estuaries and shallow embayment over different temporal scales without having recourse to expensive and time-consuming model recalibration.

The project was predicated on recent developments in measurement and data communications technology for mapping surface currents in coastal environments: deriving current profiles in the water column, *in situ* instruments for obtaining real-time environmental and oceanographic measurements, availability of radio-based wireless data telemetry options as well as web-interfaces for delivering model output in form of visualizations.

Research Objectives

There are three parts to this implementation and these are outlined here as a set of objectives:

- Part 1 – This is a theoretical development and investigative phase. In the first instance, spatial interpolation techniques such as Objective Analysis and Kriging as well as temporal data resampling were applied to the surface current measurements compensating for dropouts in data acquisition while improving the data set prior to incorporation into a transport model. The filtering of Acoustic Doppler Current Profiler (ADCP) datasets was also performed following spectral analyses of the raw data. The theory of turbulent diffusion and shear-augmented turbulent diffusion was developed within the concept of using real-time hydrodynamic data and spatially distributed dynamic coefficients in a transport

model. Algorithms were developed for evaluating diffusion coefficients from velocity measurements that would be applied to a simplified constituent transport model (Csanady, 1980).

- Part 2 – This is a field-based experimental phase to validate the algorithms developed in Part 1. This part of the study involved a series of dye-tracer that were conducted in Corpus Christi Bay to validate the algorithms developed in Part 1 and involved the development of instrumentation, data acquisition systems and real-time data visualization tools. These were deployed on a shallow-draft geo-referenced vessel equipped with a suite of instruments mounted on an undulating tow-body and capable of real-time telemetry to a shore-based unit.
- Part 3 – The third part is an applications development phase. A data-driven constituent transport model was implemented which incorporates hydrodynamic measurements and dynamic spatially distributed transport coefficients. The tools developed which includes the numerical scheme, data acquisition systems, wireless data telemetry and data analyses/visualization tools were tested within the framework of decision support systems for environmental and oceanographic assessments with particular application to emergency response activities in nearshore and coastal environments.

The various modules implemented in this three-part project are summarized.

Front-end development:

- *Estimation of Dispersion Coefficients in non-Homogeneous Flow Fields with Application to Transport Modeling*

  - Instrumentation, data acquisition and processing units provide real-time hydrodynamic data (velocity, current profile) and data pre-processing.
  - Numerical algorithm and model development:

- *Incorporation of HF Radar Surface Current Data into Plume Tracking Model (PTM)*
  - Hydrodynamic data assimilation, feeding pre-processed data into a numerical algorithm (coefficients module) that provides dynamic model coefficients.
- *Dye-tracer Study to Validate Algorithms Developed*
  - Perform validation studies through conservative tracer experiments. Perform system validation and readiness exercises prior to field deployment.
- *Constituent Transport Modeling Using Direct Observations of Hydrodynamic Data*
  - Develop constituent tracking system and application.

Back-end development:

- *Adaptive Sampling through Coupled Real-time Data Acquisition and Numerical Modeling*
  - Computing infrastructure development, data acquisition, wireless data telemetry, provision of environmental monitoring quantities in real-time on webserver, data post-processing, transmission and archival.

- *Multi-parameter Instrument Array and Control System (MPIACS): A Software Interface Implementation of Real-time Data Acquisition and Visualization for Environmental Monitoring*
    - Incorporation of real-time data visualization in a geo-referenced mobile instrument-sensing platform.
    - Rapid deployment real-time system

Methods and Materials

Determination of Transport Model Coefficients from Direct Observations

Many water quality and contaminant transport models are based on advection-diffusion numerical models (Fletcher, 1991a) giving rise to a set of parabolic partial differential equations (PDEs). The PDEs involve dispersion coefficients, which are typically assumed constant in space and time. However, dispersion experiments conducted in the Ribble Estuary by Burton et al. (Burton et al., 1995) clearly reveals that this is erroneous and other studies have shown that these coefficients have a spatial-temporal variability affected by tidal action (Riddle and Lewis, 2000). If this spatial-temporal variability is taken into account, we can expect a significant effect on predictions from numerical models as shown through model sensitivity analysis (Tchobanoglous and Schroeder, 1985). Okubo conducted a series of experiments in several bodies of water and developed a set of oceanic diffusion diagrams that gives length scale dependent dispersion coefficients in line with the well-known $4/3^{rds}$ power law (Okubo, 1971). Although these diagrams were developed from studies conducted in

the open oceans, they continue to be used within the modeling community for smaller water bodies. List et al. were able to establish temporal variability of dispersion coefficients using a set of drogues, (essentially Langrangian drifters) with global positioning (List et al., 1990) but the limitation of this approach lies in the restriction in terms of spatial extent since there is a limit to the number of drifters that can be deployed and tracked simultaneously.

The inclusion of coefficients into water quality and contaminant transport models derived from direct observation of surface current measurements will allow for the use of spatially and temporally variable coefficients and serve to improve model accuracy while providing near real-time hydrodynamic input into the numerical model. This parametric accuracy however should be distinguished from numerical accuracy stemming from truncation errors associated with discretization of the governing equations. The spatially distributed, time-dependent dispersion coefficients needed for the resulting transport equation are obtained from the spatially distributed observations of velocity over time while the dispersion coefficients are obtained through a numerical algorithm. From the literature, we find range of values for dispersion coefficients in bays and estuaries are of the order of 10^5 - 10^6 cm^2/s (Okubo 1971) while some theoretically and empirically determined expressions for obtaining dispersion coefficients (also from the literature) are given in Table 1.1 below. The list is by no means exhaustive and is presented here as a sampling of expressions relating dispersion to velocity (or time) and other theoretical and empirical relations can be found in the literature. It is noteworthy that quite a few of these are extensions of Taylor's work. In this study, a numerical

approach will be used with discretized near real-time observation of current data as input within the computational domain. No attempt was made to establish analytical forms for dispersion coefficients dependent on velocity measurements other than as described through the autocorrelation function.

Table 1.1. Mathematical expressions for longitudinal dispersion coefficients.

Dispersion Coefficient	Terms	Application	Source
$D = 63nU_T R_H^{5/6}$	D = dispersion coefficient, m^2/s n = Manning roughness U_T = maximum tidal velocity R_H = hydraulic radius	Tidal rivers and estuaries	(Harleman, 1964; Tchobanoglous and Schroeder, 1985)
$D = 10^{-6} N_R^{0.875}$	D = dispersion coefficient, m^2/s N_R = Reynolds number	Channel flow	(Davies, 1972; Tchobanoglous and Schroeder, 1985)
$D = (const)G^{1/3}l^{4/3}$	D = dispersion coefficient, m^2/s G = average rate of energy dissipation per unit mass, m^2/s^3 l = mean eddy size	Turbulent mixing, rivers, estuaries	(Batchelor, 1950; Ippen, 1966)
$D = l_L\left[\left\langle U^2 \right\rangle\right]^{1/2}$	D = dispersion coefficient, m^2/s l_L = Langrangian length scale, m U = velocity, m/s	Turbulent diffusion	(Fischer et al., 1979; Taylor, 1921)

Diffusion Coefficients in Surface Waters

Diffusion processes in surface waters govern the distribution of constituents within the water body. These constituents range from naturally occurring material such as salinity, temperature, phytoplankton, and sediment through temperature heat and other

anthropogenic material from industrial and recreational activities. A concentration profile of these constituents can be developed through numerical models that rely on coefficients, which capture the physical phenomena that lead to spreading and movement collectively termed transport coefficients. The coefficients may be determined through: i) the evaluation of the temporal variation of the currents (magnitude and direction); ii) the evaluation of the spatial variation of the velocity field; iii) the evaluation of the first and second moments of concentration distribution of a constituent and iv) inverse problem based on the advection-diffusion equation. The first two methods are based on Taylor's analysis of pipe flow (Taylor, 1954) and extended to other fluid flow regimes by Elder in his work on flow through open channels (Elder, 1958).

At the molecular scale, the process of diffusion is characterized by a molecular diffusion coefficient that depends on the degree of randomness or level of "agitation" within the fluid as indicated by fluid temperature. Analogous to this on a larger scale, turbulent diffusion is characterized by turbulent diffusion coefficient dependent on the degree of randomness or turbulence intensity measured by the currents driving the process. The extension of Taylor's pioneering work in this field have shown that turbulent diffusion in the presence of a shear structure within the current field results in a shear-augmented diffusion process, which becomes the dominant process after an initialization period determined by a characteristic vertical mixing time, t_c.

Through a series of studies conducted by Csanady in the Great Lakes (Csanady, 1966), the observation was made that there exists a variation in the dispersion of

constituents within a fluid body with the observed spreading more pronounced under certain conditions than would have been expected. The growth of a diffusing cloud would appear to be higher than could be explained if based on turbulence alone. Compounding these seemingly inconsistent observations is the fact that a weak vertical turbulent eddy diffusivity in the vertical appears to favor increased rate of lateral dispersion leading to the concept of shear augmented turbulent diffusion.

Shear diffusion becomes especially important within the coastal ocean and near-shore environments, involving the interplay between vertical turbulent diffusion and shear currents. The existence of complex shear current structures coupled with rapid variation in magnitude and direction of currents will be typical of shallow wind-driven bays and estuaries. Shear diffusion can be described as first or second stage depending on the type of shear currents encountered by fluid elements in the flow field and as noted by Elliot (Elliot et al., 1997), lateral shear is more likely to lead to first stage diffusion while vertical shear is more likely to lead to second stage diffusion. In shallow bays and estuaries and far enough away from vertical boundaries, lateral shear will be less significant in relation to the contribution to dispersion compared to vertical shear. Researchers including Bowden (Bowden, 1965) and Csanady (Csanady, 1966) have put forward expressions for determining the apparent diffusivity, $\boldsymbol{K_a}$ following on Taylor's work. Some of these expressions are presented in this paper for reference. In the case of lateral shear, the apparent diffusivity, $\boldsymbol{K_a}$ exhibits an inverse dependence on turbulent diffusivity, $\boldsymbol{K_d}$ (vertical or horizontal) while in the case of vertical shear the dependence is linear. Turbulent diffusivity itself can be evaluated through the auto-correlation

function, $\boldsymbol{R_\tau}$ of the fluctuating velocity time series based on Taylor's statistical treatment of diffusion as a random process (Taylor, 1920). Overall, mixing by diffusion is based on the interaction between a turbulent velocity field and the shear current structure generated by wind stress or tidal action.

Following Okubo & Carter (Okubo and Carter, 1966), Elliot (Elliot et al., 1997) developed expressions for shear diffusion from which the time for complete vertical mixing to occur and consequently, the relative importance of the two interacting processes can be estimated. During first stage shear diffusion, the time to complete vertical mixing $\boldsymbol{t_c}$ has an inverse relation to shear current, $\boldsymbol{S_i}$ after which the distribution of the constituent of interest (as measured through the concentration profile of a diffusing dye patch) is then governed by second stage diffusion. In each case in the presence of shear currents, turbulent diffusivity will become negligible compared to the apparent diffusivity due to shear. The overall effect is that turbulent diffusion in shallow wind-driven estuaries is augmented significantly by the shearing action. The role of vertical turbulence in shear diffusion is examined in conjunction with vertical shear in a shallow wind-driven estuary. Conditions under which shear diffusion come into play are discussed, leading to the numerical evaluation of the effective diffusivity within a shear current structure. A method of obtaining effective diffusivity from direct observation of currents was developed against the backdrop of constituent transport modeling within the prototype body of water, Corpus Christi Bay, TX. Estimates are provided for the initialization period, which has an inverse relation to the vertical turbulent diffusivity, $\boldsymbol{K_z}$. The Lagrangian correlation function, $\boldsymbol{R_\tau}$ of the velocity time-series was used in a

numerical evaluation of the turbulent eddy diffusivity, which in turn was used in the numerical evaluation of an effective diffusivity based on the shear current. In this study conducted in a shallow wind-driven bay, the shear diffusion process was found to be dominant over turbulent diffusion under certain conditions. The three-dimensional (3-D) current measurements were made with a fast response current profiling instrument simultaneous with dye-tracer experiments conducted at Corpus Christi Bay, TX between the summer and winter months of 2003.

Transport Model Development and Algorithm Selection

The scheme reduces the model equations to a single set of parabolic PDEs by replacing the usual hydrodynamic module in a coupled transport model with near real-time velocity data obtained by direct observation from HF Radar equipment. This approach effectively uncouples the hydrodynamic module from the transport module. Not only were we able to resolve numerically imposed constraints due to environmental and hydrodynamic conditions; the physical constraints imposed by bathymetry, geomorphology, and shoreline geometry are better captured using real-time measurements. This led to the development of a data-driven constituent transport model that is reduced in terms of complexity and easy to deploy regardless of the physical and geomorphologic conditions encountered. The transport model provides a concentration profile (C_i) within the domain of interest for the i^{th} constituent of interest.

Typically, these schemes are solved numerically as a coupled PDE set and for the larger, more complicated models using parallel or distributed processing which becomes

increasingly expensive with increasing model complexity (Fletcher, 1991). The diffusion coefficients are obtained either from tracer studies, or from diffusion diagrams or turbulence closure schemes.

In this implementation, the governing equations were uncoupled by using direct hydrodynamic data input from the HF radar, and as a result reducing the model to a single PDE set. Model coefficients (u, v, w and K_x, K_y, K_z) to be used in solution of the resulting transport equation were obtained from current data using the algorithm described in the preceding section and incorporated into the discretized form of the governing equation. Finally, model error analyses were performed to determine the effect of using dynamic, tidally averaged and ensemble-averaged coefficients. Given the fact that this study focuses on developing a simplified and integrated system for environmental monitoring and emergency response, this part of the research involved the selection and not so much the development of a PDE solver routine that in combination with the scheme outlined above forms the modeling framework. Noting that many schemes exist for the numerical solution of PDEs including several implicit and explicit finite differencing schemes, finite element analysis, finite volume, spectral methods etc. and is an active area of ongoing research in Computational Fluid Dynamics (Fletcher, 1991).

Tracer-study for System Evaluation and Model Validation

This part of the research was focused on system validation and integration. A towed-array of instruments consisting of conductivity, depth, temperature, fluorescence

(CDT-F) sensors, GPS and vessel navigation subsystem was deployed in Corpus Christi Bay and a series of tracer experiments were conducted to validate the algorithms and test the capability of the system to provide near real-time environmental monitoring data. The entire suite would be integrated into a rapid deployment constituent tracking and monitoring system, which will be available for conducting studies within bays and estuaries, as well as for emergency response efforts such as oil or contaminant spills in coastal environments.

The tracer study was conducted as a one-time effort using a geo-referenced towed instrument array. The towed array of sensors sampled the domain using *in situ* sensors for tracking the constituent of interest, which for the tracer study was Rhodamine WT dye. Information and data from this study was analyzed using the method of moments to evaluate the diffusion coefficients at selected locations within the bay and comparing the results with those obtained from using velocity measurements.

Modeling Framework and System Block Diagram

The overall scheme is presented in the form of a block diagram in Figure 1.1 below. Grayed out modules indicate parts of a conventional transport model that were not included in this modeling framework but would be included within typical coupled models. In the implementation of this project, equipment and tools used in this study were developed as a combination of hardware and software solutions.

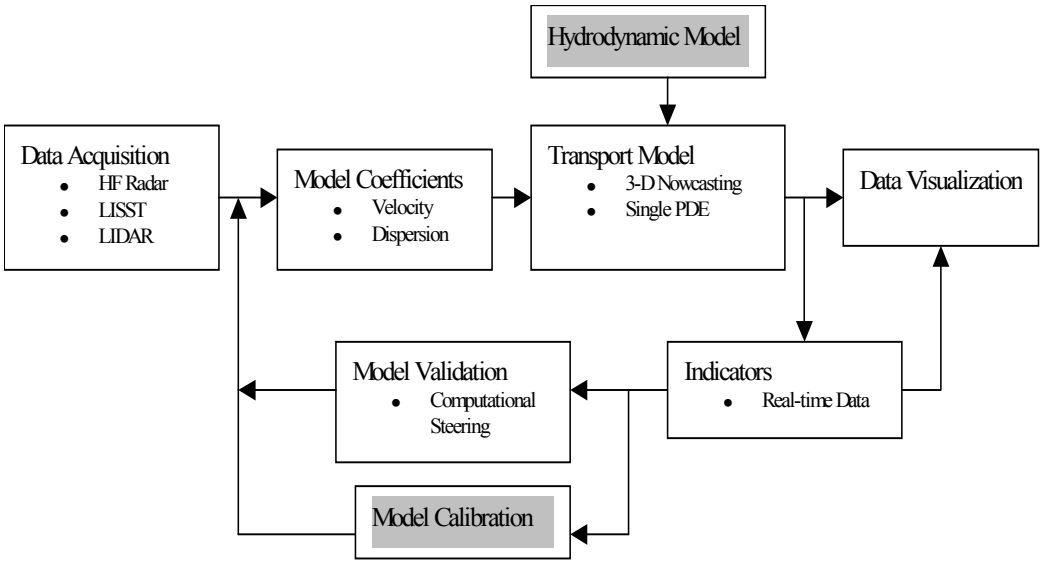

Figure 1.1. System block diagram.

Trajectory Tracking and Vessel Guidance System

A "Trajectory Tracking and Vessel Guidance System" was developed based on the improved now-cast/forecast methods enumerated earlier. This essentially is a software interface module that was developed and used for the sampling exercise to guide the tracer studies and model validation efforts. The system comprised a shipboard user interface showing color-coded tracklines corresponding to detected levels of constituents in the water body.

Integrated Sensor Interface, Data Acquisition and Computing Network

A mobile sensing platform equipped with *in situ* fluorescence and CTD sensors mounted on a towed body, with Global Positioning System (GPS) was used as the sensing platform. An instrumentation hardware and software interface was developed

and in conjunction with the Trajectory Tracking and Vessel Guidance System described in preceding section, formed an integrated data acquisition, visualization and telemetry unit that was used in an adaptive sampling scheme to facilitate and guide data acquisition exercises with improved resolution and coverage.

Site Description

The site is located within Corpus Christi Bay which is in the Texas Gulf of Mexico about 200 miles south west of Houston, TX (Figure 1.2). Being part of a system of bays that has Corpus Christi Bay as the main bay, there are four embayments connected within the system namely Oso Bay in the southwest, Nueces Bay in the northwest, Upper Laguna Madre in the south and Redfish Bay in the northeast. A shipping channel that is ~15 m deep runs east to west along the northernmost half of the bay and an intra-coastal waterway runs north to south. It is bounded on the east by Mustang and North Padre Islands and on the west by the city of Corpus Christi.

The deepest of the four, it has relatively uniform bathymetry throughout (~3 m) with a correspondingly low tidal range (± 0.5 m) as is characteristic of most of the bays in Texas. The bay is approximately 500 sq. km with the channel opening into the Gulf at the Northeastern end through Aransas Pass as the main form of exchange with the Gulf system and under the influence of the tides, the residual currents are therefore predominantly along the east-west coordinate axis with a counterclockwise circulation pattern along the shoreline. Being in a semi-arid location with freshwater inflow from Nueces River and Oso Creek, the system with a drainage area of ~49,700 sq. km

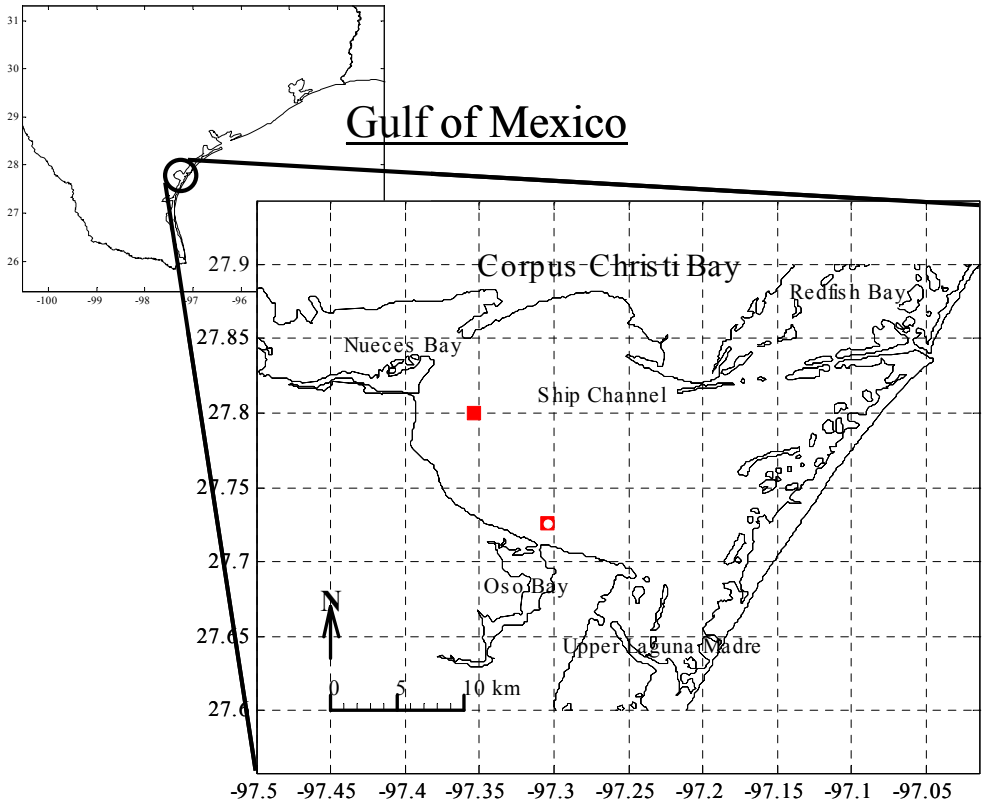

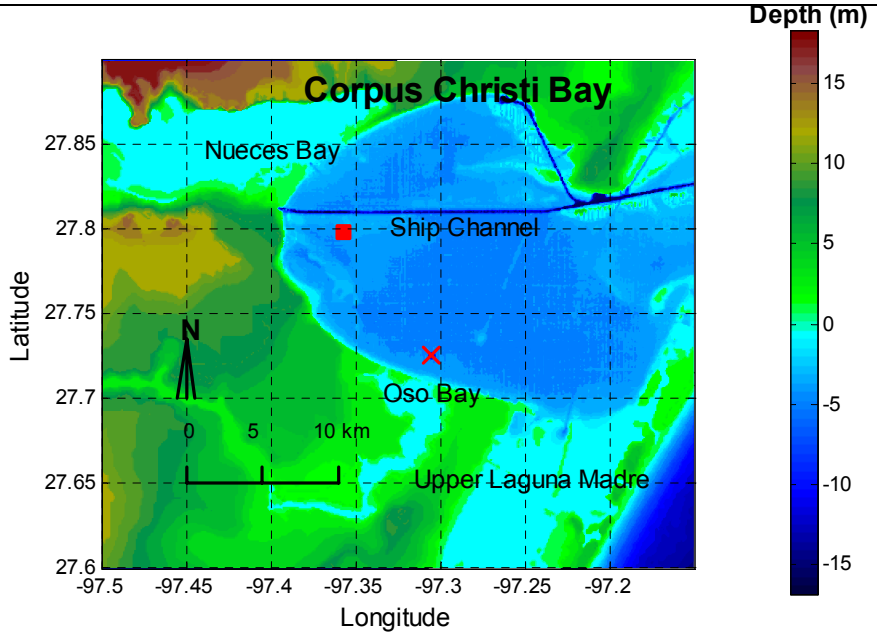

Figure 1.2. Top; map of Corpus Christi Bay in the Texas Gulf of Mexico. Approximate location for each study is indicated (■ – Study 0828_1 and 1007; ◘ -- Study 0820_2). Bottom; bathymetry of the study area.

receives a daily average freshwater flow of ~34 m^3/s and has an average salinity of 22 psu which can be as high as 33 psu. This bay, which can be classified as wind-driven is predominantly under the influence of winds blowing from a southeasterly direction while winds called "Northers" blow from the northerly direction sometimes during the winter months.

Meteorological and Experimental Conditions

Three field experiments conducted on the dates indicated in Table 1.2 below with individual identification and at the locations (also indicated in Figure 1.2). The experimental and meteorological conditions encountered during the experiments are summarized in Table 1.2 and depicted graphically in Figures 1.3 and 1.4 showing the wind pattern and oceanographic conditions respectively.

Table 1.2. Summary of experimental and meteorological conditions.

ID	Location	Date	Time (UTC)	Tide	Wind
0828_1	2747.937N, 9721.451W	Aug. 28, '03	15:44	High water, ebb	7 kn, SE
0828_2	2743.571N, 9718.297W	Aug. 28, '03	21:20		14 kn, SE
1007	2747.937N, 9721.451W	Oct. 07, '03	14:34	High water, flood	4-12 kn, NE

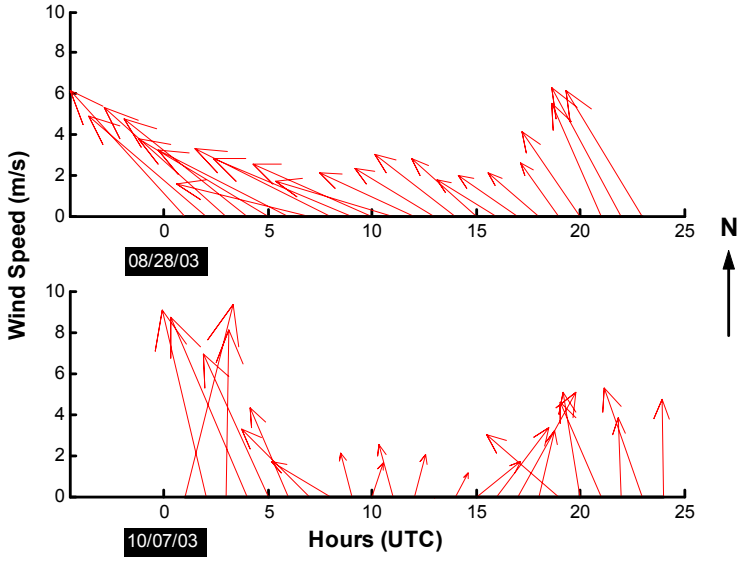

Figure 1.3. Wind speed measurements over a 24 hour period taken during the experiments. Top panel; experiment 0828_2. Bottom panel; experiment 1007. Wind strength is comparable during the two experiments reported but conditions during experiment 1007 is highly variable.

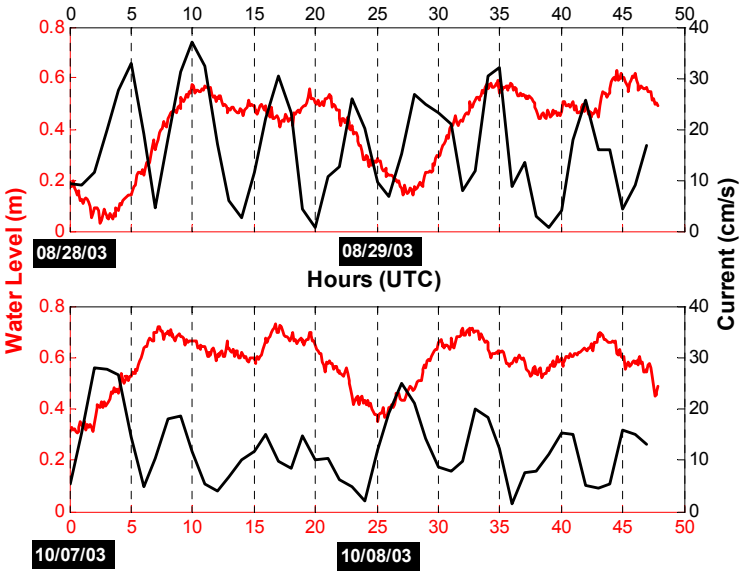

Figure 1.4. Water level (height above MLLW (─ solid line) and surface current measurements (-. dashed line) covering the duration of the experiments.

CHAPTER II

A RAPID DEPLOYMENT INTEGRATED ENVIRONMENTAL AND OCEANOGRAPHIC ASSESSMENT SYSTEM (IEOAS) FOR COASTAL WATERS: DESIGN CONCEPTS AND FIELD IMPLEMENTATION

Overview

Emergency response and spill monitoring in coastal and near shore environments is enhanced with the availability and use of real-time environmental data coupled with numerical simulation in an adaptive sampling framework. Invariably the various modules often exist on different computing platforms and a common thread is needed to achieve an integrated system suitable for application in spill or emergency response situations. In emergency response operations, information sharing between on-scene command and incident command is often required to facilitate decision-making. Wireless (802.11b) data networks coupled with use of concepts from distributed computing, can bridge the gap between data acquisition and data availability, thereby reducing the inherent latency within the system.

This in the context of environmental monitoring consists of a distributed file system (DFS), remote application services (RAS), network management and wireless data telemetry for wide area network services (WAN). This study focuses on the implementation of an integrated rapid response environmental assessment system combining *in situ* monitoring, real-time telemetry and direct numerical simulation (DNS) with web-based data access and visualization of oceanographic and environmental

parameters. The viability of the system was demonstrated in mock-spill exercises and details are presented.

Introduction

Monitoring of water quality parameters and environmental indicators in surface waters poses a challenge due to the spatial extent and dynamics involved. Design of sampling transects for routine monitoring involves a combination of science and experience but for real-time monitoring of episodic events, *a priori* design of sampling transects is impractical. The ability to observe spatially distributed time series have been made possible with the development of sensors deployed on remote platforms such as satellites, aircrafts as well as on mobile and fixed sensing platforms. The coverage of these datasets can be extensive, but limited in spatial or temporal resolution. *In situ* sensor deployments from remote platforms (fixed or mobile) are increasingly being used for data acquisition in environmental and oceanographic assessments; data that has to be made available in near real-time to the stakeholder (stakeholders including the public, the scientific community, resource managers and planners, etc.).

For instance, in emergency response operations, information sharing between on-scene command and incident command is often required to facilitate decision-making. Wireless (802.11b) data networks coupled with relational database management systems (RDBMS) can bridge the gap between data acquisition and data availability. These real-time measurements can be assimilated into numerical models either to fill in gaps in data or to improve on the spatial and temporal resolution of observations from sensing

platforms. These would include instrument measurements (such as surface currents, wind speed and direction, temperature), model predictions (fate and transport) and forensics.

This paper describes an optimized scheme that was developed to guide the monitoring of constituents of interest by coupling a real-time data acquisition routine with a numerical model and web-based data visualization. The numerical model is driven by near real-time measurements of spatially distributed coefficients leading to algorithms for estimating the temporal and spatial characteristics of an evolving constituent within the body of water. Model output in terms of trajectory and spatial distribution of the constituents of interest take into account the dynamics involved. A user interface provides real-time correlative visualization between the model output and intensity of the measured variables provided by the deployed instruments mounted on a geo-referenced mobile sensing platform to guide the data acquisition and sampling efforts.

Background

There is increasing national and global interest in field programs for the evaluation of dispersant use in nearshore waters and some regulatory agencies have opted to use a "spill of opportunity" for data gathering. Our program has helped in determining the direction of research in this area and we have been involved in coordinating such efforts (Ojo et al., 2003a) while providing the enabling infrastructure. Our group has deployed real-time *in situ* sensor instruments on fixed platforms in

targeted locations in Corpus Christi Bay to monitor important baseline parameters, such as hydrocarbon contaminant concentrations, nutrient levels, particle size distribution and characterization. In addition we have added sensor arrays to a geo-referenced boat that provide valuable information for emergency response planning activities in surface waters. The sensor-arrayed geo-referenced boat provide valuable real-time data that can be transmitted to a shore-based the Incident Command Center to aid the response decision-making process.

With the realization of the need for bridging between different computing platforms and exchange of information in real-time, the Open Software Foundation (OSF) developed the Distributed Computing Environment (DCE) (Hashimoto et al., 1996), which is comparable in certain respects to the Common Object Request Broker Architecture (CORBA, Object Management Group) (Vinoski, 1997). The growth of the Internet and development of the Transport Control Protocol/Internet Protocol (TCP/IP) opened up a completely new frontier in the area of distributed computing. Coupled with the development of wireless communications, ship-to-shore data telemetry for environmental monitoring and emergency response can be realized in a cost-effective manner using commercial off-the shelf (COTS) products. Figure 2.1 shows the architecture of the DCE, which makes it possible to have legacy code and proprietary applications in a collaborative environment running on different computing platforms, the Distributed File System (DFS) being a key component within the DCE framework.

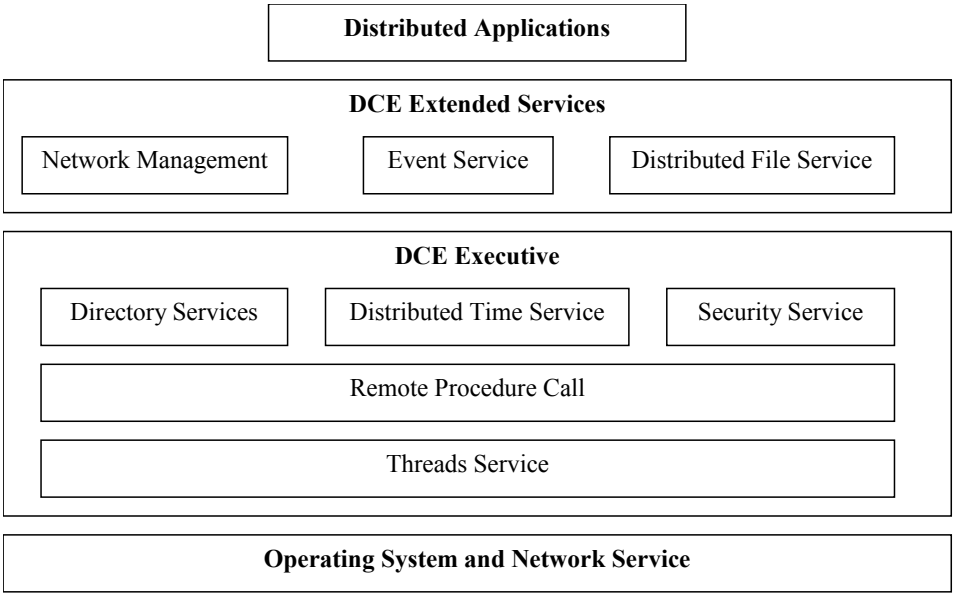

Figure 2.1. DCE architecture (Brando, 1995).

Near Term Objectives and Project Scope

The objectives of this study are summarized below:

- Develop data acquisition (DAQ) systems including hardware and software to guide sampling efforts from mobile and remote sensing platforms in surface waters particularly when responding to episodic events.
- Develop algorithms for real-time data acquisition, data analyses, post processing and visualization.
- Deploy DAQ unit with selected instruments including but not limited to current meters, particle size analyzers, fluorometers, and current meters.
- Integrate wireless data telemetry for data transmission based on 802.11b protocol.

- Implement a web server for data synthesis, making data and graphics available on the web in near real-time.

To facilitate the decision making process, integrated datasets from sensors and a numerical model operating in near real-time is to be made available for visualization in real-time via the World Wide Web (www) through the implementation of a web server with user selectable input for sensor selection and determination of coefficients needed to drive a numerical model. High-level data synthesis is to be facilitated through conformity to the widely accepted format, the Network Common Data Form, NetCDF (Rew and Davis, 1990).

Design Concept

For environmental sampling, increasing use is being made of *in situ* sensors mounted either on fixed or mobile sensing platforms (Austin et al., 2002; Schofield et al., 2002; Volpe and Esser, 2002; Wiebe et al., 2002), typically communicating with data acquisition (DAQ) units using the RS232 data transmission protocol. For our purpose, an array of sensors mounted on a tow-body capable of performing undulating profiles through the water column was used within the context of response to episodic events and mapping of surface waters for environmental parameters. The multiple subsurface instruments were interfaced with the shipboard DAQ computer using TCP/IP, thereby overcoming the limitations inherent in RS232 communications with respect to distance while at the same time multiplexing the data into a single stream. High data throughput,

reliable connectivity and seamless integration into existing data networks were some of the conceptual design considerations.

The Transmission Control Protocol/Internet Protocol (TCP/IP) serves as a common thread to weave these platforms and modules into an integrated computing system. A ship-based local area network (LAN) was established using a submersible device server that links *in situ* sensors to an onboard computer. The onboard computer performs the role of a data post-processor and communications server, linking the field sampling station with the other modules and transferring data to Incident Command. A wide area network (WAN) based on wireless broadband communications facilitates the ship-to-shore link.

Motivation to use a 10BaseT Wireless Ethernet connection for the WAN includes: easy and convenient drive mounting, restoration of dropped network connection with minimal intervention (self-healing network), and high bi-directional data throughput. Various options available for achieving the data telemetry link include wire lines, leased lines, dial-up, satellite links, microwave links and radio Frequency (RF) spread spectrum. In this study, the RF spread spectrum technology was found to be the most cost-effective, offering the advantages of continuous data transmission, moderate throughput, ease of operation, and adequate link lengths. The dial-up option was also found to be viable but lacks the bandwidth and required ease of operation.

Environmental Monitoring in Surface Waters

This sub-section provides a synopsis of environmental monitoring to highlight the challenges especially as it relates to the decision-making process in response to episodic events and emergency response efforts.

1) *Sampling*

i. Grab sampling: This method falls within the classification of *ex situ* sampling and is mostly suited for off-line processing. Samples collected are analyzed in a shore-based or onboard laboratory (Volpe and Esser, 2002). Onboard analytical laboratories are expensive and especially for smaller craft, they are often impractical. In light of these, collected samples may have to be sent off to a land based laboratory which somewhat affects the decision making process. Grab sampling methods are most suited for routine monitoring where immediate analytical results are not required or where the analytical method exclusively calls for wet-chemistry. The spatial-temporal resolution with these methods is extremely limited.

ii. Flow-through sampling: This method also falls within the category of *ex situ* sampling and is essentially a variant of grab sampling. The water samples are pumped to the surface where they are analyzed by using the same methods applicable to grab sampling. They may also be used in conjunction with some of the sensors used for *in situ* sampling (Hanson, 2000) whenever immediate results are desirable. The drawback with flow-through methods are the effects of the fluid-flow on the sample and the need to

allow for fluid flow-rates and tubing lengths when determining the exact sample location for geo-referencing purposes.

iii. In situ *sampling: In situ* sampling makes use of submersible sensors for real-time or off-line processing of environmental or oceanographic measurements. It eliminates some of the problems inherent in flow-through methods as outlined in the previous sub-section. It is especially suited for real-time processing and facilitates the decision-making process by reducing the latency in data availability when compared with off-line processing.

A combination of *ex situ* and *in situ* sampling may be necessary whenever data validation is called for. In this case, the results of laboratory analyses are used in validating the data returned by the submersible sensors and for QA/QC.

2) *Data Acquisition*

In situ instruments can be operated in batch-processing mode in which case, onboard or computer-based data loggers are used, as is the case with long-term autonomous deployments. Real-time data acquisition through vendor-supplied software may not be practical especially when interfacing more than one instrument to the DAQ unit. For real-time monitoring, data pre-processing is usually performed with embedded routines in instrument microprocessors or by using external routines on a remote computer. Post-processing may be necessary for the purpose of applying correction factors or some other instrument specific routines to the raw data in order to make the

data representative of the parameter being measured e.g. to go from raw digitized data to engineering units.

In building instrument arrays, there are advantages to be derived from using commercial-off-the-shelf (COTS) products. In some cases, the end-user chooses to develop instrument arrays from the ground up. Instrument developers often provide software to facilitate real-time data acquisition but the use of instrument specific software interface may become impractical when deploying instrument arrays using instruments from multiple vendors. In such cases, it will be necessary to have knowledge of low-level commands specific to each instrument in the proposed suite of instruments in order to facilitate the implementation of an integrated interface for real-time applications. In developing such an integrated interface, working with instrument developers may is essential for accessing any low-level instrument control routines and other instrument specific data pre-processing schemes.

Developments in sensor technology over the past decade have led to availability of *in situ* instrumentation for oceanographic and environmental measurements. These range from sensors for basic water quality measurements e.g. Conductivity, Temperature, Depth, (CTD) sensors to more specialized sensors such as particle size analyzers (Agrawal and Pottsmith, 2000), imaging devices, current profilers (Ocker, 2002), nutrient analyzers (Hanson, 2000) etc. These could be deployed by themselves or as part of an instrument array. For geo-spatial data representation, one vital piece of instrumentation is the Global Positioning System (GPS) that provides the location and time stamp for each data point returned from the submersible sensors. The *in situ*

instrument array as used in this study was built from COTS devices although the option of building instruments from the ground up was explored. The instruments used here are highly specialized and have been proven in the field, finding wide acceptance within the user community (particle size analyzers, multi-spectral fluorometers, CTD sensors, current meters). These were interfaced to a common DAQ system by accessing their low-level operating modes.

3) *Real-time Visualization*

To take full advantage of real-time data acquisition, real-time data visualization becomes imperative. This could be in form of a time-series or geo-spatial datasets, vector mapping, contour plots, and animations or a combination of these. Figure 2.2 presents the data flow structure for implementing the real-time data visualization within this framework.

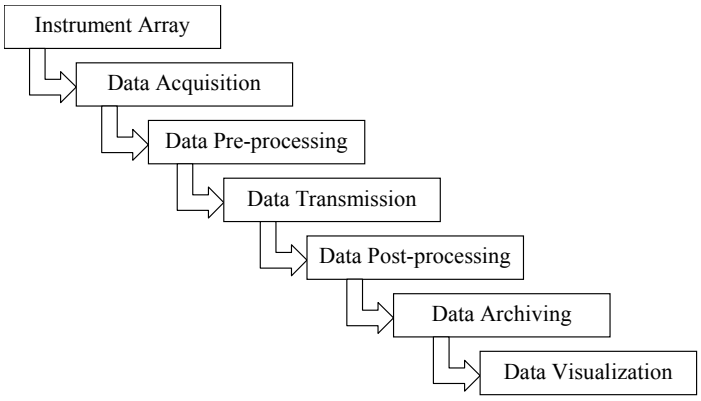

Figure 2.2. Representation of data flow for real-time data acquisition and visualization.

4) *Correlative Data Visualization*

To glean information from environmental measurements that may not be so apparent from single parameter measurements, correlative data visualization may be used between analogous multi-parameter datasets returned by single or multiple instruments (Treinish and Goettsche, 1991). For example, dissolved oxygen (DO) levels may be visually correlated with high fluorescence measurements to infer information regarding phytoplankton production which can raise or lower DO.

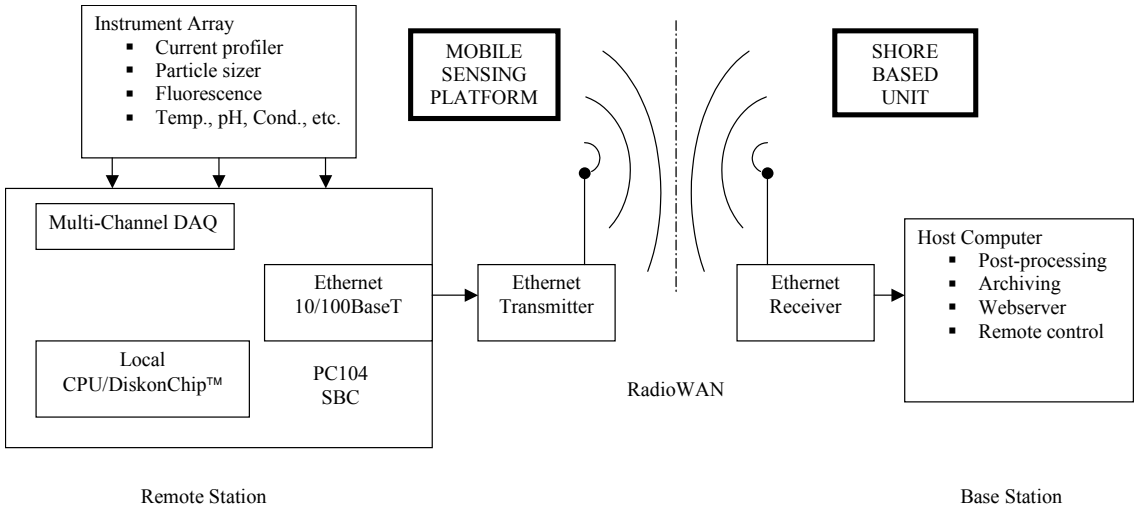

Figure 2.3. System block diagram for IEOAS.

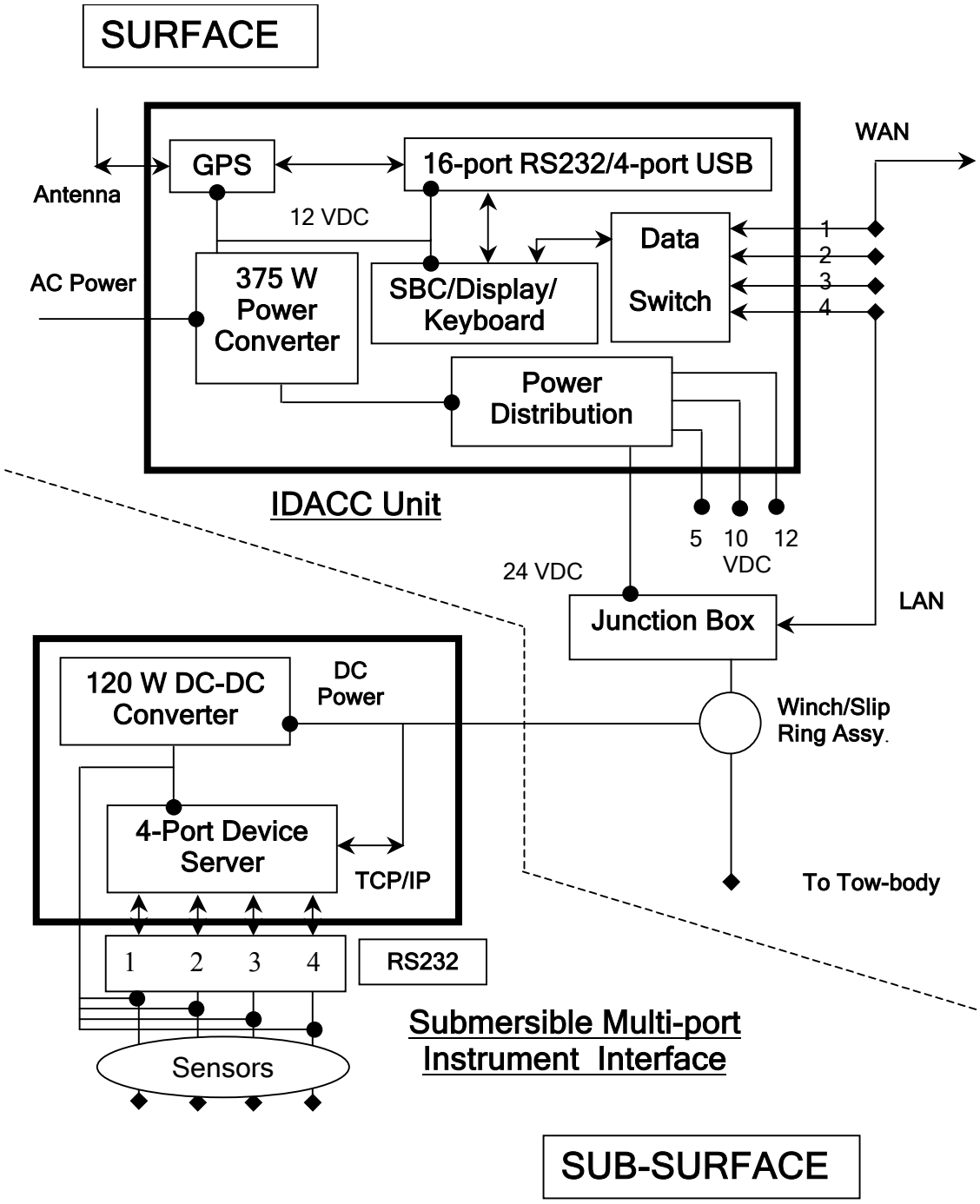

Figure 2.4. Schematic diagram of IDACC and submersible multi-port instrument interface.

System Description

Integrated Data Acquisition Communications and Control (IDACC) Unit

A block diagram representation of the IEOAS presented in the preceding sections is given in Figure 2.3. For the shipboard data acquisition unit, an Integrated Data Acquisition Communications and Control (IDACC) unit was developed as well as a submersible multi-port instrument interface. A schematic representation of the IDACC and submersible instrument interface is provided in the Figure 2.4.

As the main hardware component for data acquisition, IDACC (Figure 2.5) comprises a 15" single board flat panel industrial computer (PANEL 1150-370, Axiom Technology Company, Ltd.) mounted in a NEMA 4X sealed moisture-proof vented enclosure (Hammond Mfg., Inc.). The unit was built as a portable self-contained unit for easy transportation and fast onsite hookup and runs on regular AC power. Incorporating an AC/DC power converter, it provides a data acquisition interface to the sub-surface instruments and acts as a communications server for ship-to-shore data telemetry through a software application that was developed in-house. The IDACC interfaces with a sub-surface multi-port instrument interface, a differential global positioning system, DGPS (Furuno GP37), a 16-port RS232/4-port USB module(Edgeport/416, Inside Out Networks, Inc.) and a 5-port Ethernet switch (EtherTRAK from Sixnet, Inc.). Power from a 375 W AC-DC power converter (PFC375, Power-One, Inc.) mounted in the IDACC enclosure is fed through a power distribution box providing 5, 10, 12 and 24 VDC supply. The 24 VDC output is sent through a winch/slip-ring assembly, down the sea-cable to the tow-body and the submersible device server, which in turn distributes

power to the sub-surface sensors. The voltage drop at full load between the deck and subsurface units is ~2 V.

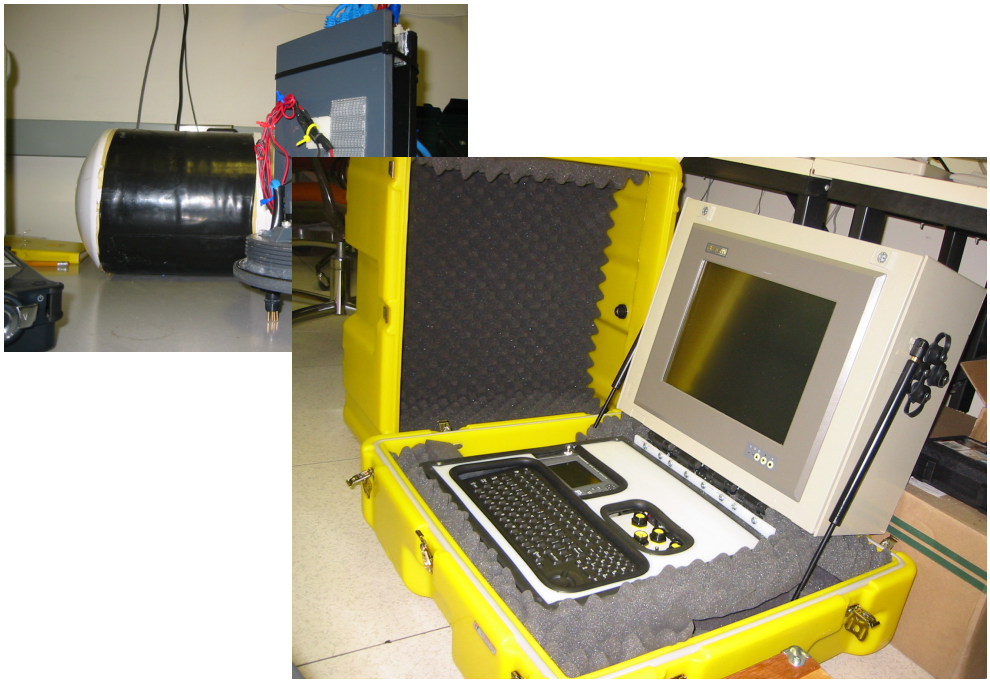

Figure 2.5. Top, inset; submersible multi-port device server. Bottom; IDACC comprising GPS unit, industrial computer in NEMA 4X enclosure, NEMA keyboard, power distribution and 4-port network interface. The main unit, which houses the electronics tilts up into operating position, supported by gas springs.

The sea cable comprises stranded twisted pair wire for both TCP/IP data communications as well as power supply. Data telemetry is facilitated by the 5-port network interface, connecting the IDACC to the subsurface device for data acquisition and sending of command signals via TC/IP to the sensors mounted on the tow vehicle. The network interface provides WAN connectivity by wireless telemetry through a radio link to shore-based network thereby ensuring real-time data accessibility for decision makers and stakeholders. In addition, IDACC allows for local data archiving on the local

hard drive through the software module, the Multi-Parameter Instrument Array and Control System (MPIACS). Built for rapid deployment, IDACC is portable, completely sealed and moisture proof. It can be deployed on the open deck of a boat, if cabin space is at a premium and requires just three quick connections; AC main power supply, DC power and data link to the subsurface device server and antenna connection for the GPS unit. A single power switch activates the entire system, booting up the main computer and the subsurface units.

For portability and transportability, the entire assembly comprising the IDACC and its ancillary modules (keyboard, GPS, power distribution) are mounted in a custom ATA shipping case (Hardigg Cases, Inc.). The case is a molded plastic grab-and-roll wheeled case with pressure equalizing valve allowing the assembly to be transported on aircrafts. The IDACC main module is a hinged assembly supported by gas-springs allowing the unit to be folded down and packed up for transportation. For on-site deployment, the top of the shipping case is simply removed, the IDACC main unit swings up into the open position and the connections made to the respective ports. The unit is powered up and made ready for data acquisition. In mounting the IDACC inside the shipping case, a set of rubber mounts was used for vibration isolation to protect the sensitive electronics from exposure to excessive vibration. Figures 2.5 and 2.6 show the IDACC interfaced to the tow-body through the submersible multi-port instrument interface.

Submersible Multi-Port Instrument Interface

The subsurface electronics are mounted on the end cap of a sealed housing made from PVC and includes power and data interface comprising of five sealed underwater connectors for power and data connection to the IDACC and up to four instruments mounted on the tow-body. This four-port subsurface unit acts as a power distribution and data communications unit. It comprises a multi-port serial RS232 device server (Digi PortServer TS, Digi International, Inc.) and a DC-DC power converter (BQ2540-7R, Power-One, Inc.), which acts as a power conditioner, receives DC supply in the range 15-36 VDC from the IDACC and distributes 15±0.07 VDC to as many as four different sensors simultaneously.

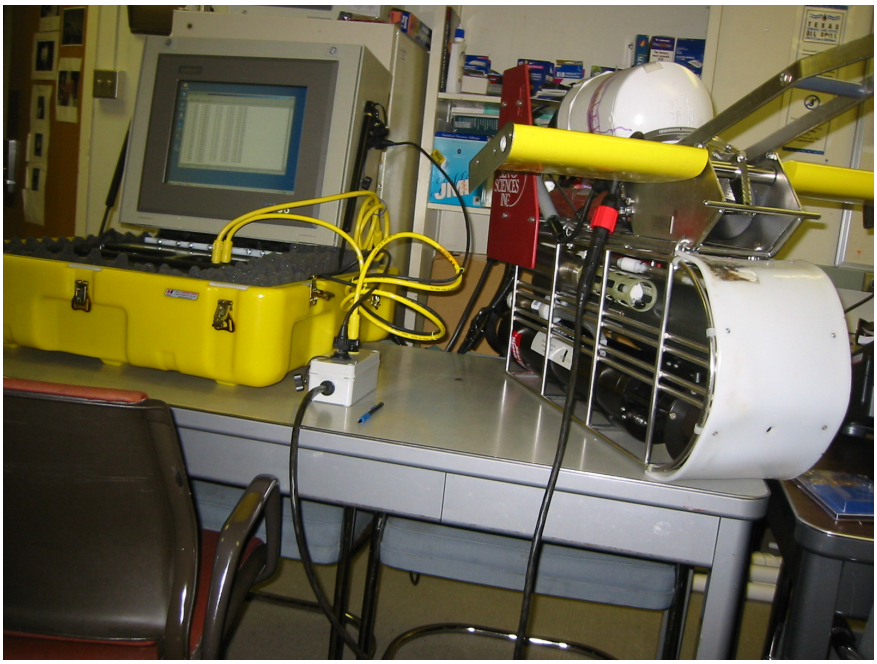

Figure 2.6. IDACC and tow-body with instrumentation and submersible multi-port device server undergoing bench tests.

To provide the data link between multiple *in situ* sensors and the shipboard IDACC unit, the device server was used to provide a multiplexed RS-232 serial instrument interface. This uses the TCP/IP protocol and addressing to implement virtual COM ports between the sensors mounted on the tow-body and the IDACC, the data being sent over twisted pair through the sea-cable. Access to the electronics is easy as the end-cap screws on to the main housing, the entire electronics and wiring being mounted on the end-cap. Driver files are required on the host PC to access the virtual COM ports on the device server, which includes a web interface for diagnostics, configuration and monitoring. The tow-body (Acrobat, Seasciences, Inc.) is an open frame undulating unit used to deploy the *in situ* instrument package. It can maintain either constant depth/elevation or undulating flight paths. It can be either controlled by a shipboard computer or manually controlled.

The Multi-Parameter Instrument Array and Control System: MPIACS

"The Multi-Parameter Instrument Array and Control System", MPIACS (Figure 2.7) is a software interface that provides real-time data visualization of up to six different parameters measured by single or multiple instruments simultaneously. These parameters could be concentration measurements from fluorometers, particle size analyzers, salinity, temperature etc. For each parameter, the percentage of the parameter (measured value relative to a pre-set peak value) generates a color trace corresponding to the horizontal travel of the instrument array through the water. This gives a visual indication of the spatial distribution of intensity of the constituent of interest or sampled

parameter. Since not all constituents of interest in environmental sampling lend themselves to visual contact, MPIACS was developed as a tool that provides instantaneous visual feedback to operators during environmental monitoring in surface waters. The interface is user-friendly allowing for quick configuration and minimal intervention from the operator. This tool has been used successfully in several deployments in simulated emergency spill response, routine bay profiling as well as dye-tracer experiments.

As a real-time environmental monitoring tool, the visual feedback aids the data acquisition process by providing immediate identification of "hot" and "cold" spots within the water body for the constituents of interest through measurements from submersible sensors. Each data point is location and time stamped through the IDACC's integrated GPS unit. The data stream is archived on the local hard drive in plain ASCII text, tab delimited file format for off-line processing. By allowing for correlative data visualization, MPIACS aids the data acquisition effort in an Adaptive Sampling framework (Stein and Ettema, 2003) by removing the "guess-work" inherent in environmental monitoring especially relating to constituents of interest that do not provide visual identification or if sampling was being performed during periods of low-visibility conditions. This visual reference will aid or guide data acquisition efforts and may be implemented in. Each color-coded trace is geo-referenced and displayed against a map outline of the study area by combining the instrument data stream with the GPS unit time and location information.

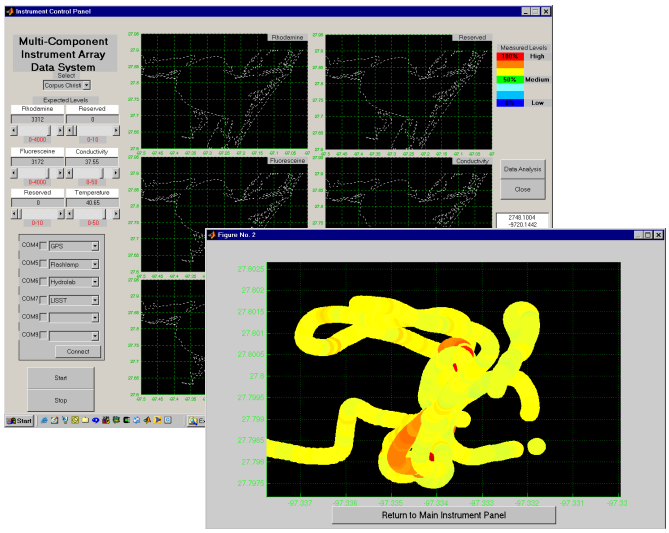

Figure 2.7. The MPIACS software interface. Lower right panel is a zoomed in portion of one of the 6 data visualization panes from the main instrument panel.

MPIACS was implemented in a modular form to facilitate expandability as well as flexibility to accommodate a wide variety of instruments. The modules comprise: Data Acquisition, Instrument Control, Data Post-processing, Data Visualization and Data Archiving. Unlike other data visualization programs that are written for off-line data visualization (He and Hamblin, 2000), the MPIACS prototype was developed with the objective of providing real-time data visualization while the data acquisition vessel is underway. A version of MPIACS was also developed, that operates in "playback" mode and suitable for off-line data visualization.

The GPS unit operates in three modes and can be set to auto-select between GPS, DGPS (differential GPS) or WAAS (wide area augmentation system) modes, depending on service availability. The accuracy of the GPS varies with the mode: DGPS mode (accuracy is within 1 m or 3 ft), WAAS mode (5 m or 15 ft), or GPS mode (10 m or 30 ft). Sampling rate of the instrument array will be governed primarily by the acquisition

rate from the GPS unit (fixed at 1 Hz) since all data points are geo-referenced. Travel speed of the sensing platform is governed by the tow-body and would typically average 5 knots and given this set of conditions, a spatial sampling resolution of ~3 m (9 ft) would be expected. Actual spatial resolution would vary depending on the operational mode of the GPS unit.

Ship-to-Shore Wireless Telemetry

For the ship-to-shore data telemetry, various options were explored including cellular, satellite, leased line links and the most cost effective option, using un-licensed radio links in the 2.4 GHz frequency range was decided upon. This link provides broadband 10BaseT wireless Ethernet transmission up to a theoretical throughput limit of 11 Mbps and distance limit of 24 km. The design considerations are presented in this section specifically addressing frequency, throughput, antenna type and mounting (with or without directional tracking). Detailed design issues for the radio link are given in this section. A number of hardware vendors were considered during the selection process looking at criteria such as ruggedness, ease of configuration, range, throughput and expandability. Hardware from two vendors were on the eventual shortlist for this project and the SpeedLAN 9000 series wireless routers supplied by Wavewireless, Inc. was chosen. The components making up the wireless units consist of a router, junction box, Ethernet interface and a signal amplifier. In selecting the antenna type and height, a link budget analysis was performed.

For the shore end of the point-to-point link, a 2.4 GHz, 14-dBi sectoral antenna (Til-Tek, Inc.) with variable horizontal beamwidth between 60º and 160º and vertical beamwidth of ±10º was used. The ship-based radio was configured as base-station for the network and for this purpose a 15-dBi omni-directional antenna (HG2415U-PRO, HyperLink Technologies, Inc.) with a vertical beamwidth of ±27º, providing 360º horizontal beamwidth was used. The omni-directional antenna was selected for the mobile platform in order to ensure a constant link regardless of the ships heading. Other options considered for the base-station were: 1) collocation of radios using multiple sectoral antennas to increase horizontal coverage and 2) directional antenna with a tracking device to re-orientate the antenna and compensate for movement of the platform. The omni-directional antenna provided the best option for our present purposes being easier to implement and more cost effective.

1) Link Budget Analysis

In designing the radio link, a number of factors have to be considered such as coverage, throughput, terrain, Fresnel zone, antenna characteristics (vertical/horizontal beamwidth, radiative power, polarization, propagation pattern etc.) and frequency. The link budget analysis is necessary to determine the available transmitted power which must be greater than the receive threshold for the receiver plus some margin. If the link is determined to be feasible, a reliability check is then performed to determine the uptime of the link, which is affected by environmental factors such as curvature of the earth, obstructions between the sites and Fresnel Zone clearance.

Generally, a line of sight (LOS) is required between the sites, and the earth's curvature is not usually taken into account for link lengths shorter than 10 km. The general formula for performing link budget analysis is provided below and for this project, it was determined that a link length of 16 km (10 mi) was sufficient to provide coverage. Figure 2.8 shows a profile of Corpus Christi Bay and the expected coverage, which is directly related to the horizontal beam width of the antenna and in turn is derived from the antenna radiation pattern.

$$A_{free} = 32.45 + 20\log_{10}(d) + 20\log_{10}(f) \quad (2.1)$$

$$RSL_{free} = (P_{TX} + G_{ANT}) - L_{loss} - A_{free} \quad (2.2)$$

$$\text{Thermal fade margin (dB)} = RSL_{free} - RTL \quad (2.3)$$

Thermal fade margin must be a positive value and a value ~10 dB is considered good for a feasible link where:

d (km) is the distance between the stations (link length)

f (MHz) is the frequency

A_{free} is free space attenuation (dB)

RSL_{free} is free space receive signal level

P_{TX} is transmitter power (dBm)

G_{ANT} sum of antenna gain for both transmit/receive

L_{loss} is the sum of all transmission losses (lines, connectors etc.)

RTL is receiver threshold level based on a minimum Bit Error Rate (BER)

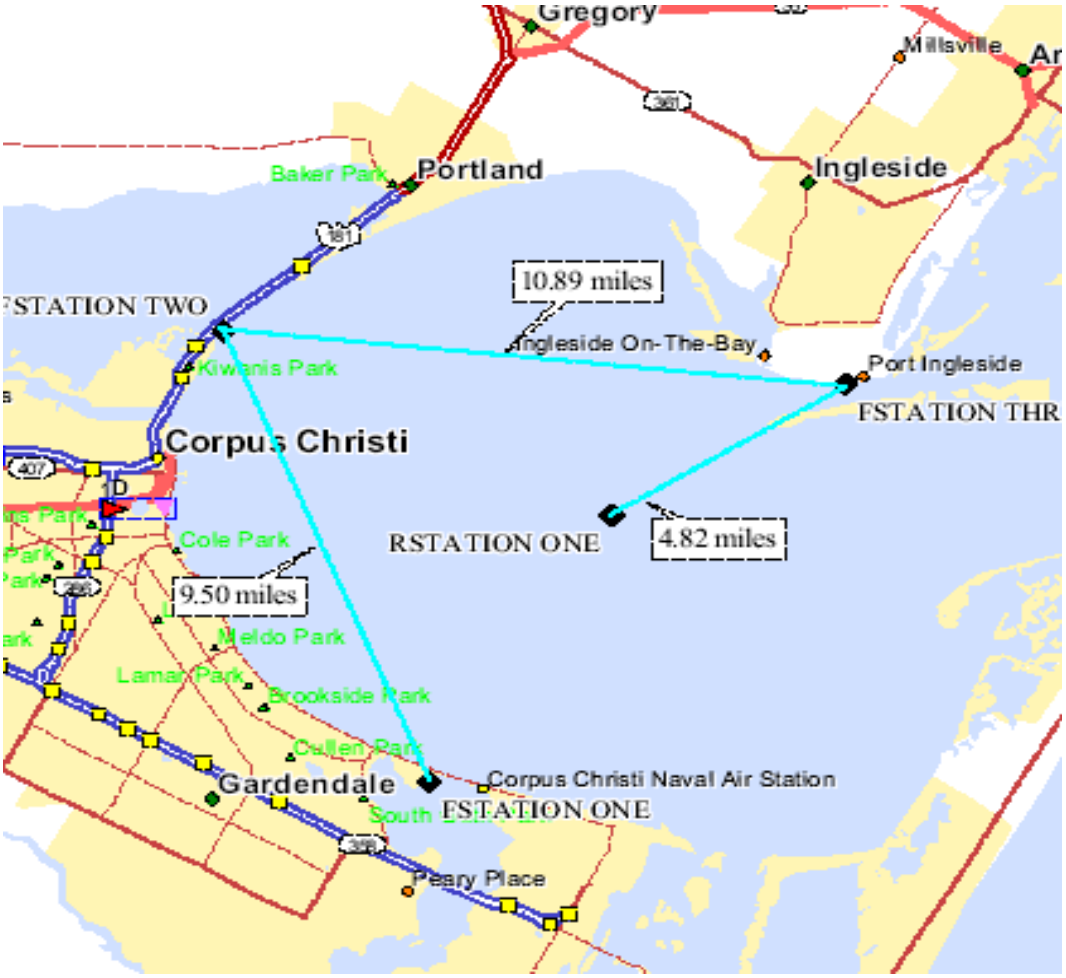

Figure 2.8. Map of coverage area.

Implementation

The novel scheme in this implementation is the ability of a shore-based Incident Command Center or stakeholder to observe in near real-time, data stream from a mobile sensing platform. In addition to data streaming, post-processed data available for display in near real-time through a web server was also investigated. The web server allows the user to run remote applications, which accepts the data stream as input. In this implementation, we were looking at DNS of constituents in surface waters, driven by data from radar surface current measurements, coupled with output from the mobile platform in an adaptive sampling framework (Thompson and Seber, 1996). Central to this is the Multi-parameter Instrument Array and Control System, MPIACS described in this section.

Data Acquisition Module

The Data Acquisition module consists of a drop down selector menu and 6 slider controls. The user selects the study area from the drop-down menu and a geo-referenced map outline of the study area is displayed in all the six panels. The expected maximum levels for each parameter to be measured are set using the six-slider controls. Based on these maximum values and a minimum value of zero, a simple algorithm is then used to scale the color-coded trace that is displayed on screen in the corresponding panel for each parameter.

Instrument Control Module

The Instrument Control module provides data communications with the instruments and consists of a set of 6 drop down selector menu. As many as 6 instruments can be interfaced through this module and depending on the instruments selected, a communications (COM) port is opened for data acquisition. Instrument specific settings are hard-coded in this implementation, but future enhancements will include a dialog box, which will allow the user to set or change instrument communication parameters such as baud rate, flow control etc. Once the individual instruments have been associated with a COM port, the "Connect" button at the bottom of the main panel is used to initiate communications and control with the instruments.

The two buttons labeled "Start" and "Stop" are then used to begin the data acquisition after all the required settings have been made. With the "Start" button, instrument data are parsed into variables corresponding to the parameter of interest. Each line of data from each instrument is location and time stamped through the GPS data, representing a sample point within the study area. This process is continuous and only terminates when the operator presses on the "Stop" button.

Data Post-Processing Module

Some instruments return raw data that need to be post-processed in order to obtain the actual measurements for a particular parameter. Instrument specific algorithms are used to convert the raw data for example, from calibration curves, or

other mathematical routines. Correction factors that may be needed are also included in these instrument modules. Following post-processing, the final instrument data are

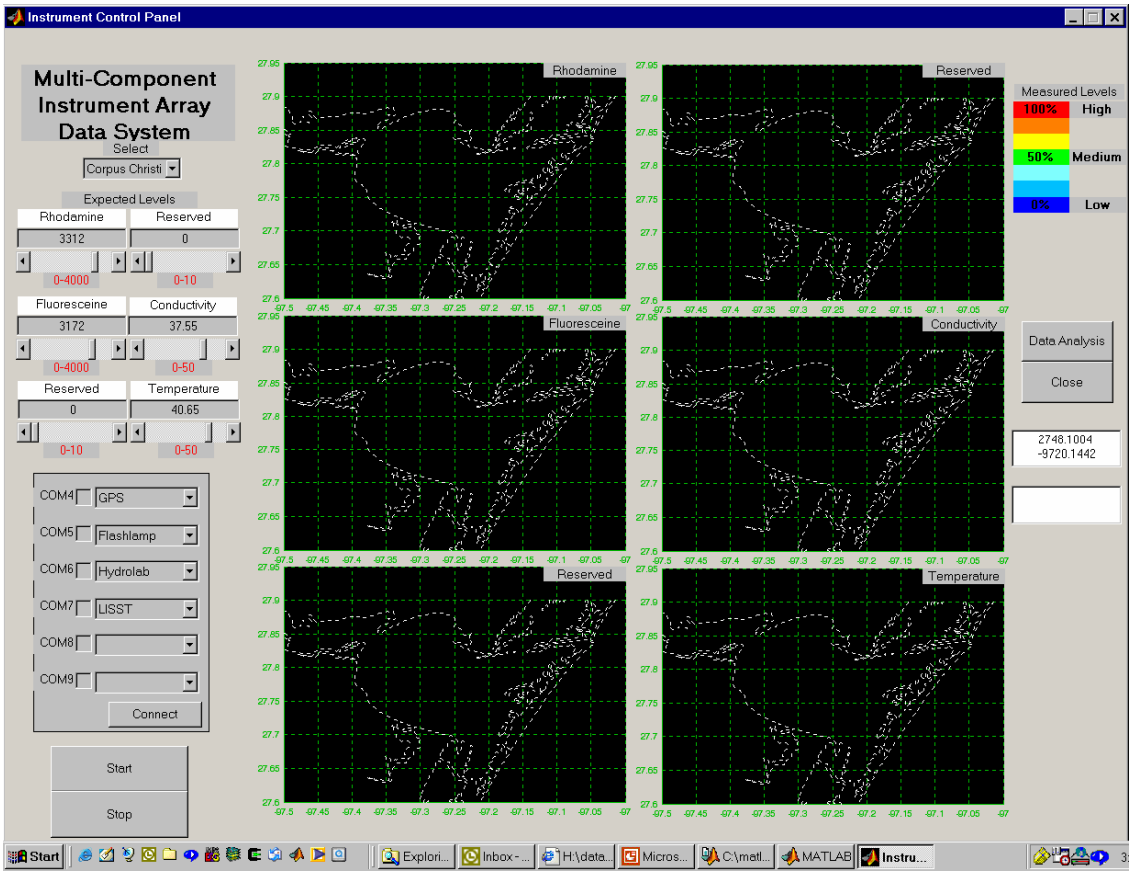

Figure 2.9. Data acquisition module with slider controls for setting instrument levels and drop down menu for selecting study area.

archived in plain ASCII tab delimited format. The instrument specific algorithms are individual modules that are called up depending on whether the instrument is included in the instrument array and connected using the Instrument Control module discussed above. It may be necessary in future enhancements, to come up with a database of such

instruments or users would have to write their own routines to accommodate sensors applicable to their deployment. The MPIACS user interface implementation is shown in Figure 2.9 comprising the individual modules described above.

Data Visualization Module

For each parameter, a percentage number variable (measured value against a pre-set peak value) generates a color trace corresponding with the horizontal travel of the instrument array through the water, giving a visual indication of the spatial distribution of relative intensity for the constituent of interest or sampled parameter. Each parameter's colored trace can be displayed in one of the six respective panels with the panels being expandable by a mouse click (for touch-screens, by touching) on any one of the six available panes. The expanded screen has infinite zoom levels and the operator can zoom in to any level of detail. The user returns to the main screen through the click of a button on the bottom of the expanded screen.

Data Archiving Module

This implementation of MPIACS includes a data archiving routine which allows for off-line analyses of the acquired data. The data files are time and location stamped and one data file is generated for each sensor in plain ASCII text, tab delimited format. This data format can be read into most spreadsheet or word-processing applications. Each data file contains metadata to allow sharing of data through the Internet and assuring quality of the data.

Results

Operational Tests

Prior to field deployment, two series of operational tests were performed for the IEOAS viz. bench tests and field tests, which were designed to test the individual modules as well as the entire system to identify parts that were in need of refinement or fine tuning. For instance, the field tests allowed independent assessment of the radio link for availability, bandwidth, throughput, reliability and range. The IEOAS could be implemented in two or three operational modes, in the final analysis, the choice would be dictated by such factors as reliability, interoperability, ease of use and rapid deployment. Most, if not all, background processes should be transparent to the user and requiring little user intervention allowing the operator to focus attention on the main tasks.

One particularly interesting mode of operation is that which allows direct streaming of data from the sensor array to the shore-based computer over a WAN with the instruments appearing to be directly connected to the shore-based computer through virtual COM ports provided by the device server to which the sensors are connected. This was made possible by TCP/IP addressing. The ship-based computer would then be freed up from the task of data post-processing and visualization and could be dedicated to other services such as navigation, communications and data archiving.

Information exchange takes place within the IEOAS through several means, paying particular attention to the native data format on the individual computers (remote or shore-based) and sensors within the network. Common data formats include ASCII

text files, streaming binary data, several flavors of image file formats (png, gif, jpeg etc.). The type of information made available in this implementation includes hydrodynamic, meteorological (wind speed, ambient temperature, weather forecasts), oceanographic (water temperature, salinity etc.), output from DNS and environmental measurements (concentration profiles). The data types are presented below.

- Directory Synchronization Process (DSP)
- Remote Access Process (RAP)
- Hydrodynamic data
- Trajectory predictions
- Meteorological information
- Forensics
- Navigational information (important for safety and post-cruise audits)
- Sampling transects

Partly, the software requirements consist of components that are integral to the computer operating system such as TCP/IP and Internet services and some third party products were used to bridge between the Integrated Data Acquisition Communications and Control (IDACC) unit and the various distributed services.

Bench Tests

The testing phase was implemented in stages, starting with the bench tests. The objective of the bench test was to run the distributed processes in real-time from the IDACC prior to field-testing and this allowed us to test the IEOAS while factoring out

performance issues related to the wireless telemetry part of the scheme (link reliability, quality, throughput, bandwidth). Bench tests include starting and stopping of remote applications and services, file management, data exchange and archiving. To facilitate the bench testing, the services listed in Table 2.1 implemented with each service running off a different computer at different locations within the IEOAS domain.

Table 2.1. Services implemented for IEOAS bench test.

Service	Description	Purpose
Hydrodynamics	Surface current measurements from radar	Near real-time data driven constituent transport model
Transport Model	Prediction of concentration profile of constituent, driven by real-time data	Provide visual indication of trajectory and extent of plume
Meteorological	Weather and other environmental variables (air/water temperature, tide etc.)	Provide information to vessel during sampling exercises
Data Acquisition	Environmental and oceanographic data from sensors	Provide actual measurements of constituent concentration and other environmental and oceanographic variables

For the bench test, the IDACC running the data acquisition service was connected to one end of a wireless radio link. Through the device server, the instruments were connected to the IDACC and with the GPS set in simulation mode, data acquisition was simulated using the MPIACS software application (Ojo et al., 2003b). This represents the part of the IEOAS on the geo-referenced mobile sensing platform. Another computer running the transport model was connected to the other end of the

radio link, representing the onshore end of the IEOAS. From the IDACC, the transport model was remotely executed using remote access process (RAP) as indicated in the preceding sections.

Through a combination of the RAP and the directory synchronizing process (DSP), the IEOAS allowed the implementation of a data-driven near real-time constituent transport model using surface current measurements from radar as input (Ojo and Bonner, 2002). Output from the model was made available to the rest of the IEOAS in near real-time using the directory synchronizing process and a web server implementation based on Apache (Thau, 1996). Remote applications service was provided using third party software (NetSupport Manager, © Productive Computer Insight, Ltd.). NetSupport Manager allowed a central command and control computer to implement file transfer between the distributed computers, broadcasting text and voice messages across the network, as well as running applications directly on remote computers.

Once a network connection had been established using TCP/IP via Ethernet, information exchange was facilitated in real-time through transferring of files using by Synchromagic (© GeloSoft, Inc.) based on DSP. The synchronizing process polls the remote or source directory at pre-defined intervals, triggered by a timer. The specified directory on the client computer is updated based on time-stamp, file size, and other file attributes that could be queried for file management normally set by the operating system. It is essential though for time-stamp query that the clocks on the various IEOAS components be synchronized. Once the files have been updated, the process initiates the

execution of the particular service for which the files or information are designated. For this bench test, the transport model requires updated surface current vector files, which are generated hourly by radar. The DSP updates the files for the transport modeling service at the end of which a model simulation run is triggered using the updated hydrodynamic data as input, while the IDACC continues to monitor all services at pre-defined intervals defined by the operator.

Field Test

The field test was designed to verify the radio telemetry link in terms of range, reliability, uptime, link quality, bandwidth and throughput under operational conditions. To achieve maximum coverage within the prototype bay (Corpus Christi Bay) it was determined that a 16 km (10 mi) link would be sufficient. The shore-based router was setup to use a 14-dBi sectoral antenna with a horizontal beam-width of 120º while the mobile sensing platform had a router setup with a 15-dBi omni-directional antenna with a 27º vertical beam-width mounted on a retractable mast. It was determined that this setup would maintain a good link under operational conditions including pitch, roll, and yaw as well as direction and speed changes of the vessel. Due to logistics, the test could not be performed at Corpus Christi Bay and so Lake Somerville in Central Texas about 200 km inland was selected. Lake Somerville is a man-made lake with a longitudinal extent of ~16 km (10 mi) which is ~100% of the maximum coverage expected at the prototype bay.

The link was setup with a fixed antenna height of 9 m (~30 ft) for the shore-based unit and variable height up to a maximum of 12 m (~40 ft) for the omni-directional antenna. The sectoral antenna had a 5º mechanical up-tilt to maintain line-of-sight LOS with the omni-directional. The antenna on the boat was mounted on a telescoping mast to allow for variable height and to ensure that the antenna could be brought down whenever the headroom requirements change such as passing under a bridge or in case of severe whether conditions.

During the link test, parameters were monitored and a maximum link of ~13 km (8 mi) at a maximum throughput of 11 Mbps was achieved. The link reliability was determined by monitoring for drops in the link during vessel movement and by how much the throughput changed depending on vessel heading.

Field Deployment

To date, three scheduled drills have been conducted; Galveston Bay, July 2002, Corpus Christi Bay, September 2002, Galveston Bay, May 2003. MPIACS allowed for real-time visualization of five parameters measured by three instruments. These include rhodamine and fluorescein concentrations from a multi-spectral fluorescence sensor (SAFire by WETLabs, Inc.), salinity and temperature from a CTD sensor (FastCAT by Sea-Bird Electronics) and total particle volume concentration from a particle size analyzer (LISST100 by Sequoia). The data was geo-referenced through a marine GPS unit (Furuno model GP-37).

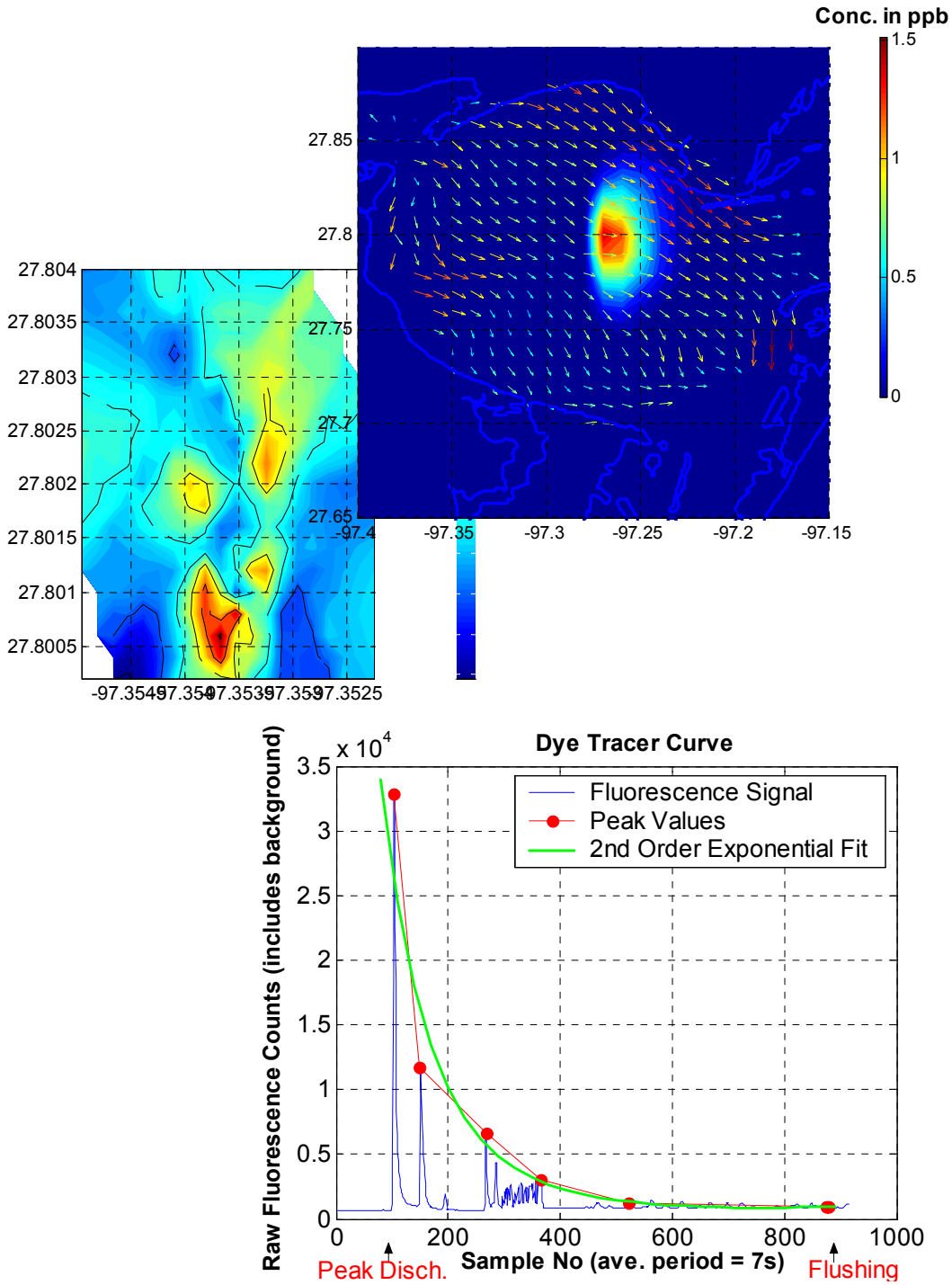

Figure 2.10. Typical output from IEOAS; contaminant plume trajectory simulation with current vectors overlay, concentration profile, and concentration-time plot.

In addition to these exercises, scientific experiments were also conducted with the system deployed during a series of dye-tracer experiments conducted in Corpus Christi Bay with the objective of validating numerical schemes developed for constituent transport and fate in surface waters.

Raw data was locally archived on the main computer by generating an ASCII text file for each sensor as well as the GPS unit. The data set was sent at pre-determined intervals by telemetry through a ship-to-shore wide area network (WAN). A shore-based computer at the Incident Command Center had a version of the MPIACS running on it and retraced the instrument color-coded tracklines in near-realtime. With a zero data dropout from the instrument array, the Incident Command computer was able to regenerate the tracklines without user intervention. A series of dye-tracer experiments were also conducted between summer and fall of 2003 including a profile of Corpus Christi Bay in July of 2003. Typical output and visualization screens from parts of the system are shown in Figure 2.10.

Discussion

Successfully designed and built a multi-sensor, multi-parameter rapid deployment instrument array for environmental and oceanographic assessments in surface waters using commercial-off-the-shelf (COTS) items. Central to the IEOAS is the IDACC, which provides the link between sub-surface instruments and onshore post-processing and archival services. The wireless telemetry link as tested provided a cost-effective implementation of Ethernet connectivity in a mobile marine environment.

Although designed for land-based connections, the routers were adapted and used in developing a portable easily deployable network for environmental monitoring. The results from field trials combined with the results from the bench tests show that the technology holds promise for environmental monitoring and emergency response in the marine environment.

The advantages of the IEOAS within the framework of environmental monitoring are summarized in this section.

- IEOAS is cost-effective built entirely using COTS devices and lends itself to rapid deployment in emergency response mode.
- Existing infrastructure can be interfaced directly with very little modification. New services can continue to run in their native format.
- Upgrades or changes can be made to one part of the system without reconfiguring the whole system. The system can be expanded without regard to memory or data storage capacity. Each service being independently optimized contributes resources into the pool including but not limited to memory, storage, CPU and data processing.
- Broadband connectivity gives the ability to transmit large sets of data with information exchange taking place over the network using TCP/IP (such as live video feeds or large image files) to shore-based units making information available to stakeholders in near real-time.

The system comprising both hardware and software modules have been deployed in Corpus Christi Bay and Galveston Bay, Texas for mock oil-spill response exercises

and used in a series of dye-tracer experiments in the summer and fall of 2003. The system can be readily deployed by a 3-man crew within a half-hour time frame on the mobile platform and it lends itself to transportability. The prototype unit particularly the IDACC is somewhat bulky and can be reduced in size and weight by specifying custom-built enclosures. Future enhancements would include an NMEA 2.0 interface to an autopilot unit, which accepts input from a waypoints module in the software interface for a full implementation of the adaptive sampling scheme.

CHAPTER III

STUDIES ON TURBULENT DIFFUSION PROCESSES AND EVALUATION OF DIFFUSIVITY VALUES FROM HYDRODYNAMIC OBSERVATIONS IN CORPUS CHRISTI BAY

Overview

Turbulent diffusion can be characterized by diffusion coefficients or turbulent diffusivity, $\boldsymbol{K_i}$ *(i = x, y, z)* dependent on the degree of randomness or turbulence intensity of the process measured through the velocity of the fluid particles. This study is an extension of Taylor's work to environmental field applications using the three-dimensional (3-D) currents field observed with a fast response current profiling instrument, as part of a series of diffusion experiments for Corpus Christi Bay, TX. The Lagrangian correlation function, $\boldsymbol{R_\tau}$ of the velocity time-series was used in the numerical evaluation of turbulent diffusivity values based on the observed current. The numerically determined diffusivity values were found to be in the range ($\sim 10^2$-10^4 cm^2/s) and in close agreement with those determined from observed concentration profiles of conservative tracer as well as those obtained using oceanic diffusion diagrams. Surface currents were obtained with HF Radar equipment deployed over the study area from which the horizontal velocity gradients were determined to be $\sim 10^{-4}$ s^{-1}. These low horizontal gradients allow for the generation of velocity time series from an ADCP mounted on a moving platform within the spatial scale of the experiment, which is of the order of 1000 m.

Introduction

Diffusion processes in surface waters are important as they govern the overall concentration distribution of constituents within the water body. These constituents range from naturally occurring material such as salinity, temperature, phytoplankton, and sediments through temperature, heat and other anthropogenic material from industrial and recreational activities. A concentration profile of these constituents can be developed through numerical models that rely on coefficients, which capture the physical phenomena that lead to spreading and movement, collectively termed transport coefficients. The coefficients may be determined through:

i) The evaluation of the temporal variation of the currents;

ii) The evaluation of the spatial variation of the velocity field;

iii) The evaluation of the first and second moments of concentration distribution of a constituent and,

iv) Inverse problem based on the advection-diffusion equation.

The first two methods are based on Taylor's work on the analysis of fluid flow through pipes (Taylor, 1954) and extended to other fluid flow regimes by Elder in his work on flow through open channels (Elder, 1958). There have been very few applications in the open waters typical of bays, estuaries and the coastal ocean but an example of the adaptation of this method to the open ocean was in a study conducted at the 106-Mile ocean disposal site (Paul et al., 1989). The authors are aware that this is the first attempt to directly apply this method in shallow waters using measurements taken with an

Acoustic Doppler Current Profiler (ADCP) within an Eulerian framework to evaluate turbulent diffusivities.

Turbulent diffusion in surface waters is analogous to molecular diffusion as a stochastic process (Taylor, 1920) and a coefficient of turbulent diffusivity or eddy diffusivity can be developed which will be found to be several orders of magnitude higher than molecular diffusivity values. In addition, constituent transport in the turbulent regime can be modeled as Fickian diffusion with constant coefficients, conditionally dependent on a Lagrangian time scale of turbulence.

This study is aimed at extending this concept into the area of environmental field applications with emphasis on the nearshore environment. The objectives of this study are: (1) to examine the error associated with the development of velocity time series from a spatial series generated from a moving platform; (2) to evaluate from the resulting currents, the time scale of the turbulent process and subsequently determine the eddy diffusivity for Corpus Christi Bay within an Eulerian framework. These diffusivity values will be compared with those obtained from dye-tracer concentration profiles as well as in the literature; (3) to develop a numerical scheme for the evaluation of turbulent diffusivity from observations of the 3-D current profile that can be applied at different spatial and temporal scales.

Part of our research focus is to develop an integrated system for environmental monitoring efforts within Corpus Christi Bay in particular and the Texas Gulf of Mexico region in general. The overall objective is to be able to completely characterize the area in terms of physical, bio-chemical, environmental and oceanographic parameters using

current state-of-the-art in *in situ* sensors and remote sensing. Currently, a system of High Frequency (HF) Radar has been deployed around the Texas Gulf of Mexico covering areas around Corpus Christi, Matagorda and Galveston Bay providing real-time surface current measurements (Kelly et al., 2004) and efforts are underway to expand the capability for response to episodic events (Kelly et al., 2002; Ojo and Bonner, 2002; Ojo et al., 2003a).

A system of fixed and mobile platforms complement the radar system using *in situ* instrumentation, which provide environmental measurements from within the study area, variables that can be assimilated into numerical schemes operating in a predictive mode (Ojo et al., 2003b; Ojo et al., 2003c) within the framework of environmental and oceanographic assessments. The integrated scheme combining these real-time measurements with numerical transport modeling (Sterling et al., 2004a; Sterling et al., 2004b) needs to be effectively characterized and parameterized (Ernest et al., 1991; Lee et al., 2000) in order to be fully operational. This work is important for the parameterization under different meteorological, oceanographic and geomorphologic regimes, of the diffusive component of the resulting constituent transport model and the methodology for achieving this objective was developed through this study.

Turbulent Diffusivity

A method of obtaining turbulent diffusivity values from the direct observation of currents in surface waters was developed as part of this study against the backdrop of

constituent transport modeling within a body of water, by relating the statistical process of diffusion to a diffusion coefficient, K given below:

$$d\sigma^2/dt = 2K$$

$$d\sigma^2/dt = 2\overline{u'^2}\int_0^t R(\tau)d\tau \qquad (3.1a)$$

$$R(\tau) = \frac{\overline{u'(t)u'(t+\tau)}}{\overline{u'(t)^2}}$$

where σ^2 is the variance of a cloud of diffusing particles, τ is a lag time between successive observations of the velocity, u of a fluid particle and $\overline{u'^2}$ is the mean-square of the velocity fluctuation of fluid particles in random motion and relates to the degree of randomness or turbulence intensity. Taylor adopted a Lagrangian correlation coefficient, R of the form $e^{-\tau/T_L}$ from which an expression for K can be derived using (3.1a) where T_L is the integral time scale of diffusion. For times when $\tau \gg T_L$, it follows that the diffusing cloud grows at a constant rate with diffusivity given by:

$$K = \overline{u'^2}\int_0^t R(\tau)d\tau \qquad (3.1b)$$

The time, T_L, which can be determined from the area under the R curve, is regarded as the 'persistence time' of the particle velocities after which the particles have

lost all memory of their initial velocities. With respect to a set of coordinate axes and in terms of the respective time scale, T_i,

$$K_i = \overline{u_i'^2} T_i$$

$$T_i = \int_0^t R_i(\tau) d\tau \qquad (3.2)$$

$$u_i(t) = \overline{u_i(t)} + u_i'(t)$$

for $i = x, y, z$ corresponding to the coordinate axes. The quantity $u_i'(t)$ is the i^{th} component measured at time t, of the Lagrangian velocity fluctuation around a supposedly steady mean velocity, $\overline{u_i(t)}$ of a tagged particle experiencing turbulence in a fluid, and τ [0 ∞] is a lag time for the ensemble of velocity measurements.

This introduces the following concepts:

a) Turbulence intensity given by $\overline{u_i'^2}$;

b) Characteristic velocity given by $\sqrt{\overline{u_i'^2}}$, the rms of the velocity fluctuations and

c) Gustiness given by $\sqrt{\overline{u_i'^2}} \Big/ \overline{u_i}$

the overbar indicating an ensemble mean of realizations u_i of the velocity components over a period of time, with $R_i(0) = 1.0$ and $R_i(\infty) = 0$. This implies that R_i is bounded and at large enough times, there is an asymptotic convergence of turbulent diffusivity values

following which the diffusive component of the transport model can be modeled as a Fickian diffusion process. Several models have been proposed for R_i by researchers to describe specific flow regimes (Frenkiel, 1953) including the simple exponential form used by Taylor in his classical work on turbulence. This allows for the integral in (3.2) to be performed leading to the evaluation of K_i if the mean of the flow velocity, u_i is known. In oscillating flows commonly experienced in tidal or wind-driven bays and estuaries, u_i can be evaluated using a running average over a suitably large number of ensembles.

Certain requirements for $R_i(\tau)$ are imperative in order to find analytical forms for K_i but in complex flow regimes typical of bays and estuaries within temporal scales of the order of minutes and spatial scales of the order of a few thousand meters, the difficulty lies with finding the Lagrangian values in equation (3.2) from the Eulerian statistics that current meter measurements would typically return. In the work of Paul et al., long-term current meter readings were used in estimation of the dispersion of waste sludge under high- and low-turbulence conditions on a spatial scale of the order of 100 km and temporal scales of the order of 100 days.

By obtaining the probability distribution of the velocity measurements along independent coordinate axes, the variance-covariance property of the distribution was used based on the assumption that the averaged mass-distribution of a constituent would be described as a multiple of the velocity distribution. In related work, (O'Connor et al., 1985) the turbulent process in open waters was categorized using three broad classifications viz. small, intermediate and large.

- Small Scale -- temporal scale < 24 h, spatial scale between 0-10 km.
- Intermediate Scale -- temporal scale between 1-100 days, spatial scale between 10-300 km.
- Large Scale -- Temporal scale > 100 days, encompassing the ocean basin.

This study is restricted to small-scale processes where tidal and inertial motions are considered advective and the velocity fluctuations about the tidal mean are responsible for diffusion or turbulent mixing. This is in contrast to intermediate and large-scale processes where the tidal and inertial currents will be considered diffusive. This scale dependence of the turbulent diffusion process was compiled into a set of oceanic diffusion diagrams (Okubo, 1971) based on data obtained for the open ocean, which may not find much applicability within the coastal and nearshore environments. In light of this, similar diffusion diagrams are needed specifically for the coastal ocean but data on the diffusive process within these areas will have to be developed.

A series of dye experiments conducted in the Baltic (Schott, 1978) using a set of vector-averaging current meters (VACM) extended previous studies in meteorological applications (Hay and Pasquill, 1959) to the oceanographic field. These two studies investigated the relationship between the Lagrangian and Eulerian statistics through a scaling of the time axis for $R_i(\tau)$. The relation equivalent to (3.2) is:

$$K_i = \beta \overline{u_i'^2} \int_0^t R_i(\beta\tau) d\tau \qquad (3.3)$$

The empirical coefficient β serves the purpose of preserving the shape of the autocorrelation and ranges in value between 1-4. A value of ~4 was found to give adequate results for meteorological applications with no specific prescription for oceanographic applications. It is hypothesized here that the value of β is dependent on the method by which the currents field is measured, which in turn is determined by the type of instrumentation.

Bowden-Fairbairn deployed two fast response current meters that were capable of responding to fluctuations with a period of ~2 s (Bowden and Fairbairn, 1952) in the Mersey Estuary (Great Britain) from which they were able to directly obtain the values of $R_i(\tau)$. Bowden and Howe used the same approach within the same study area but using an electromagnetic flowmeter that could sample fluctuations with periods ~1 s (Bowden and Howe, 1963). By comparison, the VACM used by Schott averaged currents over a period of 112 s and it is possible, with the higher sampling frequency used by Bowden et al. for the direct application of (3.2) which is equivalent to setting β = 1 in equation (3.3).

Our approach is similar to that used by Bowden et al. using a fast response current profiler and direct numerical analysis of the velocity time series for the evaluation of $R_i(\tau)$ through discretized forms of equations (3.1) and (3.2). The current profiler employed was capable of sampling with a period ~0.5 s returning measurements that allowed for the direct application of (3.2).

Noting that linear growth is a necessary but not a sufficient condition for equation (3.2) to be applicable within the context of the governing equations of transport (Fischer et al., 1979) an integral length scale l_i could be defined as follows:

$$l_i^2 = \overline{u_i'^2} T_i^2 \tag{3.4}$$

This length scale then is the distance that a fluid particle must traverse before it loses memory of its initial velocity. This establishes scale-dependence for turbulent diffusion, which ranges from microseconds for Brownian motion through 0.1 s for laboratory-scale turbulence to 100 s for atmospheric applications. This is important in the sense that the process of turbulent diffusion can be characterized by a length scale that depends on a characteristic velocity and a time-scale which in turn depends on the asymptotic property of the velocity autocorrelation function. Stated differently,

$$d\sigma_i^2 / dt = 2K_i = 2\overline{u_i'^2} T_i \tag{3.5}$$

and for K_i = constant

$$\sigma_i^2 = 2\overline{u_i'^2} T_i^2 = 2l_i^2 \tag{3.6}$$

If L_i^2 represents the size of the diffusing cloud of particles along a particular coordinate axis, then the turbulent diffusion process can be modeled as Fickian diffusion with a constant diffusivity, K_i in the regime where the cloud size is much larger than the length scale of the turbulence i.e.:

$$L_i^2 \gg 2l_i^2 \tag{3.7}$$

Methods and Materials

The study was conducted as part of a series of dye-tracer experiments conducted within Corpus Christi Bay through the summer and winter of 2003. The analyses given in the preceding sections were applied to Corpus Christi Bay for the characterization of the turbulent diffusion process using the velocity autocorrelation derived from 3-D current measurements.

This section reviews some analytical forms of the autocorrelation function and examines the errors that may result from the development of a velocity time series using an ADCP mounted on a moving platform. The generation of velocity autocorrelation, and subsequently the evaluation of turbulent diffusivity using the velocity history of fluid elements are described. The condition for the application of Fickian diffusion dependent on T_i was determined for the selected bay, presented in the form of a vertical profile of the K_i values.

Summary of the three studies conducted are given below. For reference purposes identification numbers have been assigned to each study. Two studies were conducted on

August 28, 2003 at two different locations and at different times within the tidal cycle. A third study was conducted on October 7, 2003 at the first location but at a time within the tidal cycle different from the time of the first study conducted at that location. This experimental design was for the purpose of elucidating information relating to the hypothesis on spatial-temporal variability of diffusivity values due to the coupling between meteorological conditions and oceanographic forcing within the study area. Table 1.2 gives a summary of the study sites, experimental and meteorological conditions.

Review of Analytical Models of Velocity Autocorrelation Function, ACF

If the turbulence is a stationary stochastic process with no organized flow structures (which will be typical of wind-driven shallow bays and estuaries), then $R_i(\tau)$ should be independent of time, and be an even function whose integral given by (3.2) is bounded and well defined (as $\tau \rightarrow \infty$). The behavior and suitability of four different analytical models of $R_i(\tau)$ are summarized in Table 3.1 and serves as backdrop for the numerical approach used in this study especially in reference to the time-scale from which the turbulent eddy diffusivity can be derived. Four models have been selected in this study. The basic exponential form put forward by Taylor (T), two sets F1 and F2 (Frenkiel, 1953) and the fourth, ATG (Altinsoy and Tugrul, 2002).

Table 3.1. Various models proposed for the analytical evaluation of R_L. T -- Taylor (1921); F1 and F2 -- Frenkiel (1953); ATG -- Altinsoy and Tuğrul (2002).

Model		Computed T_L	
		$T_L = 10$	$T_L = 100$
T (Taylor)	$R_L(\tau) = \exp\left[-\tau/T_L\right]$	10.00	99.99
F1 (Frenkiel)	$R_L(\tau) = \exp\left[-\tau/2T_L\right]\cos\left[\tau/2T_L\right]$	9.92	99.16
F2 (Frenkiel)	$R_L(\tau) = \exp\left[-\pi\tau^2/4T_L^2\right]$	10.00	100.00
ATG (Altinsoy & Tugrul)	$R_L(\tau) = \exp\left[-\pi\tau^2/8T_L^2\right]\cos\left[\tau^2/2T_L^2\right]$	9.99	99.96

Figure 3.1 and Table 3.1 present the forms for the autocorrelation function. Figure 3.1a shows each of the four models (T, F1, F2, ATG) of $R_L(\tau)$ with $T_L = 10$ s while Figure 3.1b is the same plot but with $T_L = 100$ s. Note that from (3.2) and (3.4), T_L is the area under each curve and the numerically computed values are given for each of the models in Table 3.1. These models will subsequently be compared with the numerically computed R_i values from direct observations of current fluctuations. Note that the first model prescribed by Taylor and the second one from Frenkiel appear to be more suitable whereas the first model by Frenkiel and that proposed by Altinsoy and Tuğrul appear to produce undesirable negative effects. A more in-depth study of the behavior of $R_i(\tau)$ for all four models was carried out (Manomaiphiboon and Russell, 2003) against certain prescribed requirements (Pope, 2000) for turbulent flows.

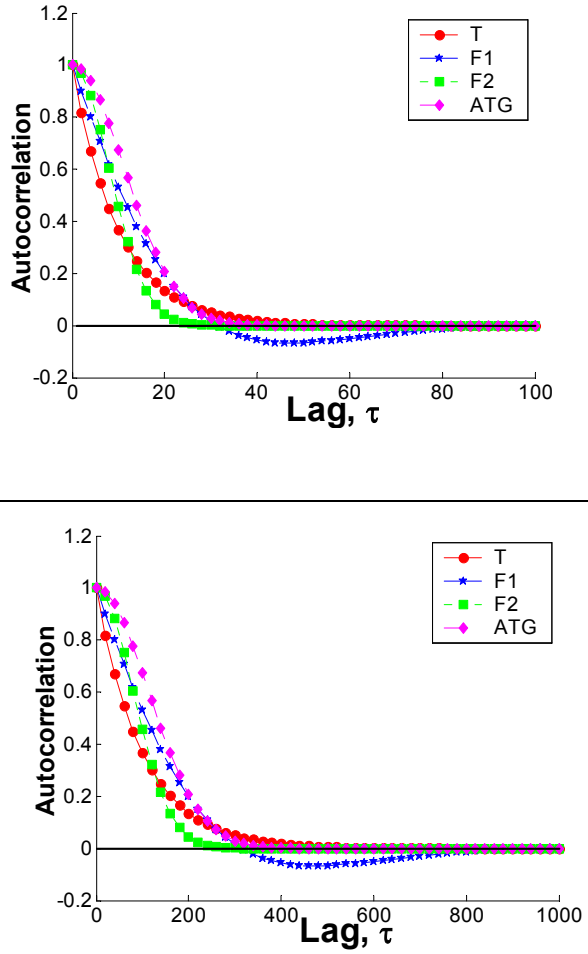

Figure 3.1. Analytical forms of $R_i(\tau)$ proposed by several researchers for T_c = 10 (upper panel) and T_c = 100 (lower panel) . —●— T; —*— F1; —■— F2; —◊— ATG.

Time Series Generation from Spatial Series of Velocities Taken from a Moving Platform

Suppose the first measurement was taken at time t_0 at position P_1 and given a uniform velocity gradient S ($S = \frac{\delta u}{\delta x}$) within the sampling area.

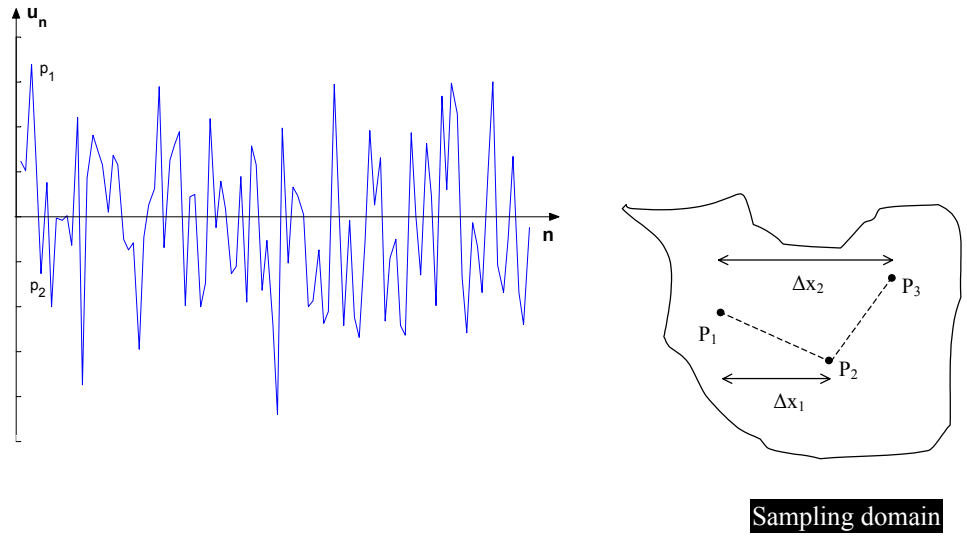

Figure 3.2. Illustration of sampling scheme and spatial series of current measurements generated from ADCP mounted on a moving platform.

At time t_1,

$$u_{P_2} = u_{P_1} + S \cdot \Delta x_1$$

At time t_2,

$$u_{P_3} = u_{P_1} + S \cdot \Delta x_1 + S \cdot \Delta x_2$$

At time t_3,

$$u_{P_4} = u_{P_1} + S \cdot \Delta x_1 + S \cdot \Delta x_2 + S \cdot \Delta x_3$$

At time t_{n-1},

$$u_{P_n} = u_{P_1} + S \cdot \left(\Delta x_1 + \Delta x_2 + \ldots + \Delta x_{n-1}\right) \tag{3.8}$$

$$u_{P_n} = u_{P_1} + S \cdot \sum_{1}^{n} \Delta x_{n-1} \tag{3.9}$$

Δx_{n-1} being the separation between sample points P_1 and P_n within the sampling domain where u_{P_1} and u_{P_n} are the measurements taken at the respective points, the time t_{n-1} (= $n.T_s$), being the time the n^{th} sample was obtained given that T_s is the instrument dependent sample period. Equation (3.9) could be written as follows:

$$u_{P_1} = u_{P_n} + \vartheta \tag{3.10}$$

where ϑ $(= S \cdot \sum_{1}^{n} \Delta x_{n-1})$ is an error term associated with the sampling scheme and derives from the spatial displacement of the instrument platform from point P_1. Hence, at sample point P_1 the time series of measurements is given by the spatial series of velocity measurements that includes an error term in addition to the instrument error. Equation (3.10) is rewritten for point P_1 as a time series dependent on ADCP measurements (u_{adcp}) as follows:

$$u(t) = u_{adcp} + \vartheta \tag{3.11}$$

Let $\Delta x_{n-1} = X_N$ (X_N being the position of sample point P_n in relative coordinates to point P_1, $N = 0,1,\ldots,n\text{-}1$) then,

$$\sum_{1}^{n} \Delta x_{n-1} = \sum_{0}^{N} X_N = n \cdot \overline{X} \tag{3.12}$$

$\overline{X}$ is the average displacement of the instrument platform relative to P_1 after n samples. equation (3.11) then becomes:

$$u(t) = u_{adcp} + n \cdot S \cdot \overline{X} \tag{3.13}$$

For transects made up of monotonically increasing set of sampling points, $\overline{X} = X_N/2 = \alpha \cdot (n-1) \cdot T_s/2$ (α being the travel speed of the moving platform). The time series representation from the spatial series would therefore appear to increase in error as the square of the number of samples with the error given by

$$\vartheta = \alpha \cdot n(n-1) \cdot S \cdot T_s/2 \tag{3.14}$$

By creating a running average of the n samples, the time series at point P_1 becomes:

$$u(t) = \overline{u}_{adcp} + S \cdot \overline{X} \tag{3.15}$$

and the associated error is given by $\vartheta = \alpha \cdot (n-1) \cdot S \cdot T_s/2$, a linear dependence on the number of samples.

Instrumentation and Data Acquisition

3-D current profiles of the bay were obtained using a fast response 1200 kHz broadband workhorse Acoustic Doppler Current Profiler, ADCP (RD Instruments, Inc., San Diego, CA, USA) installed on a rigid mount on the bow of a 10 m small-watercraft. Additional instrumentation was mounted on a separate tow-body capable of undulating through the water column while simultaneously performing horizontal profiling. These were comprised of a SAFIRE multi-spectral fluorometer (WET Labs, Inc., Philomath, OR, USA) for obtaining the concentration distribution of the dye, a CTD (conductivity-temperature-depth) sensor for basic water parameters (Sea-Bird Electronics, Inc., Bellevue, WA, USA), and a LISST-100 (Laser *In situ* Scattering and Transmissometry, type 100) particle size analyzer for particle size distribution measurements (Sequoia Scientific, Inc., Bellevue, WA, USA).

Data logging was carried out on-board the craft with an integrated data acquisition (DAQ) computer incorporating a GPS unit. The bottom-tracking capability of the ADCP allowed for absolute current measurements to be taken on a moving platform by taking into account the velocity of the moving platform and was set to sample at a rate of 2.5 Hz. The current profiles were obtained within a 300-500 m radius dictated by the spatial extent of the dye patch and velocity time series were generated over a period between 120-150 minutes. The profile was well localized both temporally and spatially enough to filter out horizontal variations in current structure and the effects of tides.

Surface currents and horizontal shear were obtained from HF Radar (Seasonde™ by CODAR Ocean Sensors, Inc.) operated as part of our coastal environmental field facility and permanently deployed in Corpus Christi Bay. It operates on the principle of Bragg Scattering of high frequency (HF) electromagnetic waves incident on surface waves (Barrick et al., 1977). The Doppler shift between transmitted and returning waves provides a measure of the speed of the surface wave with the transmitted and reflected waves also providing a means of georeferencing the resulting currents over the entire spatial domain. The Seasonde has a spatial resolution of about 1km with a range of 50-70 km allowing for horizontal surface current mapping over the domain of observation.

Data Analysis

Data post-processing and analysis were performed with the Signal Processing Toolbox in MATLAB® and a set of routines that were developed in our laboratory. The ADCP collects bottom-tracking data simultaneous with the current measurements and this was used in compensating for the motion of the instrument platform as well as subsequent referencing to geographic coordinates. Spectral analysis was subsequently performed on the velocity time-series using Welch periodogram method to get the frequency signature of the ADCP data. Following this, a low-pass filter was applied to the velocity signal, the size of the filter determined based upon the observed frequency spectrum. Application of the filter serves to remove systemic noise from the observed signal, thereby isolating the current fluctuations.

For each coordinate axis, the result was an N x 30 matrix of velocities in 30 equally spaced vertical bins through the water column with N, the size of the samples dependent on the duration of the exercise and instrument sampling rate. These were numerically analyzed using the cross-correlation function in the signal processing toolbox with different values of lag τ (in seconds) to obtain the velocity autocorrelation $R_i(\tau)$ in three absolute coordinate axes x, y, z respectively. A suitable value of τ was found by inspecting the properties of $R_i(\tau)$ for convergence and non-negativity as discussed in preceding section. The $R_i(\tau)$ values were then used in the numerical evaluation of T_i and turbulent diffusivity values, K_i ($i = x, y, z$) using (3.2), the numerical integration performed using the trapezoidal method.

The horizontal shear structure was obtained from the velocity gradients using the 2-D currents from HF radar. The currents were resolved into components along each of the x,y-coordinate axis following which the shear structure was determined. The resulting shear structure was subsequently used in equation (3.15) along with the velocity series from ADCP to evaluate the error associated with generating velocity time series from a moving platform.

Site Description

The study sites for the field data acquisition were located within Corpus Christi Bay as described in Chapter I and illustrated in Figure 1.2 while Table 1.2 summarizes the meteorological and oceanographic conditions that are depicted graphically in Figures 1.3 and 1.4 respectively.

Results

The results of numerically evaluating turbulent diffusivity from direct observations of the 3-D currents field are presented in this section. The findings are compared with previous work using similar numerical approach and those using analytical techniques. From the three studies, velocity time-series measurements were obtained during each exercise along with fluorescence and CTD data.

Velocity Time Series from a Moving Platform – Error Analysis

Within the sampling domain the horizontal velocity gradient, S were derived from data obtained through surface current mapping using high frequency (HF) radar deployed over the study area by our research staff. S has a maximum value ~ $6x10^{-4}$ s^{-1} occurring along the x-coordinate direction and these gradients are represented in the contour plot of Figure 3.3 derived for the instance when the gradients were at a maximum. As would be expected for surface waters, these gradients are relatively low with the highest values occurring around the shoreline and around regions of high flow.

Given transects made up of n = 1 to 100 samples with T_s = 0.39 s, and α = 2.2 m/s, and using the maximum value of S the error associated with the sampling scheme will have the values represented in Figure 3.4. From the foregoing analyses for a monotonically increasing transect set although averaging reduces the error significantly, it appears that there can still an unacceptable amount of error in the resultant time series of velocities generated from a moving platform (Figure 3.4).

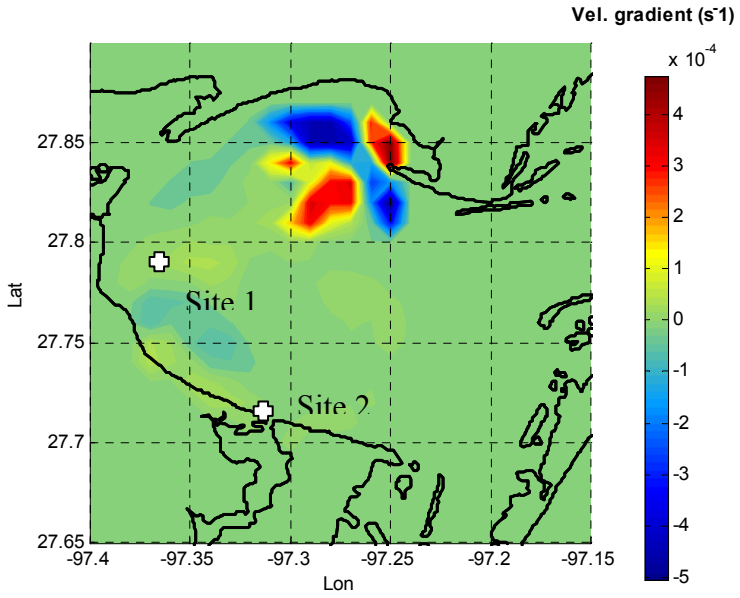

Figure 3.3. Horizontal velocity gradients from surface current mapping of the study area at the instant when gradients were at a maximum. The shear structure was determined from HF radar surface current mapping. Approximate location of the 2 study sites is indicated. These sites are in the region marked by very weak horizontal shear.

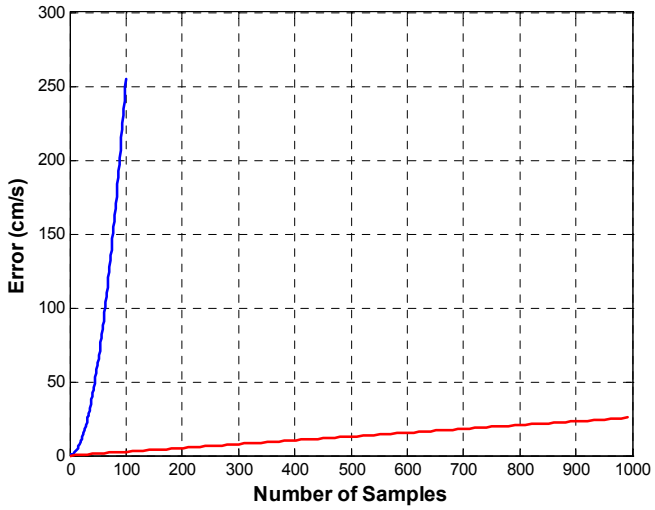

Figure 3.4. Errors resulting from velocity time series generated from spatial series evaluated against number of samples in series. The error increases as the square of number of samples for monotically increasing transect design while the relationship is linear based on a running average of the transect set.

For instance, averaging over 1000 samples produces an error of ~25 cm/s while averaging over 100 samples would produce an error of ~2.5 cm/s, a 10-fold reduction. Hence, for these types of transect design, the number of samples would have to be kept small enough to achieve acceptable error levels.

Another type of transect design like the one used in this study, which is not monotonically increasing but made up of a normally distributed set of points is examined. The normal probability plots for this (typical) distribution of sampling points within the domain (Figure 3.5) reveals the characteristics of the distribution in comparison with a plot (straight line in the figure) from the ideal normal distribution. As seen from the plot, the distribution exhibits linearity between the 1st and 3rd quartiles indicating that the distribution is indeed normal. The mean (50th percentile) of the sampling points (in relative coordinates) $\overline{X}$ = 0 cm and the standard deviation falls within the range 250-350 m.

The fact that this distribution is normal is largely due to the large number of samples taken, a condition that must be met in order for a distribution to exhibit characteristics of a normal distribution. One may be tempted to then apply equation (3.13) directly for generating the time series since the zero mean $\overline{X}$ effectively eliminates the sampling error. Equation (3.15), which is a running average of the spatial series however allows for using fewer number of sample points and is the preferred method for error reduction as there is no direct dependence on the number of samples when compared to equation (3.13). There is of course an indirect dependence on the number of samples even with the application of equation (3.15) noting that fewer sample

points imply a departure from a normal distribution. It can be argued though that $\overline{X}$ would still be small enough (~0 cm) such that in combination with the low value of the horizontal gradient *S* therefore, effectively eliminates the sampling error.

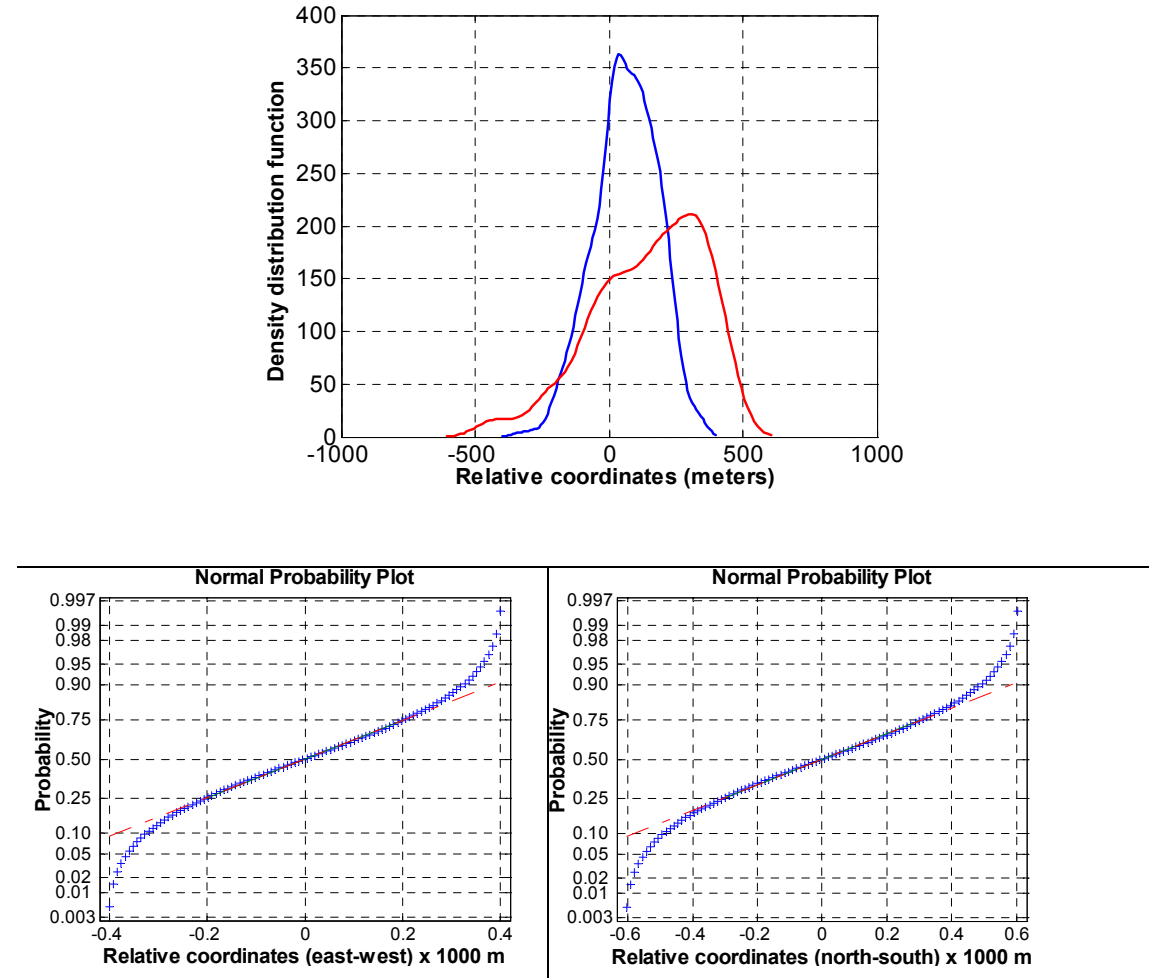

Figure 3.5. Top panel; distribution of sampling points in relative coordinates in both east-west (blue) and north south (red) directions. Bottom; normal probability plot. Left is for east-west and right is for the north-south distribution of (relative coordinates) of the sampling points plotted in blue. The red line is the straight-line plot from the ideal normal distribution.

It is imperative to note that filtering the spatial series eliminates instrument errors as well but the number of samples required for the running average and hence the filter size is increased to accommodate the additional error inherent in the sampling scheme. For comparison, whereas 10 samples may have been adequate to reduce instrument error by one-third, this number of samples will not be sufficient to produce a distribution that approximates a normal distribution. Increasing this sample size to 100 would produce a better approximation resulting in a 10-fold reduction in instrument error while at the same time reducing the error due to the sampling scheme.

A time series can therefore be produced from a spatial series by careful design of the sampling transects and subsequent application of a suitable filter to the spatial series. The transect should not be composed of monotonically increasing sampling points and ideally the distribution of sampling points should approximate a normal distribution with the mean (in relative coordinates) approaching zero. Typical time series of the horizontal and vertical velocity components u_i ($i = x, y, z$) corresponding to the East-West, North-South, Up-Down coordinate axes are shown in Figure 3.6. In Figure 3.7 typical results from the numerical computations of the autocorrelation function are presented along with the analytical model of the autocorrelation function F2.

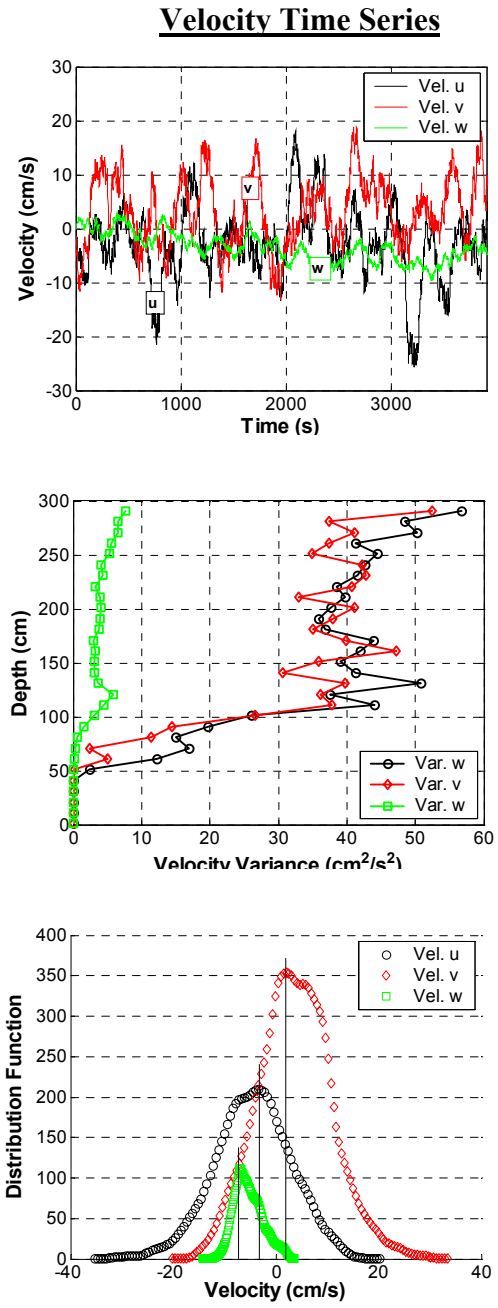

Figure 3.6. Top, typical time series of velocity fluctuations along *x, y, z* coordinate axes respectively; middle, corresponding depth profile of average velocity variance; bottom, corresponding velocity distribution function.

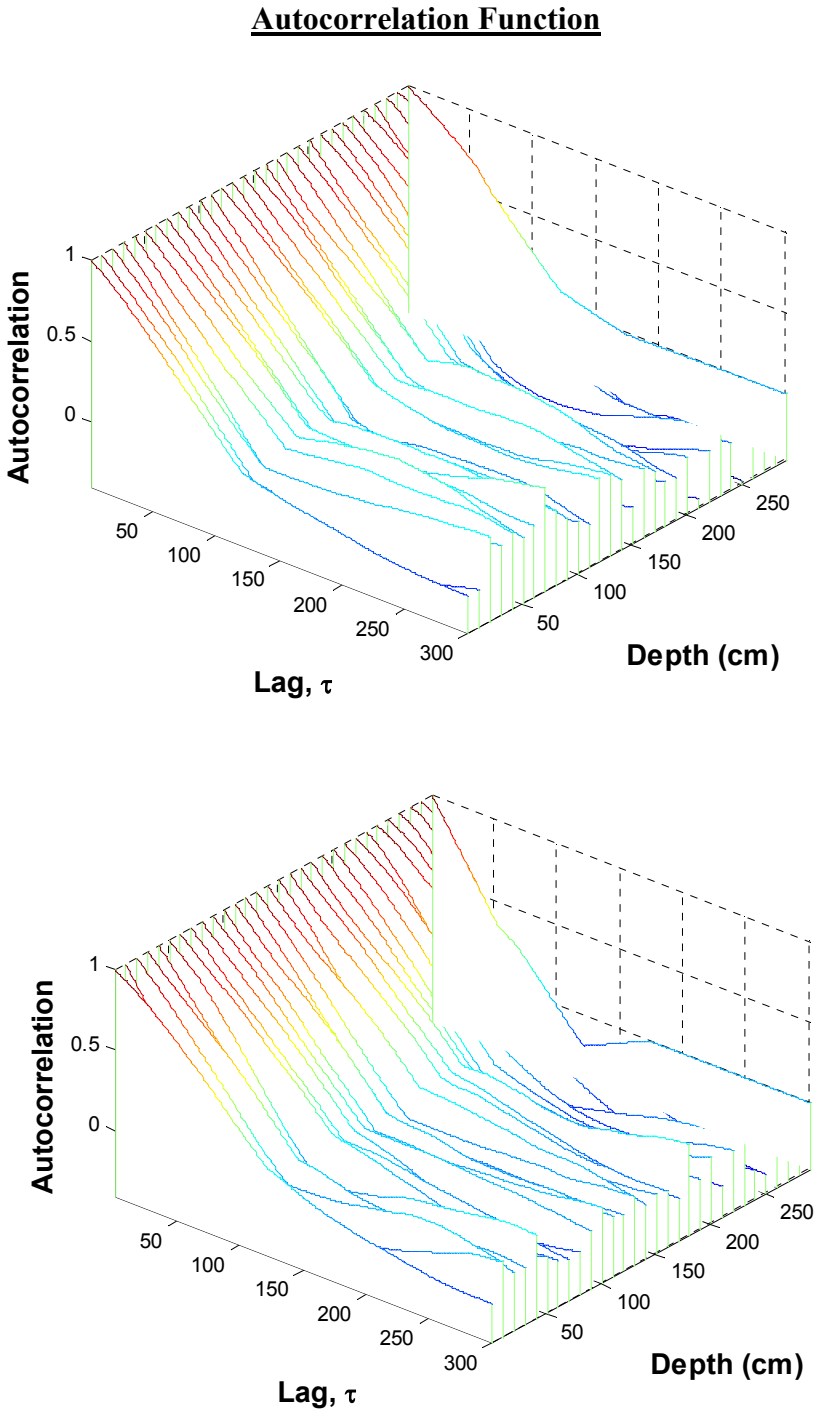

Figure 3.7. From top to bottom, Lagrangian (scaled) velocity autocorrelation function derived from velocity time series along *x, y,* coordinate axes respectively (similar for the *z*-axes).

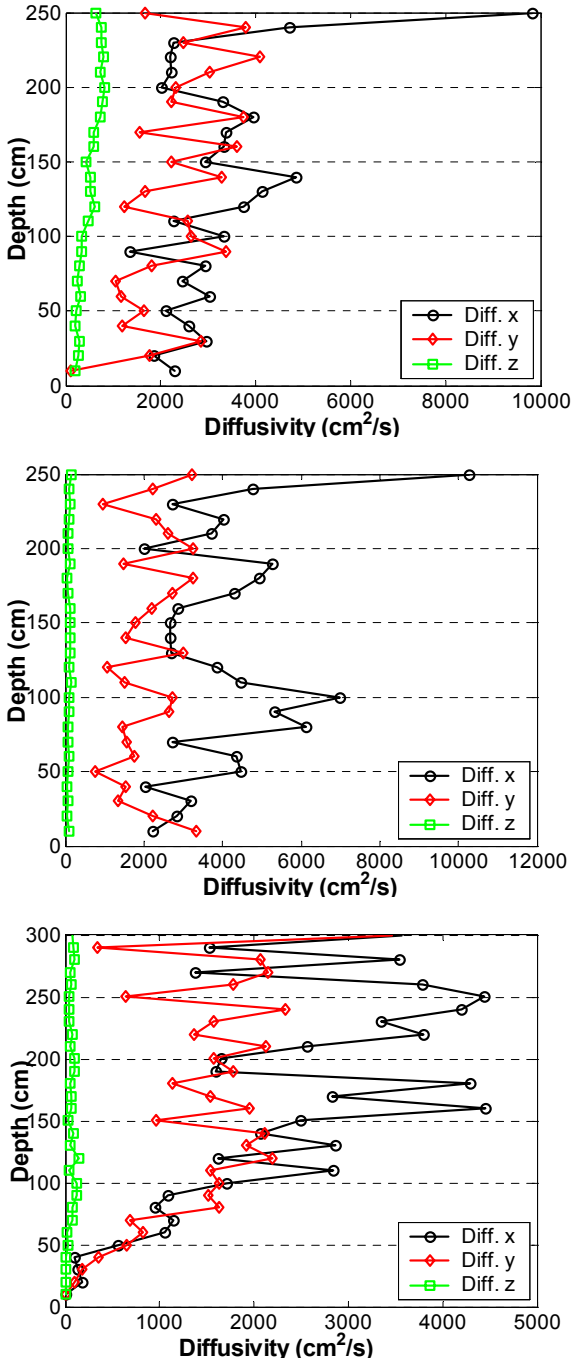

Figure 3.8. From top to bottom; depth profile of turbulent diffusivity for each of the three studies. Top, study 0828_1; middle, study 0828_2; bottom, study 1007. Open circle (—○—), *x*-coordinate; diamond (----◊---), *y*-coordinate; open squares (---□---), *z*-coordinate.

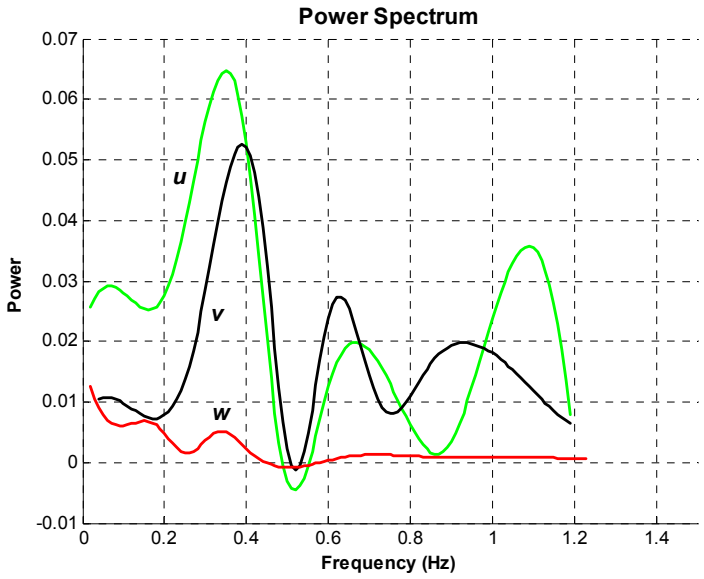

Figure 3.9. Typical frequency spectrum of velocity time series up to the Nyquist frequency. Identified ~3 s period events (corresponding to ~ 10 ensembles) used in sizing low-pass filter for noise and error reduction.

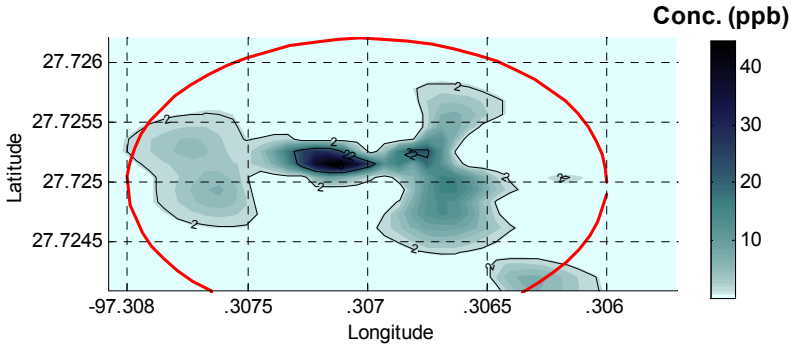

Figure 3.10. Observed dye patch from study 0828_2, 6202 s after instantaneous release. Outlined (- - -) is the 68% numerical estimate of spread within 2σ based on computed turbulent parameters (K_x = 1.03 x 10^4, K_y = 0.33 x 10^4).

Computed diffusivities are shown in Figure 3.8 while the power spectrum of a typical velocity time series is shown in Figure 3.9, the main events identified with a period of ~3 s (close to the observed wave pattern) corresponding to ~10 ensembles based on a sampling period of 0.39 s. It is imperative to note that the error reduction resulting from averaging of the time-series using a low-pass filter with a window size corresponding to 10 ensembles is about one-third. In Figure 3.10, the estimates of the spatial extent of a cloud in turbulent diffusion are compared to actual observations of the spread of a given dye patch.

Autocorrelation Function

For each study and each coordinate axes, the autocorrelation, R_i was computed from the velocity time series using (3.2). These numerically computed values (Figure 3.7) when compared with the analytical models T, F1, F2 and ATG discussed earlier and represented in Figure 3.1 (models from Taylor, Frenkiel, Altinsoy et al.) were found to be in conformity with that prescribed using the analytical model F2. Care must be taken however in applying this close to the boundaries as it was observed that at certain depth cells particularly the bottom layers, the values of R_i became negative which would be seen as a direct violation of its properties as previously outlined. For the most part, R_i was bounded, asymptotically decreasing as prescribed and the results compare with those obtained by Bowden using similar numerical methods.

Scale of Turbulent Diffusion

The time and length scales of turbulence were computed using the integral in (3.2) and the expression in (3.4) respectively. The numerically computed values of the time scale, T_i and the mean and maximum length scale, l_i for the various depth cells and coordinate axes are presented in Table 3.2. Generally, the values of T_i were determined to fall within the range 5-84 s but between the depth cells, the values were found to fall within a relatively narrow range, suggestive of the fact that the turbulence structure does not vary significantly with depth. The length scales on the other hand range in value from 0-680 cm. There is significant difference in values between the East-West (mean, 205-337 cm), the North-South (mean, 157-245 cm) and the vertical (mean, 35-184 cm) directions.

Turbulent Diffusivity

From the dependence of turbulent diffusivity on the turbulence intensity and the time scale of diffusion in equation (3.2), the diffusivities along each of the three coordinate axes were computed and the results are displayed in Figure 3.8 showing the depth profile of the numerically computed turbulent diffusivity values for each coordinate axis. The maximum diffusivity is 1.03×10^4 cm^2s^{-1} while the mean turbulent diffusivity is $\sim 0.4 \times 10^4$ cm^2s^{-1} for the East-West (i.e. '*x*') coordinate axis. For the North-South (i.e. '*y*') coordinate axis the maximum value was 0.41×10^4 cm^2s^{-1}, about one order of magnitude less than the values for the East-West axis, while the mean value was $\sim 0.20 \times 10^4$ cm^2s^{-1}.

Table 3.2. Summary of turbulent diffusivity results for all three studies conducted.

		Time Scale of Diffusion, T_i (seconds)			**Length Scale, l_i (cm)**			**Turbulent Diffusivity (x 10^4 cm^2s^{-1})**		
		Mean	Max.	Std. Dev.	Mean	Max.	Std. Dev.	Mean	Max.	Std. Dev.
Study 0828_1										
Coordinate axis										
	x	25	47	8	284	680	106	0.32	0.98	0.16
	y	27	42	9	245	380	94	0.23	0.41	0.10
	z	71	84	10	184	260	52	0.05	0.08	0.02
Study 0828_2										
Coordinate axis										
	x	28	42	8	337	640	116	0.4	1.03	0.18
	y	24	37	8	224	353	77	0.21	0.33	0.08
	z	27	40	7	50	79	15	0.01	0.02	0.00
Study 1007										
Coordinate axis										
	x	21	34	9	205	387	116	0.22	0.45	0.14
	y	19	31	7	157	284	75	0.14	0.35	0.08
	z	23	40	8	35	73	18	0.01	0.01	0.00

Mean and maximum values of the diffusivity, integral time and length scales computed during each study for each of the three coordinate axes, *x, y,z.*

Similarly, the maximum vertical turbulent diffusivity was 0.08 x 10^4 cm^2s^{-1}, about two orders of magnitude less than the corresponding values along the *x*-coordinate and one order of magnitude less than the values along the *y*-coordinate directions respectively. These values are summarized in Table 3.2 and compares in value to those obatained from data for different bodies of water taken from the literature (Murthy, 1975; Riddle and Lewis, 2000; Ward, 1985).

Discussion

The results of this study are important in the light of episodic events in shallow embayments and the diffusive effects of turbulence occurring within the first few hours following a pulse discharge. Ward had conducted horizontal dye-diffusion experiments under geomorphologic conditions similar to the ones reported in this paper and although no data was reported specifically for Corpus Christi Bay (except the Upper Laguna Madre), the results obtained for horizontal diffusivity values are comparable. Also the values reported by Riddle and Lewis for bodies of water similar in depth to Corpus Christi Bay show comparable vertical diffusivities to the figures reported in this study. It is pertinent to note that the mean value of the turbulent length scale (~3 m) is comparable to the average depth of the bay. This is to be expected as the size of the turbulent eddies would be limited by the existence of a boundary either physical or virtual, virtual boundaries which may be due to stratification within the water column.

Through this study, the dependence of the turbulence process on the *degree of randomness* as measured through the intensity of turbulence, akin to the dependence of

molecular diffusivity on the temperature of the bulk fluid, was examined for Corpus Christi Bay. A numerical algorithm was developed for evaluating diffusivity values from direct observations of the 3-D currents field and these values were comparable with those obtained through dye-tracer experiments as well as those obtained from oceanic diffusion diagrams. The study was deliberately limited in terms of spatial and temporal scales in order to filter out the gross effects of tidal and inertial motion on the diffusion process. Future studies will allow the extension of this concept to the entire bay premised on the availability of surface current mapping data to coincide with the turbulent processes that drive constituent transport on the scale of days to months.

Using the maximum values of turbulent diffusivities, an estimate of the spatial extent of a diffusing clouds over a given period or diffusion time of ~6000 s was obtained assuming $2\sigma_t$ (68% of distribution) as representative of the spread of the cloud along each coordinate axis. The estimated horizontal spatial extent for study 0828_1 was 220 m and 142 m in the *x, y*-direction respectively, giving an aspect ratio of 1.6 for the diffusing patch. For study 0828_2, the corresponding values were 226 m and 128 m respectively with an aspect ratio of 1.8 while the values for study 1007 were found to be 149 m and 132 m respectively with aspect ratio of 1.1. These values for a cloud in turbulent diffusion was compared to actual observations of a given dye patch obtained during the different studies and presented in Figure 3.10 for study 0828_2. The time and length scales of turbulent diffusion were found to be within the range expected of oceanographic processes being ~100 s and ~10 m respectively.

For study 1007, although the turbulent diffusivity values (hence the computed spatial extent) were much lower than the values from the other two experiments, actual dye patch observations were much higher indicative of onset of shear diffusion. This shear diffusive process has been observed in pipe and channel flows by several researchers (Csanady, 1966; Elder, 1958; Elliot, 1986; Taylor, 1954). Figures 1.3 and 1.4 presents the meteorological and hydrodynamic conditions obtained for the duration of the experiment, noting the difference in meteorological conditions prevailing during the various experiments, particularly the wind pattern during experiment 1007 showing much variability in direction. This may have been a contributory factor to this shear-effect among other factors, which include water column stability.

Conclusion

The ability to characterize diffusion processes from hydrodynamic information is important as it can be applied to different bodies of water especially when viewed against the backdrop of the logistical challenge and expense associated with conducting dye-tracer experiments. As was determined from this study, the process of diffusion in surface waters particularly wind-driven bays such as described is not always shear-dominant but depending on prevailing conditions, may be dominated by pure turbulence. This is significant against the backdrop of general and ocean circulation models that employ turbulence closure schemes premised on the assumption of shear-diffusion. The algorithm developed was calibrated against observed spread of a dye patch, which will allow for the inclusion of diffusivity values within the framework of a data-driven

transport model using direct hydrodynamic observations. This capability forms a logical extension of existing oceanographic instrumentation to environmental assessments and precludes the application of turbulence closure schemes that base estimates of diffusivity on the assumption of prevailing shear.

Although this study does not answer all the questions regarding the enigma of turbulence, observations from these set of experiments contributes to the data on diffusion processes available for coastal and nearshore environments with emphasis on Corpus Christi Bay, data that is usually not found through the use of available oceanic diffusion diagrams. Considering that current profilers of the type used in this study are readily available, more experiments of this type can be conducted in a cost effective manner and this study establishes the methodology for such experiments with a view to better characterize the diffusive process within the study area. Additionally, future work will investigate the shear-diffusion process for Corpus Christi Bay with a view to developing similar algorithm necessary for evaluation of shear-diffusivity values from observed hydrodynamic data. These algorithms will be applied within a data-driven transport model in a related part of this study and which forms part of the ongoing development process within our laboratory.

CHAPTER IV

OBSERVATIONS OF SHEAR-AUGMENTED DIFFUSION PROCESSES AND EVALUATION OF EFFECTIVE DIFFUSIVITY FROM CURRENT MEASUREMENTS IN CORPUS CHRISTI BAY

Overview

Studies on the process of diffusion in fluids have shown that in the presence of a shear structure within the currents field, the observed spreading of a marked fluid can be augmented significantly. Shear-diffusion becomes the dominant diffusion process after a time $\boldsymbol{T_n}$, the initialization time has elapsed. For vertical shear, a characteristic vertical mixing time, $\boldsymbol{T_c}$ having an inverse relation to the vertical turbulent diffusivity, $\boldsymbol{K_z}$ governs this initialization time.

This study focuses on the observation of shear-augmented diffusion process in a shallow wind-driven body of water leading up to the development of numerical algorithms for obtaining an *effective diffusivity*, $\boldsymbol{K_e}$ from shear-current measurements at spatial scales ~1000 m. This was part of a series of dye-tracer experiments conducted in Corpus Christi Bay, Texas. Numerical estimates are provided for $\boldsymbol{T_c}$ using the value of $\boldsymbol{K_z}$ determined from the temporal current fluctuations based on the Lagrangian correlation function, $\boldsymbol{R_\tau}$ of the velocity time-series. It was found that in the presence of shear-current structure, $\boldsymbol{K_e}$ values obtained along two orthogonal directions were ~10^4 and 10^5 cm^2/s respectively, about 10-20 times higher than estimates obtained based on

turbulence alone and confirmed through visual observations and numerical estimates of the size of the diffusing dye cloud.

Introduction

This is the second part of a series of studies in support of ongoing efforts within our research group aimed at developing an integrated environmental and oceanographic assessment system for monitoring the coastal environment. The scheme combines real-time measurements from fixed and mobile platforms with data-driven numerical transport modeling and it is imperative that the coefficients required within this framework be quantifiable from direct observations of hydrodynamic data. In the first part of these related studies on mixing processes within the bay, the authors examined the role of turbulent diffusion with a view to develop a numerical scheme for the evaluation of coefficients required to drive a transport model using direct observations of water currents.

Constituent transport and water quality models are often employed in environmental studies in order to derive the time evolution and concentration profile of constituents of interest. The underlying advective-diffusive numerical models rely on coefficients that are used in characterizing the physical phenomena that lead to the evolution of the concentration with time of constituents of interest in surface waters. Collectively termed transport coefficients, there exists essentially two components viz. the advective component and the diffusive component. A number of different methods

can be applied to determine the diffusive component and four of these, from the literature are outlined:

- Method I – This method is based upon the temporal variation of the magnitude and direction of currents;
- Method II – This method is based upon the spatial variation of the currents field;
- Method III -- Using the first and second moments of the distribution of the concentration profile over time of a diffusing cloud, typically a dye patch;
- Method IV – An inverse solution of the governing transport equation of advection and diffusion, similar to Method III in that it requires the concentration profile of a diffusing substance over time.

Methods I and II, following on Taylor's analysis (Taylor, 1954) has been extended to other fluid flow regimes such as flow through open channels (Elder, 1958). Method I was applied to surface waters in the first part of this study by using direct observations of the currents field returned by an Acoustic Doppler Current Profiler (ADCP) and a numerical scheme (Ojo et al., 2004c).

Through a series of studies conducted by Csanady in the Great Lakes (Csanady, 1966), the observation was made that there exists a marked variation in the observed diffusion of constituents within a fluid body, the spreading being more pronounced under certain conditions than would have been expected. In other words, the growth of a diffusing cloud would appear to be much higher than expected if one were to consider only turbulence. Compounding these seemingly inconsistent observations is the fact that weak vertical turbulence appears to favor an increased rate of horizontal spreading

hence, the concept of shear-augmented diffusion similar to that observed by Taylor and Elder in pipe and channel flow respectively.

Shear diffusion involving the interplay between vertical turbulent diffusion and shear-currents become especially important within the coastal and near-shore environments (for instance in shallow wind-driven bays and estuaries) where the existence of complex shear current structures coupled with rapid variation in magnitude and direction of currents will be typical. Two different stages of shear diffusion have been identified namely first and second stage depending on the type of shear currents encountered by fluid elements in the flow field or whether boundaries (physical or virtual) have been encountered. In a general sense, lateral shear will be more likely to lead to first stage diffusion while vertical shear will be more likely to lead to second stage diffusion (Elliot et al., 1997). Particularly for shallow bays and estuaries, far away from vertical boundaries, lateral shear will therefore be less significant in terms of the contribution to shear diffusion when compared to vertical shear.

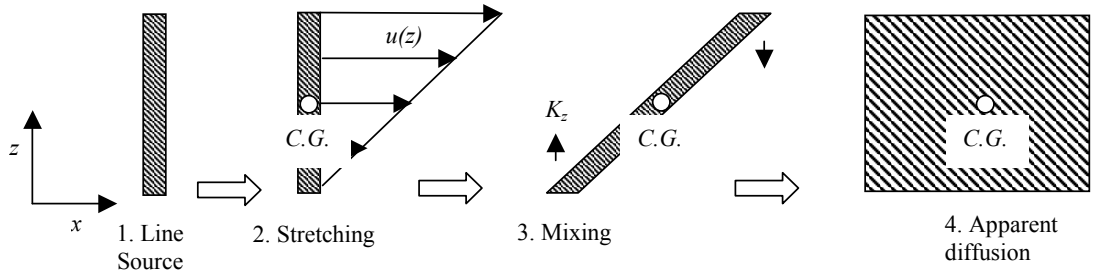

Figure 4.1. This is a depiction of the effect of a vertical shear current on a line source leading up to shear diffusion. 1. The line source is introduced. 2. The line source is displaced under the influence of the velocity (linear) profile, shifting the center of mass. 3. Next, vertical (turbulent) mixing redistributes the constituent as shown. 4. The overall effect is the apparent diffusion of a line source into a plane under the combined effect of a vertical shear current and vertical mixing.

During the first stage of diffusion, K_e will have a linear dependence on turbulent diffusivity, K_d (vertical or horizontal) and during the second stage, say for vertical shear, there exists an inverse dependence on vertical turbulent diffusivity, K_z. Turbulent diffusivity itself can be evaluated either by Methods I, III or IV. Method I uses the auto-correlation function, R_τ of the fluctuating velocity time series and is based on Taylor's statistical treatment of diffusion as a random process (Taylor, 1920).

Researchers (Bowden, 1965; Csanady, 1966) have put forward expressions for determining the effective diffusivity, K_e following on Taylor's work and based on Method II. Following on previous work done in this area (Okubo and Carter, 1966), Elliot developed expressions for K_d from which the time taken to complete vertical mixing or the characteristic mixing time, T_c can be determined (Elliot et al., 1997). From observation, it was determined that in the presence of shear currents, the direct contribution by turbulence to the overall diffusivity value becomes negligible when compared to the contribution from shear. In light of this, the process of turbulent diffusion in shallow wind-driven bays and estuaries can be augmented significantly by the shearing action of a spatially varying currents field as depicted in Figure 4.1.

The objectives of this study are: (i) to examine the role of vertical turbulence with respect to shear diffusion in conjunction with vertical shear in a shallow wind-driven bay; (ii) determine conditions under which shear diffusion becomes significant; (iii) develop a scheme for the numerical evaluation of the effective diffusivity.

This study was based on the observations in a wind-driven bay, Corpus Christi Bay, Texas where the ADCP was used to elucidate information on the shear current

structure within the bay. Predicated on recent developments in surface current measurements and the availability of current profilers, the numerical scheme developed which was used in evaluating effective diffusivity values is important within the framework of constituent transport and water quality models with specific application to the nearshore and coastal environment (Ernest et al., 1991; Sterling et al., 2004a; Sterling et al., 2004b).

Background Theory

The phenomenon manifesting as shear-augmented diffusion, first observed and published in the mid-part of the last century (Taylor, 1954), has been extended by other researchers to different flow regimes in both natural and engineered systems. The concept of an effective diffusivity is introduced within the framework of diffusive transport processes. Shear-augmented diffusion can be modeled as Fickian diffusion with constant coefficients, conditionally dependent on the time to complete vertical mixing (Taylor, 1953).

Shear-Augmented Diffusion and Effective Diffusivity

Following the work of Taylor on laminar and turbulent flow through pipes, the subject of research spanning the successive years has been the extension of this work to natural systems as is the focus of this paper. Under the effects of lateral or vertical shear currents structure and turbulence, a dye patch will spread at a rate that has been observed to be much higher than could be attributed to turbulence only. In a shallow wind-driven

bay, the velocity gradients that produce shear will be more pronounced in the vertical than in the lateral (horizontal) plane, except near the shore or close to land boundaries. Estimates on the value of horizontal shear (Elliot, 1986; Ojo et al., 2004c) indicates up to six orders of magnitude difference between these velocity gradients (vertical and horizontal) in coastal waters, which in subsequent analysis, will be an important factor especially as it relates to the onset of second-stage shear diffusion in a shallow embayment.

Analogous to the Lagrangian time-scale of turbulence (a statistical property), the condition for the application of the Fickian diffusion model in shear-diffusion is the initialization time, T_c. However, unlike the treatment of turbulent diffusion, Taylor's starting point for the analysis of shear-diffusion was not statistical. Rather the advection-diffusion equation incorporating knowledge of the shear structure in pipe flow was used in deriving analytical forms for the shear diffusivity, K_e and subsequently establishing the basis for its application through certain prescriptions. The premise was to write a constituent transport equation in terms of cross-sectional averages of the variables in the governing equation resting on the following assumptions:

a) The concentration distribution is at steady-state relative to a plane moving at the mean speed of the flow;

b) The flux through the boundaries is zero;

c) The effect of advection in the longitudinal direction is late to appear relative to that due to the cross-sectional variation of velocity.

For clarity, let us begin by writing a simplified form of the transport equation (the final result can be extended to three-dimensions), which considers advection in the horizontal, and mixing by diffusion within the water column

$$\frac{\partial S}{\partial t} + u\frac{\partial S}{\partial x} = \frac{\partial}{\partial z}\left(K_z \frac{\partial S}{\partial z}\right) \tag{4.1}$$

where S = solute concentration as time t, u is the velocity relative to a moving plane in the x-direction, K_z is the turbulent diffusivity in the z-direction.

In Elder's treatment for flow through a channel, the solution to equation (4.1) given the boundary and initial conditions stated in (a)-(c) above results in an expression for effective longitudinal shear diffusivity, K_x (along the x-coordinate axis) of the form:

$$K_x = -h^2 \int_0^1 (2\zeta)^n u' \left[\int_0^\zeta \frac{1}{K_z}\left(\frac{1}{\zeta}\right)^n \left(\int_0^\zeta (\zeta)^n u' d\zeta \right) d\zeta \right] d\zeta \tag{4.2a}$$

$$u(z,t) = \overline{u(t)} + u'(z,t) \tag{4.2b}$$

where h is the cross-sectional depth, $\zeta = z/h$, $\overline{u(t)}$ is the cross-sectional mean (depth average) of the velocity, and $u'(z,t)$ is the deviation from the cross-sectional mean. The parameter n takes the value $n = 0$ for a two-dimensional channel while $n = 1$ corresponds

to Taylor's treatment of flow through a pipe. Hence, for two-dimensional flow the expression for K_x becomes,

$$K_x = -\frac{1}{h}\int_0^h u' \left[\int_0^z \frac{1}{K_z} \left(\int_0^z u' dz \right) dz \right] dz \tag{4.3}$$

Bowden simplified this further by taking a functional form of both the velocity profile and vertical eddy diffusivity along the cross section given by,

$$\begin{aligned} u' &= uf(\zeta) \\ K_z &= Kg(\zeta) \end{aligned} \tag{4.4}$$

u = maximum value of velocity, and K = maximum value of vertical eddy diffusivity taken at the surface. From (4.3) and (4.4) the result is,

$$\begin{aligned} K_x &= -\left(h^2 u^2 / K\right) \overline{f(\zeta) F(\zeta)} \\ F(\zeta) &= \int_0^\zeta \left\{ [1/g(\zeta)] \int_0^\zeta f(\zeta) d\zeta \right\} d\zeta \end{aligned} \tag{4.5}$$

with the overbar indicating depth averaging. Using several analytic forms of the velocity and vertical diffusivity profiles together with further simplifications and assumptions, Bowden presented different expressions for K_x. One of such assumptions in reference to $F(\zeta)$, and applied to the case of wind drift in shallow water was that K_z (= K) remained constant over the entire depth an assumption that will be found to be valid for a shallow bay typified by the one considered in this study. For practical purposes, it is desirable to have an expression of the form

$$K_x = \Omega\left(h^2 u^2 / K\right) \tag{4.6}$$

and following Bowden's analysis, Riddle and Lewis were able to derive expressions of this form for K_x by carrying out a parametric fit between Ω^{-1} (the shear parameter) and a coefficient β obtained from a power law general expression for shear-current (Riddle and Lewis, 2000). Considering the variability and complexity of the shear current encountered in natural systems, it may be difficult to represent the depth profile of the current by typical analytical expressions necessary for performing the integral in equation (4.3). There is therefore a limitation when considering the applicability of equations (4.5) and (4.6) to natural systems such as bays or estuaries. Fischer developed a method for performing this analysis through the introduction of dimensionless quantities into equation (4.3) leading to a general form for K_x as in equation (4.6) (Fischer et al., 1979):

$$K_x = \left(h^2 \overline{u'^2} \Big/ \overline{K_z} \right) I$$

$$I = -\int_0^1 u'' \left[\int_0^{z'} \frac{1}{K_z'} \left(\int_0^{z'} u'' dz' \right) dz' \right] dz \tag{4.7}$$

where I is a dimensionless integral having dependence on dimensionless quantities $u'' = u' \Big/ \sqrt{\overline{u'^2}}$, $K_z' = K_z \Big/ \overline{K_z}$, $z' = z/h$, the overbar again indicating cross-sectional averages. This reveals the rather interesting inverse dependence of shear diffusion on vertical turbulent diffusivity and the mean-square, S_i of the deviation of the velocity from the cross-sectional average. The form of equation (4.7) was used in this study by numerically integrating the discretized data set obtained from the various current measurements.

This is conditional though considering the steady-state condition as prescribed for the cross-sectional concentration distribution relative to a moving frame i.e. the solute concentration is well mixed vertically. For this condition to apply, there is consideration of the initialization time, T_n proportional to a characteristic time scale, T_c and is given by,

$$T_n = \psi h^2 / \overline{K_z} = \psi T_c$$

$$T_c = h^2 / \overline{K_z} \tag{4.8}$$

The quantities $\sqrt{\overline{u'^2}}$, $\overline{K_z}$ are the characteristic velocity and characteristic turbulent diffusivity respectively. Different values have been suggested for the constant of proportionality in equation (4.8), the dimensionless time, Ψ by several researchers who have studied diffusion processes in both natural and engineered systems as summarized in Table 4.1.

Table 4.1. Typical values proposed for the value of dimensionless time, Ψ based on different shear current structures.

Proponent	**Dimensionless Time, ψ**
Chatwin (1972)	1.0
Fischer (1968)	0.4
Sayre (1969)	0.5
Okubo and Carter	$1/\pi^2$ ($\approx$ 0.1)
Yasuda (1984)	0.5

This implies another form of (4.7) that can be written as follows:

$$K_x = \overline{u'^2} T_c . I \tag{4.9}$$

where the dimensionless integral, I quantifies the structure of the shear as well as its variability, and by analogy to Ω in equation (4.6), I can be described as a shear coefficient. Typical values of I suggested for rivers and estuaries (Fischer, 1973) fall within a very narrow range from 0.06 to 0.15 and for practical applications, a suggested value of 0.1 would suffice. The implication of (4.8) and (4.9) is that for times $t \geq T_n$, the size of the diffusing cloud measured by its variance grows at a constant rate and the process can be modeled as Fickian diffusion with constant diffusivities.

Similar expression can be found for effective diffusivity, K_y in the orthogonal y-direction, hence the general expression in two dimensions:

$$K_i = \overline{u_i^{'2}} T_c . I_i$$

$$I_i = -\int_0^1 u_i^{''} \left[\int_0^{z'} \frac{1}{K_z^{'}} \left(\int_0^{z'} u_i^{''} dz^{'} \right) dz^{'} \right] dz \qquad (4.10)$$

for $i = x, y$ and $u_i^{''} = u_i^{'} \Big/ \sqrt{\overline{u_i^{'2}}}$ being derived from the respective horizontal components of the current along the respective x, y coordinate axes.

Although the preceding analyses would apply in the case of lateral shear (first stage diffusion) as well, this study was limited to the case of vertical shear on the premise of the study area being within a shallow body of water, far enough away from land boundaries against the backdrop of Elliot's findings. In other words, the assumption was made that the process of shear diffusion proceeded as second-stage diffusion after a

time $t \geq T_n$ that will be determined as part of this study. An effective diffusivity along the x,y-coordinate axis, K_i computed on the basis of equation (4.10) with dependence on the vertical turbulent diffusivity, K_z and vertical shear current (collectively embodied in the quantity I_i) as well as T_c will apply.

Method

The preceding analyses were applied to a shallow wind-driven bay by examination of shear-augmentation of the diffusion process using vertical turbulent diffusivity evaluated from the velocity autocorrelation, the dataset being derived from 3D current measurements. The condition for the application of Fickian diffusion dependent on the initialization time was determined for the selected bay as well as the characteristic time and the value of the dimensionless time.

Current measurements of the area in 3D were obtained using a fast response Acoustic Doppler Current Profiler, ADCP (RD Instruments, Inc., San Diego, CA). The ADCP was installed on a rigid mount on the bow of a small craft that also had a towed instrument array used for obtaining horizontal profiles of the concentration distribution of the dye along with CTD and particle size distribution measurements. The current profiles were obtained within a 300-500 m radius dictated by the spatial extent of the dye patch over a period between 0-150 minutes following dye application. The profile was well localized both temporally and spatially enough to filter out horizontal variations in current structure and the effects of tides, an important factor in emphasizing the turbulence and vertical shear structure within the scale of the experiment.

Summary of the three studies conducted are given Table 1.2. For reference, identification numbers have been assigned to each study. Two studies were conducted at two different locations on August 28, 2003 at two different times in the tidal cycle (study 0828_1 and 0828_2). Studies 0828_1 and 1007 were conducted at location 2747.937N, 9721.451W on two different dates (August 28 and October 7, 2003) and at different times in the tidal cycle. With this experimental design, information can be obtained as to the existence of a spatial-temporal variability of diffusivity values due to the coupling between meteorological conditions and oceanographic forcing within the study area.

Site Description

Located within Corpus Christi Bay in the Texas Gulf of Mexico about 200 miles south west of Houston, TX (Figure 1.2) the study area is part of a system of bays. Comprising of four interconnected embayments namely Oso Bay in the southwest, Nueces Bay in the northwest, Upper Laguna Madre in the south and Redfish Bay in the northeast, Corpus Christi Bay is the main bay within the system. Along the northernmost half of the bay, a shipping channel that is ~15 m deep runs east to west while an intra-coastal waterway runs north to south.

The deepest of the four, it is bounded on the east by Mustang and North Padre Islands and on the west by the city of Corpus Christi. Other characteristics of the bay are:

Size:	Approximately 500 sq. km
Bathymetry:	Relatively uniform, ~3 m

Tidal Range:	Relatively low, ± 0.5 m
Residual currents:	Predominantly along the east-west coordinate axis; counterclockwise circulation, tidally driven.
Main forcing:	Winds from a southeasterly direction. "Northers" from the northerly direction during the winter months.
Drainage area:	~49,700 sq. km, daily average freshwater flow of ~34 m^3/s.
Average salinity:	22 psu and as high as 33 psu.

Instrumentation

The ADCP was a 1200 kHz broadband workhorse that was installed in a bottom-tracking, downward-looking configuration on the bow of a 27 ft. watercraft as part of an instrument array for environmental measurements that included a CTD, a fluorometer and particle size distribution analyzer. The other instruments were mounted on a tow-body capable of performing undulating profiles throughout the water column. Data logging from the instruments were carried out on-board the craft with an integrated data acquisition (DAQ) computer incorporating a GPS unit.

The ADCP was equipped with bottom-tracking capability that allowed absolute current measurements to be taken on a moving platform by compensating for the velocity of the moving platform. A time series of the horizontal and vertical velocity components u_i ($i = x, y, z$) corresponding to the East-West, North-South, Up-Down coordinate axes were returned in layers or bins spaced equally at 0.1 m apart throughout

the water column. Given the bathymetry of the study area as shown in Figure 2 with depth ~3-4 m, the maximum number of bins used in this study was thirty taking into account 0.25 m blanking zone for the instrument. Three dye-tracer studies were carried out between the summer and winter months of 2003 within Corpus Christi Bay during which ~20000 current samples were obtained during each exercise along with fluorescence and CTD data. Analysis of the data from ADCP current measurements used in this study is described below.

Data Analysis

With the ADCP set for single pings at 2.5 Hz sampling rate, data post-processing which includes spectral analysis and low-pass filtering was performed on the ensemble of velocity measurements to generate the velocity time-series having acceptable error levels. Along with the bottom-tracking data, ship movement was compensated for and the current measurements referenced to the geographic coordinate axes. For each coordinate axis, a matrix (N x 30) of velocities (where N, the size of the samples depends on the duration of the exercise and sampling rate, 30 being the number of horizontal layers or bins in the water column at 0.1 m apart) was analyzed.

The velocity autocorrelation $R_i(\tau)$ was first obtained and then applied in the numerical evaluation of vertical turbulent diffusivity, K_z based on Method I that is described in the first part of this series of studies as mentioned before. Following this, numerical evaluation of the dimensionless integral, I_i given in equation (4.10) was subsequently performed using these results along with the value of T_c determined from

equation (4.8) leading to values for shear diffusivity, K_i ($i = x, y$). All data post-processing and analysis were performed with a set of MATLAB® based routines developed in our laboratory for this study as part of the integrated scheme for environmental and oceanographic assessments. The derivation of equation (4.3) and the discretization for the numerical scheme following from the derivation of equation (4.7) is presented below.

$$\frac{\partial S}{\partial t} + u' \frac{\partial S}{\partial x} = \frac{\partial}{\partial z}\left(K_z \frac{\partial S}{\partial z} \right)$$

with the quasi - steady state assumption, frame of reference moving at the mean flow velocity, solute fully mixed in the vertical

$$\frac{\partial S}{\partial t} = 0$$

$$u' \frac{\partial S}{\partial x} = \frac{\partial}{\partial z}\left(K_z \frac{\partial S}{\partial z} \right)$$

The vertical profile of the solute is therefore given by

$$\frac{\partial S}{\partial x} \int_0^z \frac{1}{K_z} \int_0^z u'(z) dz dz = S(z)$$

The mass flux can be written as follows :

$$\dot{M} = \int_0^h u'(z)S(z)dz = \frac{\partial S}{\partial x}\int_0^h u'(z)\int_0^z \frac{1}{K_z}u'(z)dzdzdz$$

Alternatively the x - sectional (mass per length) flux can also be written as :

$$\dot{M} = -hK_e\frac{\partial S}{\partial x}$$

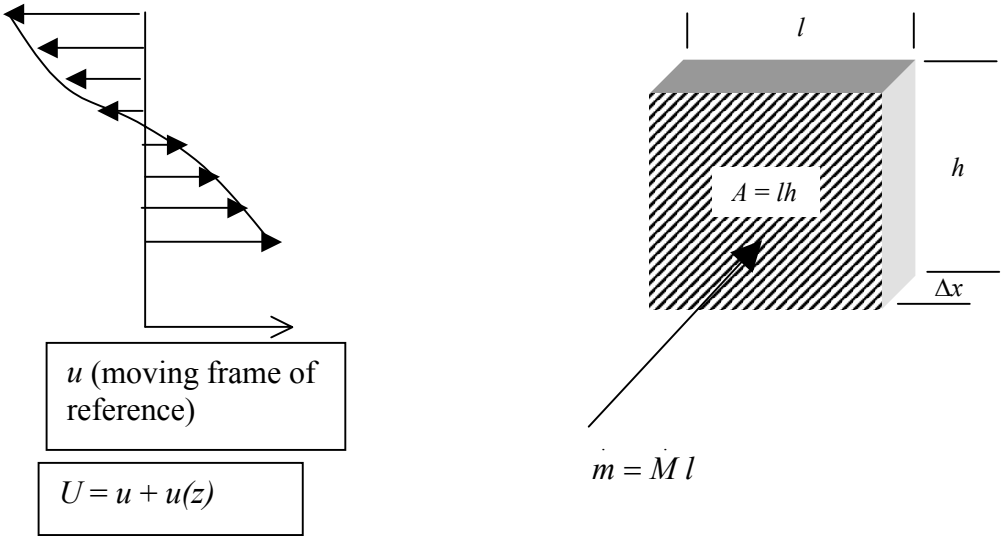

Figure 4.2. Illustration of fluid element under the influence of vertical current shear.

Figure 4.2 illustrates this process in a simplified form and finally by comparing the two expressions for mass flux,

$$-hK_e = \int_0^h u'(z) \int_0^z \frac{1}{K_z} \int_0^z u'(z) dz dz dz$$

and we arrive at equation (4.3)

$$K_e = -\frac{1}{h} \int_0^h u'(z) \int_0^z \frac{1}{K_z} \int_0^z u'(z) dz dz dz$$

The discretized form of equation (4.7), which derives from equation (4.3) is as follows :

$$-\left[\frac{h^2 \sum_0^h u_z^2 - \left(\frac{1}{h} \sum_0^h u_z \right)^2}{\sum_0^h K_z} \right] \sum_0^1 \left\langle \frac{u_z - \frac{1}{h} \sum_0^h u_z}{\sqrt{\frac{1}{h} \sum_0^h u_z^2 - \left(\frac{1}{h} \sum_0^h u_z \right)^2}} \text{x} \ldots \right.$$

$$\left. \ldots \sum_0^{z/h} \left\{ \frac{\sum_0^h K_z}{hK_z} \left[\sum_0^{z/h} \left(\frac{u_z - \frac{1}{h} \sum_0^h u_z}{\sqrt{\frac{1}{h} \sum_0^h u_z^2 - \left(\frac{1}{h} \sum_0^h u_z \right)^2}} \right) \right] \right\} \right\rangle$$

Results

The results of numerically evaluating shear diffusivity from direct observations of the 3-D currents field are presented in this section. The values determined for I from this study were compared with Fisher's. Using the computed values of K_i, estimates were made of the size of an evolving dye patch and compared with the observed spatial distribution of the evolving dye patch reconstructed using the fluorescence measurements that were taken during the study.

Characteristic Velocity Distribution, Dimensionless Integral and Initialization Time

Figures 4.3-4.5 show typical shear-current vertical (depth) profiles of the velocity components along the respective coordinate axis as well as vector plots of the currents field from each of the three studies at selected times. The statistics of the sampling distributions of characteristic velocities are presented in Figure 4.6 for each of the three studies while the density distribution functions are displayed in Figure 4.7. These distributions are seen to be normal with a narrow spread (some noticeable outliers in the data), the East-West characteristic velocities showing a mean of ~40-50 cm/s while the North-South characteristic velocities show a mean of ~20 cm/s.

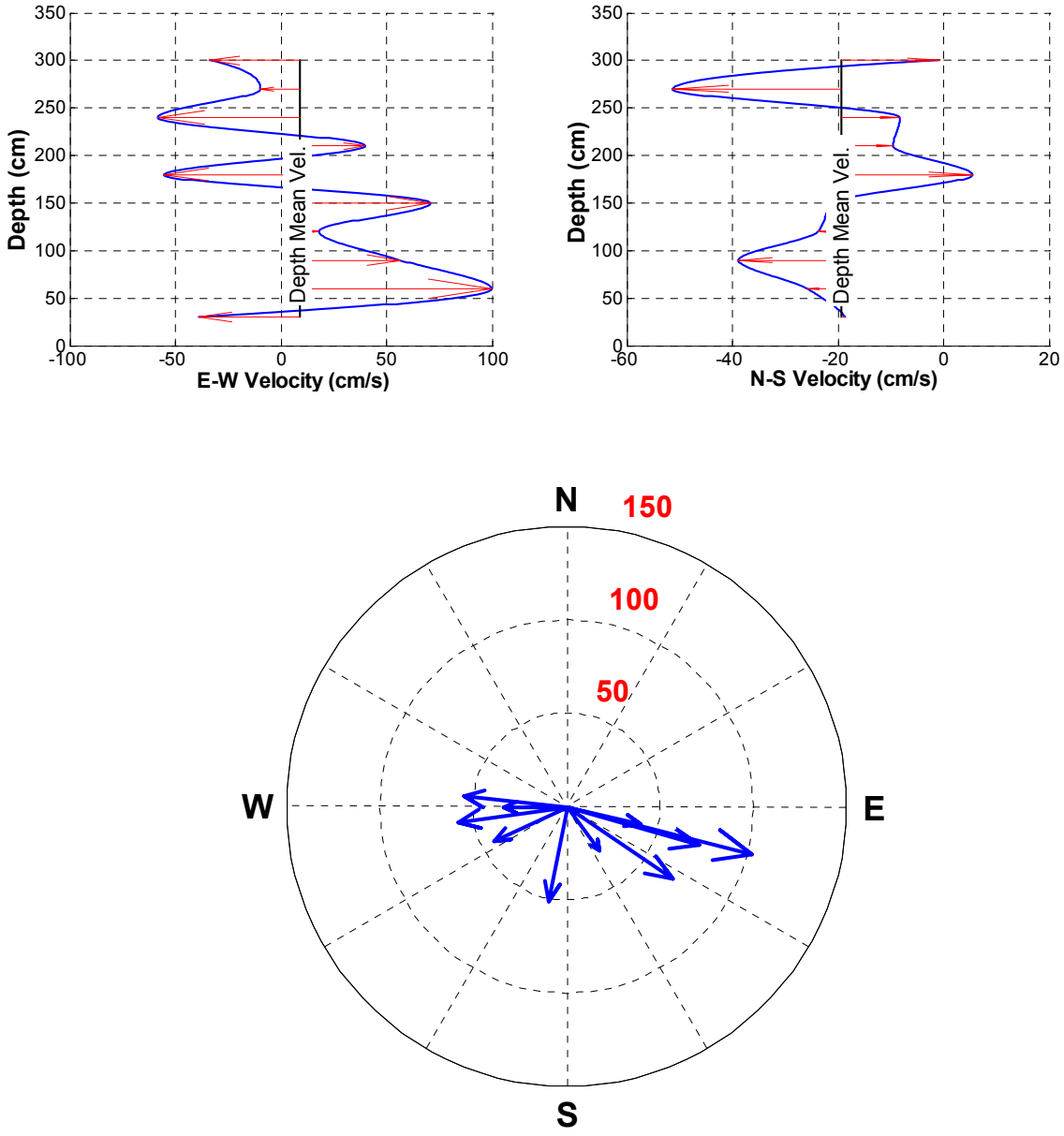

Figure 4.3. Study 0828_1. Top-left panel -- E-W shear current profile at 0.3 m depth intervals; top right panel – N-S shear current profile at 0.3 m depth intervals; bottom panel – compass plot of velocity vectors.

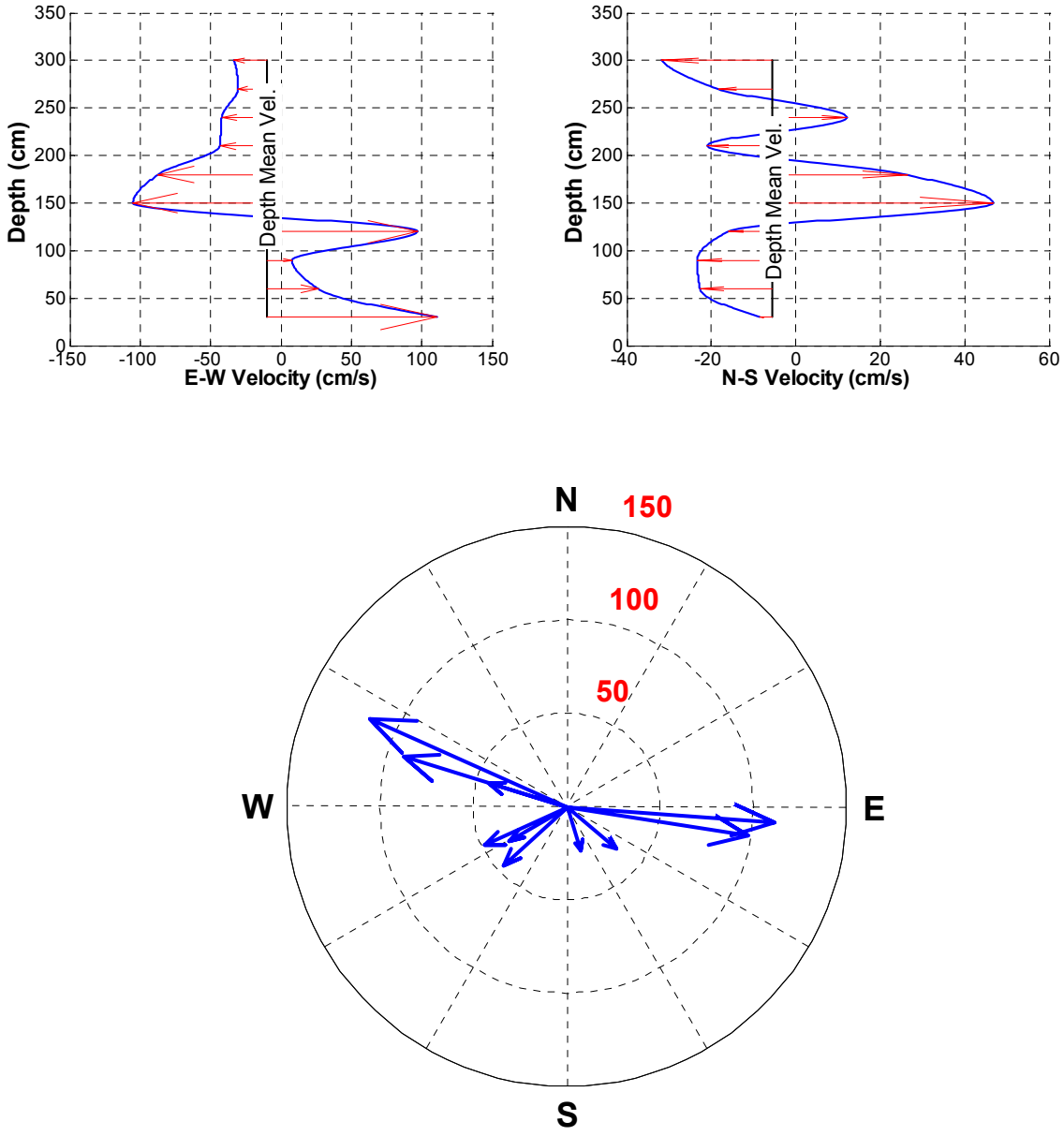

Figure 4.4. Study 0828_2. Top-left panel -- E-W shear current profile at 0.3 m depth intervals; top right panel – N-S shear current profile at 0.3 m depth intervals; bottom panel – compass plot of velocity vectors.

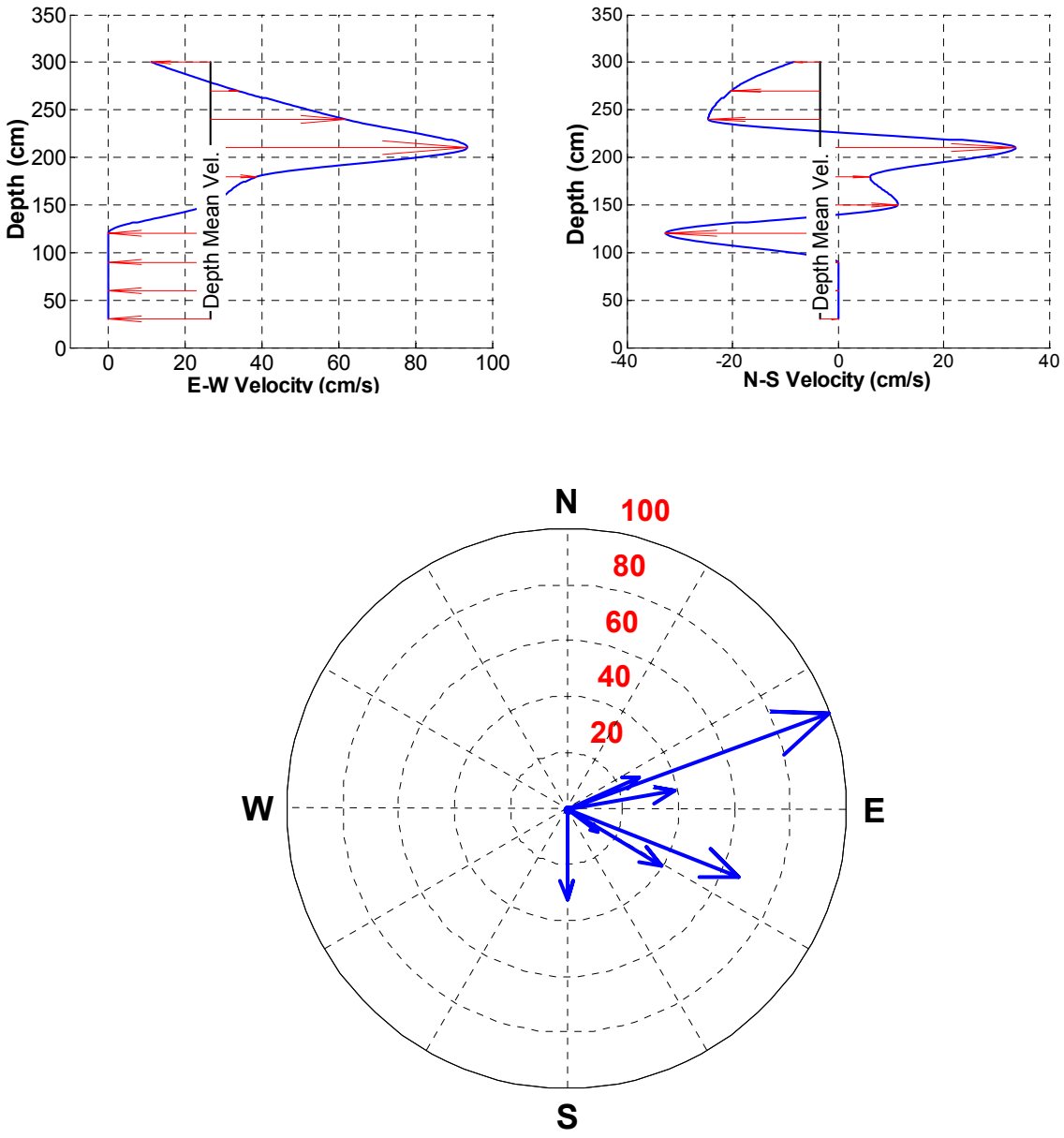

Figure 4.5. Study 1007. Top-left panel -- E-W shear current profile at 0.3 m depth intervals; top right panel – N-S shear current profile at 0.3 m depth intervals; bottom panel – compass plot of velocity vectors.

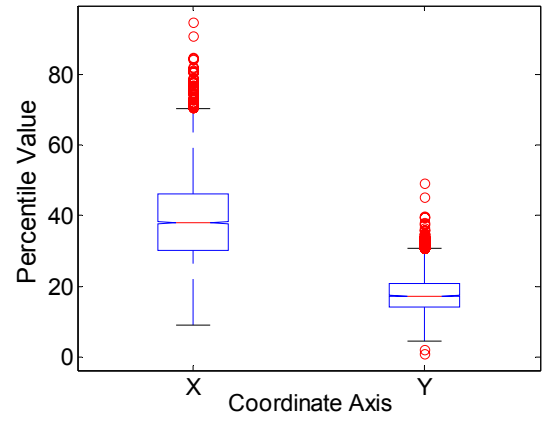

Study 0828_1

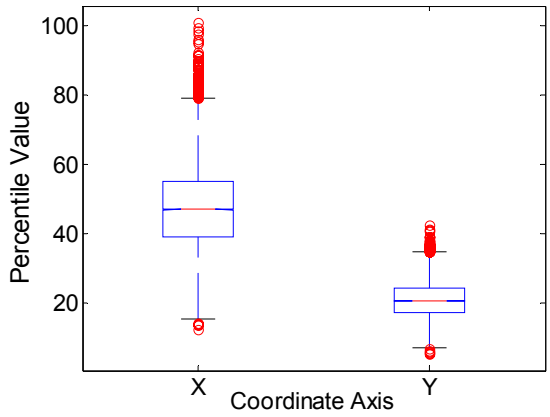

Study 0828_2

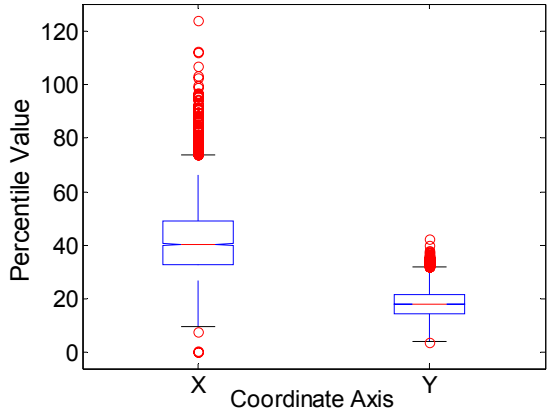

Study 1007

Figure 4.6. Statistical summary of characteristic velocities. Top -- study 0828_1; middle -- study 0828_2; bottom -- study 1007. Open circle, --o-- outliers within dataset.

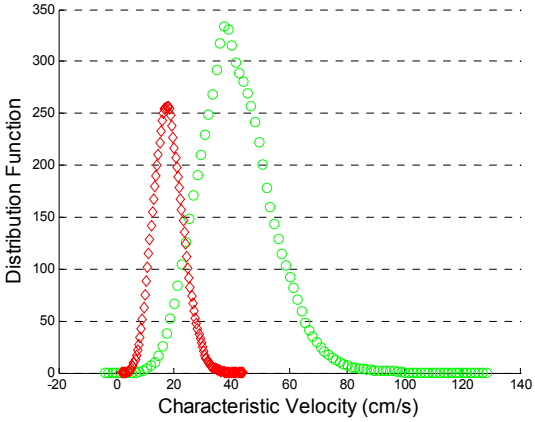

Study 0828_1

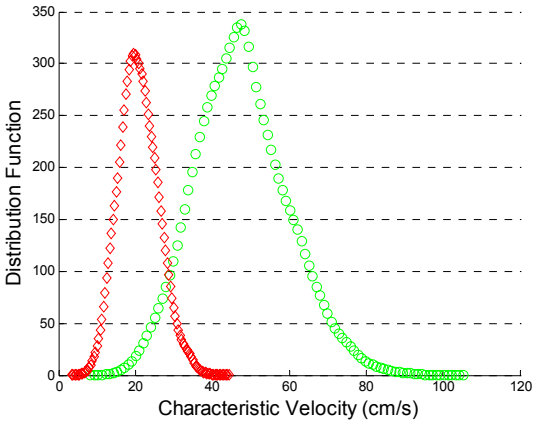

Study 0828_2

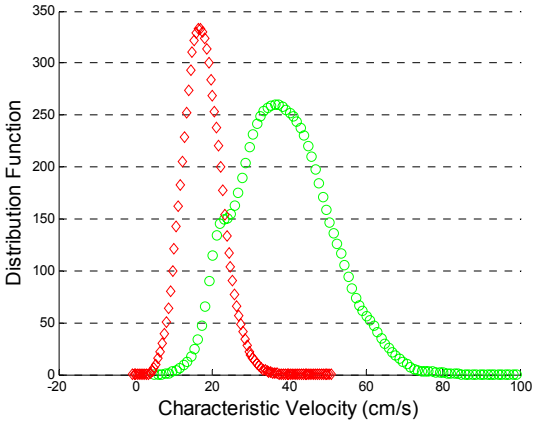

Study 1007

Figure 4.7. Density distribution function of characteristic velocity computed from shear-current. Top – study 0828_1; middle – study 0828_2; bottom – study 1007 (-○- east-west; -◊- north-south).

Table 4.2. Summary of shear diffusivity results for all three studies conducted. Mean and maximum values of the dimensionless integral, initialization time and shear diffusivity are given for each of the coordinate axes, *x, y*.

	Dimensionless Integral, I			**Initialization Time, T_n (seconds)**		**Characteristic Velocity, $\sqrt{\overline{u'^2}}$ (cm/s)**			**Characteristic Diffusivity, $\overline{K_z}$ (cm^2/s)**	**Shear Diffusivity, K_{ie} x 10^5 (cm^2/s)**
	Mean	**Max.**	**Std. Dev.**	**Ψ= 0.1**	**Ψ= 0.4**	**Mean**	**Max.**	**Std. Dev.**		
Study 0828_1										
East-West	0.12	0.22	0.03	177	709	41.65	123.93	12.76	50	3.67
North-South	0.12	0.22	0.03			18.24	42.18	5.10		0.70
Study 0828_2										
East-West	0.11	0.24	0.04	85	342	47.52	101.06	12.15	104	2.15
North-South	0.11	0.24	0.04			20.84	42.60	5.15		0.41
Study 1007										
East-West	0.12	0.19	0.02	114	456	38.60	94.85	11.74	76	2.09
North-South	0.12	0.21	0.02			17.50	49.27	4.96		0.43

The quantities from equation (4.10) used in the computation of shear diffusivities (dimensionless integral, I and initialization time, T_n) are presented in Table 4.2 along with the statistics on the distribution of the characteristic velocity. The numerically determined values for I were found to have a mean that was ~0.12 and a range of 0.06-0.24 and these figures were found to be in agreement with the values recommended by Fisher as previously stated. The T_n values were determined using Ψ values of 0.1 and 0.4 giving a lower bound of 85 s and upper bound of 709 s. These values for T_n implies that the constituent of interest, in this case a pulse discharge of tracer at the surface would become fully mixed into the water column within minutes following application.

Shear Diffusivity

The numerically computed diffusivity values were ~2-4 x 10^5 cm^2/s along the x-coordinate direction and ~4-7 x 10^4 cm^2/s along the y-coordinate direction. In all the studies, the E-W shear-diffusivity was found to be about one order of magnitude higher than the N-S diffusivities. These values are in line with the observation of the evolution of the dye-patch and within order of magnitude estimates of the diffusivities from concentration profiles of the diffusing dye-patch. Using the numerical estimates of the diffusivities, the variance σ_i^2 (i =x, y) and standard deviation, σ_i, (i =x, y) of the dye-patch over the duration of the experiments were obtained, taking 68% of the dye to be within $2\sigma_i$, ($\sigma_t^2 = 2K_{ie}t$) leading to a size estimate of ~500-600 m along the x-coordinate axis and ~200-300 m along the y-coordinate axis.

Comparing these size estimates with actual observations of a diffusing cloud, we find close agreement within the limits of uncertainties associated with mass-balance computations in such natural systems. Confounding this is the relatively high background fluorescence in the body of water and the lower detection limit of the fluorescence-measuring instrument, which implies that such size estimates based on fluorescence measurements tend to be lower than actual. In fact, other researchers have noted these uncertainties and Okubo suggested that 50-75% accuracy would be acceptable for most experiments involving dye releases (Okubo, 1971). The numerical size estimates taken within $\pm \sigma_I$, or 68% of the diffusing cloud was close to 100% of the size estimates from the actual dye release in study 1007. One could also infer that these numerical estimates give the lower bound of the spatial extent of the plume (~200 m along the *y*-coordinate axis and ~500 m along the *x*-coordinate axis). Similar estimates of the spatial extent using turbulent diffusivity values were found to be 3-5 times lower.

This suggests therefore by the order of magnitude difference in the estimated values of diffusivity that shear diffusivity dominated over turbulent diffusivity within the study area for experiment 1007 and that the diffusive process can be characterized by shear diffusivity values obtained from the numerical scheme as described earlier. Figure 4.8 presents the above results in graphical form, outlining numerical size estimates of a diffusing cloud based on turbulence and shear against the actual dye patch size several minutes after release.

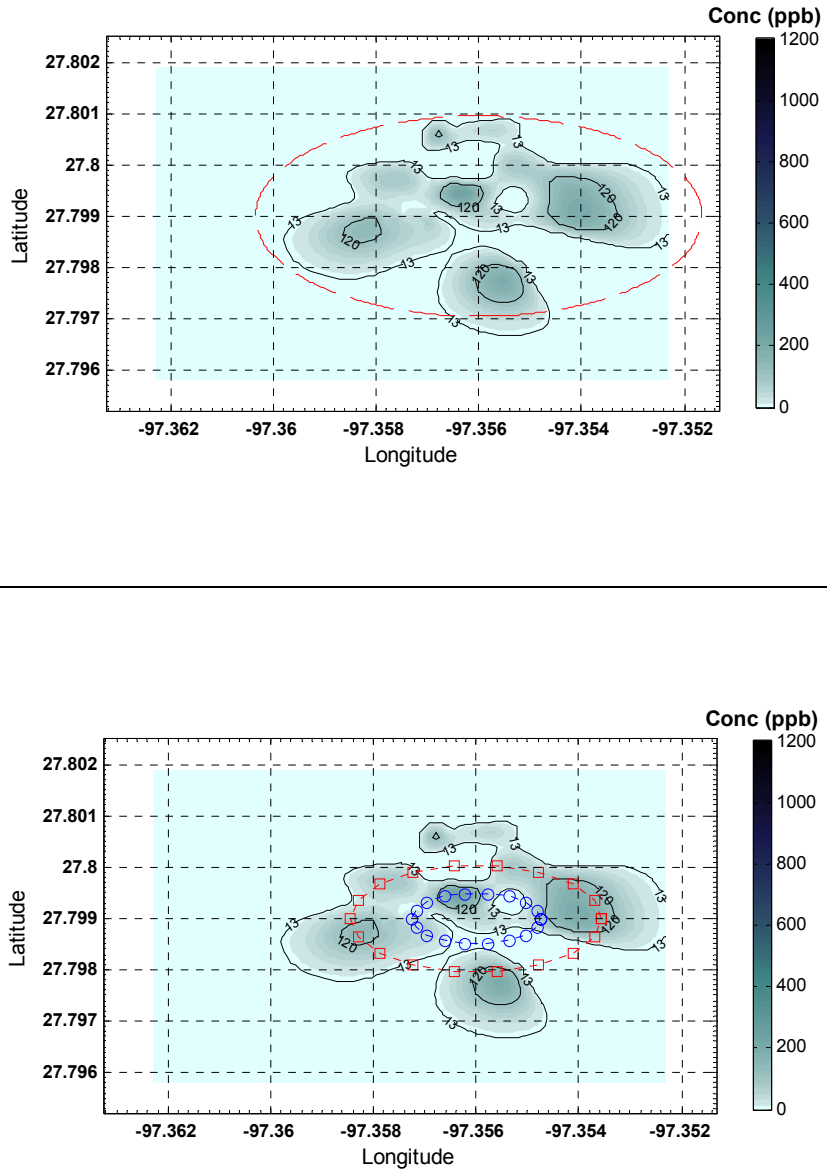

Figure 4.8. Top; observed dye patch, 5557 s after instantaneous release. Outlined (- - -) is the 68% numerical estimate of spread with 2σ based on shear (K_x = 2.09 x 10^5, K_y = 0.43 x 10^5). Bottom; same dye patch outlined open circles (-o-) is the 68% numerical estimate of spread with 2σ based on turbulence and open squares, the 99% numerical estimate also based on turbulence (K_x = 1.69 x 10^4, K_y = 0.30 x 10^4). The estimates based on turbulence presents an underestimation of the concentration distribution.

The explanation for the shearing effect being observed in one study and not in others may be found in the different meteorological and oceanographic conditions (Figures 1.3 and 1.4) encountered in study 1007 compared to study 0828_1 and 0828_2. Noting that the wind pattern observed during study 1007 as being highly variable in direction, this might have contributed to the shearing effect being more pronounced in this particular experiment compared to the other two.

Discussion

The onset of shear-augmented diffusion was determined for the study area and found to be influenced by the variability with depth and time of the magnitude and direction of the current as well as the vertical turbulent diffusivity. Algorithms were developed for characterizing the diffusive processes and for the evaluation of diffusivity values using the 3D currents field that was obtained with a vessel-mount ADCP. In the initial stages following the introduction of a constituent into the bay (on the order of seconds) and for times less than T_n, the diffusion process will be governed by turbulence. Following this, and for times greater than T_n (which is of the order of minutes, depending on the bathymetry, turbulence intensity and shear structure of the currents field), the diffusion process will be governed by vertical shear.

It is imperative to note that the initialization time could be influenced by the existence of a virtual boundary or diffusion floor within the water column such as a thermocline or pycnocline. In other words, the argument relating this study to shallow bays could be extended to deeper bodies of water if there is evidence to support the

existence of a diffusion floor. The diffusion floor effectively limits the further vertical transport of the constituent and ultimately affects the time for complete vertical mixing or initialization time, T_n. In addition, water column stability will be an issue as it affects the eventual mixing, on which the mechanism of shear-augmentation of the diffusion process depends (Bowden, 1965; Okubo and Carter, 1966).

Using the numerical estimates of shear diffusivities, the estimated variance and therefore the spatial extent of a plume over a given time period were obtained. The results obtained from the numerical analyses of direct observation of currents were compared with observations of a dye-patch from the tracer experiments and the estimated spatial extent of a diffusing cloud undergoing shear diffusion was ~3-5 times higher than for turbulent diffusion. This is in close agreement with actual observations of the dye plume in study 1007 being ~3 times greater in size than the size observed from study 0828_1 and 0828_2 suggesting that shear diffusion was the dominant process in study 1007.

Although the analyses in this paper indicate that shear diffusion would prevail in all three studies, this was not confirmed for studies 0828_1 and 0828_2. The presence of a reversing flow during the early part of the ebb cycle as indicated by the flow structures in Figures 4.3 and 4.4 taken from study 0828_1 and 0828_2 respectively may have resulted in a negation of the shearing effect with respect to the diffusion process. When one compares the flow structure in Figure 4.5 taken during the fully developed flood cycle of study 1007, a clearly defined boundary layer can be observed at about the 1 m depth-mark without any reverse flows. This combined effect of having a clearly defined

boundary layer without any reversed flows may have resulted in an augmentation of the diffusion process as observed in study 1007 but not observed in the other two studies conducted even though the preceding analyses indicate shear augmentation for all three studies. In addition, we believe that the highly variable wind pattern observed during study 1007 (Figure 1.3) contributed to the shear structure of the currents within the water column, in contrast to what was observed during studies 0828_1 and 0828_2.

Thus the application of rigorous analytical techniques to the characterization of shear diffusion processes in natural systems such as the one described in this study will be predicated on the fulfillment of conditions beyond those prescribed earlier. Recall a sufficiently low T_n relative to the vertical extent of the water column and vertical turbulent diffusivity K_z in the presence of a shear current structure. This study indicates that even where T_n is sufficiently low (which will be true for shallow bodies of water or for deeper waters having a diffusion floor due to stratification) the shear current may not always lead to diffusion augmentation. Particularly in bays and estuaries where flow reversal and stratification is common, it will be necessary to be able to qualify or categorize those prevailing conditions when in concert with T_n and the shear coefficient, I produce shear diffusion in natural systems as observed in study 1007. It is worthy of note that inherent in the application of turbulence closure schemes common to some well known ocean and general circulation models, is the assumption of shear turbulence and as has been demonstrated through these set of experiments, this may not always hold.

Noting that the diffusion process was enhanced up to 10-20 times and if one were to attribute this to and increase in turbulence, this would require a 3-5 times increase in

the level of the velocity fluctuations going by the relation of turbulent diffusivity to the variance of the velocity field. The meteorological conditions and geomorphology of the study area did not vary to the extent of being able to justify this level of increase in turbulence leading to the conclusion that shear-current structure rather than increasing turbulence produced the diffusion augmentation in this shallow body of water observed in study 1007.

Future Work

The ability to be able to characterize diffusion processes from hydrodynamic information is important as it can be applied to different bodies of water especially when viewed against the backdrop of the logistical challenge and expense associated with conducting dye-tracer experiments. Given the state of the art in currents measurements in surface waters, this ability will form a logical extension of existing instrumentation for oceanographic and environmental assessments.

In order to be able to apply this comprehensively, the effect of water column stability will have to be examined in order to develop conditions for which the shear augmentation of the diffusion process will prevail subject to T_n and I. This will result in a classification similar to the development of atmospheric stability classes for the application of the Pasquill-Gifford (Pasquill, 1962) dispersion model in meteorological and air quality applications.

CHAPTER V

DIFFUSION AND MIXING EXPERIMENTS IN CORPUS CHRISTI BAY, TX: DYE-TRACER STUDY TO DETERMINE DIFFUSIVITY VALUES

Overview

A series of dye tracer experiments were conducted within Corpus Christi Bay, TX to determine horizontal diffusivity values, $\boldsymbol{K_i}$ ($i = x, y$ along the East-West and North-South, coordinate axes respectively) from the observed concentration profiles of a diffusing patch of Rhodamine WT dye. These dye-tracer studies covering horizontal length scales between 10-1000 m (with corresponding time scales of ~10^4 s) were conducted for validating a numerical scheme developed for evaluating diffusion coefficients from turbulent characteristics of the currents field in surface waters. In one of the studies, the diffusion process in this shallow wind-driven bay was enhanced by the vertical shear current structure resulting in diffusivity values that were 10-20 times greater than estimated based on turbulence. In general, the East-West diffusivities were found to be ~10^4-10^5 cm^2/s, an order of magnitude higher than the North-South diffusivities which were found to be ~10^3-10^4 cm^2/s. These results will be useful within the framework of constituent transport modeling and contributes to available data on diffusion processes within the coastal and near-shore environments.

Introduction

The coupling of physical, chemical and biological processes in natural systems as captured in the governing equations of fate and transport in conjunction with system hydrodynamics is important in describing the evolution of constituents over space and time. Development of a concentration profile of constituents of interest can be achieved through the solution of these governing equations predicated on the parameterization of the diffusive component expressed as the diffusion coefficient or diffusivity. Diffusivity values on the horizontal plane exist for length scales of 1-100 km in the open and coastal oceans as well as lakes (Murthy, 1970; Stummel, 1949). Such data have been compiled into oceanic diffusion diagrams (Okubo, 1971) but limited data exist at smaller scales particularly in the near-shore environment covering length scales in the range 10-1000 m and corresponding time scales on the order of minutes to hours. Tracer experiments have traditionally been the accepted method of obtaining diffusivity values in surface waters (Elliot et al., 1997; Okubo, 1971; Riddle and Lewis, 2000) but these are logistically challenging to conduct as well as being so time consuming.

A numerical scheme was developed in our laboratory for computing diffusivity values from hydrodynamic observations (Ojo and Bonner, 2002; Ojo et al., 2004c) and the primary objective of this dye-study is to validate this scheme. This scheme depends on the evaluation of the turbulence and shear structure of the flow field in surface waters and by conducting a series of dye tracer experiments simultaneously with current measurements in a prototype bay, an independent determination of diffusion coefficients was made and then compared with the numerically determined values. Validation of the

numerical scheme will allow for a logical extension of existing instrumentation to elucidating information regarding physical processes that drive transport phenomena in surface waters, given the current state of the art in current measurements (Kelly et al., 2002; Kelly et al., 2003). The second objective is to determine the effect of variable geomorphology and meteorological conditions on diffusivity values and the third objective is contributing to the available data on the diffusive process and particularly those for Corpus Christi Bay, Texas.

This work is important in light of ongoing efforts within our research laboratory to develop an Integrated Environmental and Oceanographic Assessment System (IEOAS) for the nearshore environment (Ojo and Bonner, 2004). The scheme couples real-time oceanographic observations with a numerical model (Ernest et al., 1991; Lee et al., 2000; Sterling et al., 2004a; Sterling et al., 2004b) to facilitate complete spatial-temporal characterization of surface waters with emphasis on bays and estuaries.

Methods and Materials

Site selection within the study area as well as timing of the experiments was to facilitate the establishment of varying experimental conditions in order to determine whether there exists a spatial-temporal variation in diffusivity values with respect to meteorological and geomorphologic variation. Several testing and preliminary runs were performed within Corpus Christi Bay as part of the data acquisition equipment development process, prior to the actual series of dye releases. Three dye releases were subsequently carried out for the actual studies during which known amounts of

Rhodamine WT dye were released at different locations and at different times in the tidal cycle.

The dye patch was followed for the duration of the experiment and repeatedly sampled for fluorescence at a rate of ~1 Hz. Subsequent data processing allowed reconstruction of the concentration profile from which the computations described in the Methods section were performed. Simultaneous readings of the 3-D currents field were obtained with the ADCP. The instrumentation as well as data acquisition software and hardware are described in this section. Also described is the method of data analysis (pre-processing and post-processing).

Study Site

The study sites for the field data acquisition were located within Corpus Christi Bay as described in Chapter I with the bathymetry as shown in Figure 1.2 which also shows the approximate locations of the two study sites. The Texas A&M University – Corpus Christi operates and maintains environmental and meteorological stations at these locations (Kelly et al., 2004; Kelly et al., 2003) and these stations were sited because of their proximity to identifiable flux points within the bay. Instruments and sensors on these platforms provided complimentary data during these experiments as well as a visual reference for the origin of the dye application. Each one of the three studies have been assigned a reference number as indicated in Table 5.1 which also presents information relating to the actual dye release. During studies 0828_1 and

0828_2, 1000 g of 20% dye were released on each occasion while 4000 g of 20% dye was released during study 1007.

Table 5.1. Experimental and meteorological conditions for dye diffusion experiment.

ID	Location	Date	Time (UTC)	Duration (mins)	Sal. (psu)	Water Temp. (ºC)	Tide	Wind
0828_1	2747.937N, 9721.451W	Aug. 28, '03	15:44	138	33	30	High water, ebb	7 kn, SE
0828_2	2743.571N, 9718.297W	Aug. 28, '03	21:20	104	32	30	High water, ebb	14 kn, SE
1007	2747.937N, 9721.451W	Oct. 07, '03	14:34	145	25	26	High water, flood	4-12 kn, NE

Instrumentation

The diffusing dye patch during each experimental run was monitored over a period using a towed instrument array consisting of a fluorometer (SAFIRE from WET Labs, Inc., Philomath, OR, USA), a CTD sensor (FastCat from Sea-Bird Electronics, Inc., Bellevue, WA, USA) and a particle size analyzer (LISST-100 from Sequoia Scientific, Inc., Bellevue, WA, USA). These instruments formed part of a suite of oceanographic and environmental sensors that also included an Acoustic Doppler Current Profiler (ADCP from RD Instruments, Inc., San Diego, CA, USA). Fluorescence measurements were obtained with the SAFIRE, a combination spectrophotometer and spectrofluorometer exciting the target at six discrete wavelengths while sensing discrete levels of 6 absorptive and 16 emission (fluorescence) wavelengths. Instrument

calibration established excitation/emission wavelengths for Rhodamine WT dye at 487/620 nm for this instrument and a working range of 100-1500 ppb corresponding to ~650-32000 raw counts of fluorescence.

The instrument array was towed at a constant depth of ~1 m below the water surface, the depth being maintaned by the control system of the undulating tow body, a Seasciences Acrobat (Seasciences, Inc. USA) tow body. Calibration parameters were applied to the raw fluorescence counts by the data acquisition computer for conversion to concentration units. In addition to the fluorometric data, salinity and temperature measurements were obtained with the FastCat while current measurements were obtained with the ADCP throughout the duration of each of the experiments. The duration of the experiments were determined by the instrument detection limits and the extent of the dye plume that can be sampled at the towing speed of the instrument platform.

Data Acquisition

Fluorescence and auxiliary measurements from the subsurface instruments was facilitated through a software interface developed in our laboratory for conducting environmental and oceanographic assessments in surface waters (Ojo et al., 2003b; Ojo et al., 2002). The Multi-Parameter Instrument Array and Control System, MPIACS software interface provided real-time data visualization of fluorescence, salinity, temperature and volume concentration of particulates simultaneously by geo-referencing the instrument raw data through a data acquisition GPS unit. Visual indications of the

spatial distribution and the intensity for each constituent of interest or sampled parameter guided the sampling efforts through color-coded tracklines representing low to high levels of concentration.

The spatial resolution achievable was dependent on the data rate of the GPS employed (typically 1 Hz) and the travel speed of the tow body (~3 m/s). The GPS unit was run in the auto-selection mode during this exercise, allowing the unit to operate in GPS, DGPS (dynamic GPS) or WAAS (wide area augmentation system) mode, depending on service availability. The accuracy of the GPS varies with the mode: DGPS mode (accuracy is within 1 m), WAAS mode (5 m), or GPS mode (10 m). Under this set of conditions, a spatial sampling resolution of ~3-10 m was achieved.

Data Analyses

The coefficients required in the advection-diffusion equation of transport can be obtained from studies using passive tracers such as fluorescent dyes for short time scale studies or radioactive gases for longer time scales on the order of weeks (Clark et al., 1996; Ledwell, 1991). Any one of two well-established methods can be used for analyzing the concentration data in order to deduce the required coefficients. First is the method of moments using statistical regression analyses and the second method essentially is an inverse formulation of the underlying equations using optimization schemes. Both methods rely on data obtained from the observed concentration profile of a diffusing cloud of tracer. In this study, fluorometric measurements were obtained from a diffusion dye patch of Rhodamine WT on time scales ~10^4 s, which corresponds to the

early stages of the diffusion process. Following is a review of two of the commonly used methods in dye-tracer studies and provides a background for selecting the most appropriate method for achieving the stated objectives.

Method A

With this method, complete homogeneity within the patch is assumed and the approach is to consider the variance in orthogonal directions separately also assuming the diffusive processes along those directions to be acting independently from each other. The diffusivity values are then computed from the time rate of change of the variance. This requires the evaluation of the diffusing cloud at successive time intervals. One may choose to simplify the analysis by assuming a radially symmetric patch for which an equivalent radius is obtained and then computing the variance based on the equivalent radius. A two-dimensional (2-D) concentration profile from the observed fluorescence data will be sufficient in computing the horizontal diffusivity values or even an evaluation of the centerline concentration along each axis will be adequate.

In general, a power-law relationship exists between the variance, S_i^2 of a diffusing cloud and the diffusion time, t the elapsed time since release (Murthy, 1975)

$$S_i^2 = at^m \qquad (5.1)$$

The values of *a* and *m* are obtained from a log-log plot of the time evolution of observed variance of the diffusing dye patch from which, assuming homogeneity in the concentration distribution within the patch,

$$K_i = \frac{1}{2}\frac{dS_i^2}{dt} \tag{5.2}$$

$$K_i(S_i) = \frac{m}{2} a^{1/m} S_i^{2(1-1/m)} \tag{5.3a}$$

$$K_i(S_i) = qS_i^p \tag{5.3b}$$

for $i = x, y$ corresponding to the x, y coordinate axes, $q = (m/2)a^{1/m}$ and $p = 2(1-1/m)$. From lake studies, Murthy determined that the value of *m* lies between two and three and for practical purposes, models of diffusion based on equation (5.3b) and different values of *m* can be developed as summarized in Table 5.2. Equations (5.3a), (5.3b) express the dependence of diffusivity, K_i on the length-scale of diffusion, L_i generally taken as $3S_i$ and the following expressions relate properties needed for the evaluation of K_i to the concentration profile *c(x,y,z,t)*:

$$M_o = \int_{-\infty}^{\infty}\int\int c(x,y,z,t)\,dx\,dy\,dz \tag{5.4}$$

Table 5.2. Diffusion models prescribed on the basis of parameter *m*.

m	p	Diffusion Properties		
		Law	Parameter	Model
1	0	K = constant		Fickian
2	1	$K = qL$		Linear length scale
3	4/3	$K = \varepsilon^{1/3} L^{4/3}$		Inertial sub-range

$$x_o = \frac{1}{M_o} \int_{-\infty}^{\infty} \iiint xc(x,y,z,t)\,dxdydz \tag{5.5a}$$

$$y_o = \frac{1}{M_o} \int_{-\infty}^{\infty} \iiint yc(x,y,z,t)\,dxdydz \tag{5.5b}$$

$$S_x^2(t) = \frac{1}{M_o} \int_{-\infty}^{\infty} \iiint (x - x_o)^2 c(x,y,z,t)\,dxdydz \tag{5.6a}$$

$$S_y^2(t) = \frac{1}{M_o} \int_{-\infty}^{\infty} \iiint (y - y_o)^2 c(x,y,z,t)\,dxdydz \tag{5.6b}$$

Equations (5.4) - (5.6) represent the zeroth, first and second moments corresponding to the total mass, the center of mass and the variance of the diffusing dye patch respectively. These are used along with equation (5.3) in obtaining the effective diffusivity along the respective coordinate axes. For a two-dimensional dye patch the

equivalent variance, S_r^2 of a radially symmetric patch can be found using equation (5.7a) while the equivalent variance, S_{xy}^2 of an elongated patch is given by equation (5.7b),

$$S_r^2 = 2S_x S_y \tag{5.7a}$$

$$S_{xy}^2 = S_x^2 + S_y^2 \tag{5.7b}$$

Given the analytical solution of the advection-diffusion equation (with constant diffusivities values, K_x, K_y, K_z) in three dimensions relating the concentration profile $c(x, y, z, t)$ from an instantaneous point discharge M_o,

$$c(x,y,z,t) = \frac{M_o}{8(\pi)^{3/2}(K_x K_y K_z)^{1/2} t^{3/2}} \exp\left[-\frac{1}{4}\left\{ \frac{(x-u_x t)^2}{K_x t} + \frac{(y-u_y t)^2}{K_y t} + \frac{(z-u_z t)^2}{K_z t} \right\} \right] \tag{5.8}$$

the concentration at the center-of-mass of the dye cloud can be obtained from,

$$c(x_o, y_o, z_o, t) = \frac{M_o}{8(\pi)^{3/2}(K_x K_y K_z)^{1/2} t^{3/2}} \tag{5.9}$$

where at time, t the center-of-mass of the dye cloud traveling with velocity, $\boldsymbol{v}(u_x, u_y, u_z)$ will be located at coordinates (x_o, y_o, z_o) relative to the origin of the point discharge. The

expression in (5.9) is of the form $at^{-3/2}$ having a straight line fit on a log-log plot of observed peak concentration against time provided K_x, K_y, K_z are constants. An estimate of the velocity, $\boldsymbol{v}$ can therefore be obtained from the displacement of the center-of-mass of the diffusing cloud relative to the origin over successive time intervals.

Method B

This method is based on the governing equation of transport. Written for a single conservative substance and using 2-D depth integrated concentration observations from fluorescence,

$$\frac{\partial c}{\partial t} = -\frac{\partial}{\partial x}\left(u_x c\right) - \frac{\partial}{\partial y}\left(u_y c\right) + \frac{\partial}{\partial x}\left(K_x \frac{\partial c}{\partial x}\right) + \frac{\partial}{\partial y}\left(K_y \frac{\partial c}{\partial y}\right) \qquad (5.10)$$

where over the depth range $z = [0, h]$, $c = \int_0^h c(x, y, z, t)dz$ is the depth integrated concentration profile assuming homogeneity in the vertical and u_x, u_y are the horizontal velocity components of the currents field. Using a forward time, central space (FTCS) finite difference approximation on a spatial [j x k] -temporal [x n] grid, equation (5.10) above can be written as a discretized algebraic equation (DAE). The localized values for u_x, u_x, K_x and K_y will be taken as constant in this representation.

$$\frac{\Delta c_{j,k}^{n+1}}{\Delta t} = -u_x \frac{c_{j+1,k}^n - c_{j-1,k}^n}{2\Delta x} - u_y \frac{c_{j,k+1}^n - c_{j,k-1}^n}{2\Delta y} + K_x \frac{c_{j+1,k}^n - 2c_{j,k}^n + c_{j-1,k}^n}{\Delta x^2} + K_y \frac{c_{j,k-1}^n - 2c_{j,k}^n + c_{j,k+1}^n}{\Delta y^2} \tag{5.11}$$

Equation (5.11) can be written in matrix form as follows:

$$\frac{\Delta c_{j,k}^{n+1}}{\Delta t} = \begin{bmatrix} \frac{-u_x}{2\Delta x} & \frac{-u_y}{2\Delta y} & \frac{K_x}{\Delta x^2} & \frac{K_y}{\Delta y^2} \end{bmatrix} \begin{bmatrix} c_{j+1,k}^n - c_{j-1,k}^n \\ c_{j,k+1}^n - c_{j,k-1}^n \\ c_{j+1,k}^n - 2c_{j,k}^n + c_{j-1,k}^n \\ c_{j,k+1}^n - 2c_{j,k}^n + c_{j,k-1}^n \end{bmatrix} \tag{5.12a}$$

$$\boldsymbol{r} = \boldsymbol{SC} \tag{5.12b}$$

$\boldsymbol{r}$ is evaluated as the time rate of change of concentration at a node (j, k) on the spatial grid having a concentration, $c_{j,k}$ at time-step n; $\boldsymbol{S}$ is a matrix of coefficients and $\boldsymbol{C}$, a matrix of concentration differentials evaluated at surrounding node points. This formulation of an unsteady advection-diffusion transport with appropriate boundary-conditions (B.C.) and forward-stepping with time has a truncation error of $O(\Delta t, \Delta x^2, \Delta y^2)$ the time-step, Δt and B.C. being selected appropriately.

The matrix in (5.12) can be inverted in order to evaluate the coefficient matrix, $\boldsymbol{S}$ from observed concentration matrix, $\boldsymbol{C}$ in a least-squares sense, Δt being determined by the time interval between observations.

$$\boldsymbol{S} = \boldsymbol{rC^{-1}} \tag{5.13}$$

Using optimization techniques, both the diffusivity values and velocity field can be obtained and if the velocity field is known, diffusivity values alone will be obtained. Since the objective of this study is the validation of a numerical scheme developed for the evaluation of diffusivity from the velocity field, *Method A* is the preferred method as it allows the determination of characteristics of the evolving dye-patch for comparison with existing data on the process of diffusion viz. center of mass, variance, and diffusion length scale.

Primary data used in this study consisted of the geo-referenced fluorescence measurements representing concentration distribution of the Rhodamine dye. The concentration profiles were accurately reconstructed for the diffusing patch of dye at successive time intervals using the time and location stamp from each data point. The observed fluorescence measurements in raw counts were first converted to actual concentration (in ppb) by applying predetermined calibration parameters for the fluorometer. These concentration values were corrected for background fluorescence, which can be relatively high in Texas waters (Ward, 1985). Objective analysis was subsequently performed on these converted, background corrected measurements to obtain 2-D concentration profiles of the dye over uniform grid spacing at successive time intervals. Finally the expressions in equations (5.4) – (5.6) were applied to the uniformly gridded datasets, producing the variance, S_i^2 ($i = x, y$) from which plots of S_i^2 against

time were generated leading to the computation of diffusivity, K_i ($i = x, y$) from using equation (5.2).

Results

Results from two of the dye-tracer experiments conducted are presented in this section. The time series of the dye concentrations returned by the fluorometer for studies 0828_2 and 1007 are shown in Figure 5.1 while the peak concentrations against time using log-log plots as expressed in equation (5.9) are shown in Figure 5.2. Reconstructed dye-tracer patches (at successive time intervals) and a log-log plot of the variance against diffusion time are shown in a series of isopleths in Figure 5.3 and Figure 5.4 respectively from study 0828_2. Similarly, for study 1007, reconstructed dye-tracer patches are shown in Figure 5.5 while the log-log plot of the variance against diffusion time is shown in Figure 5.6. The computed variance at different diffusion times and the characteristics of the diffusing patch are summarized in Table 5.3. From the log-log plots, (Figures 5.4 and 5.6) a trend line was fitted through the actual data points with subsequent application of equation (5.2) for the evaluation of K_i.

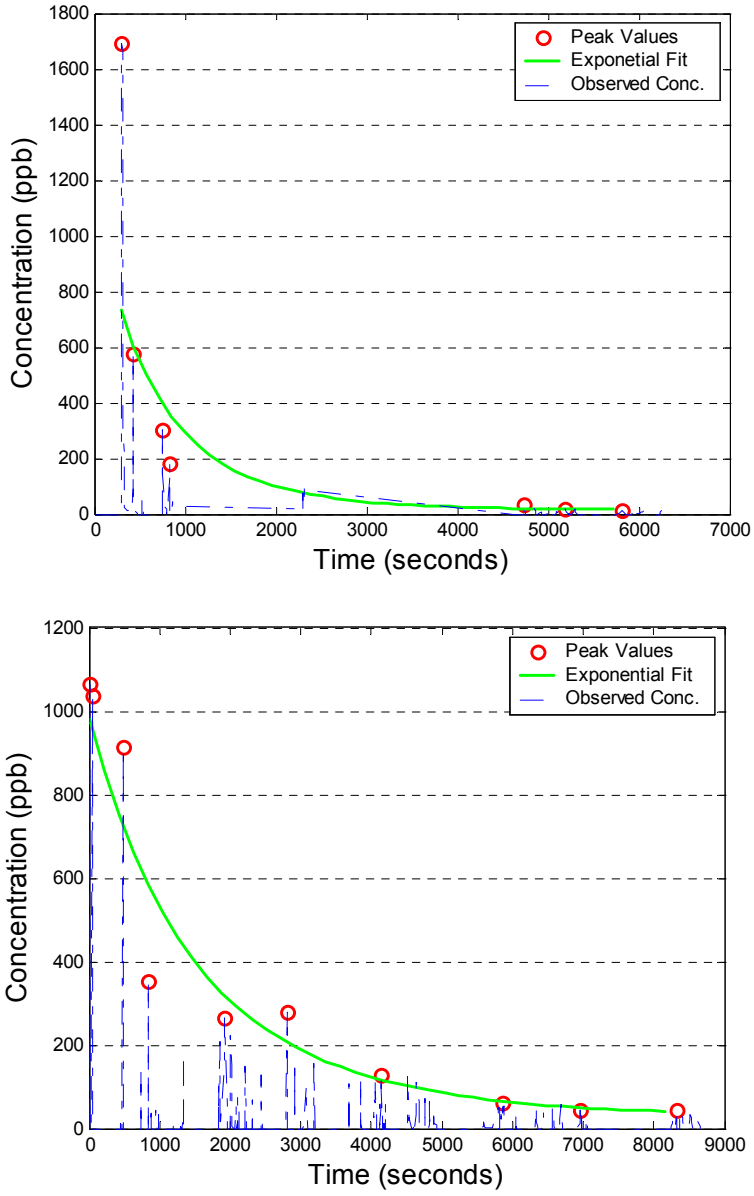

Figure 5.1. Time series of concentration. Solid line (-); observed concentration; dashed line (--) exponential fit to observed data; open circle (o) peak concentration (approx. center of mass). Top, study 0828_2; bottom, study 1007.

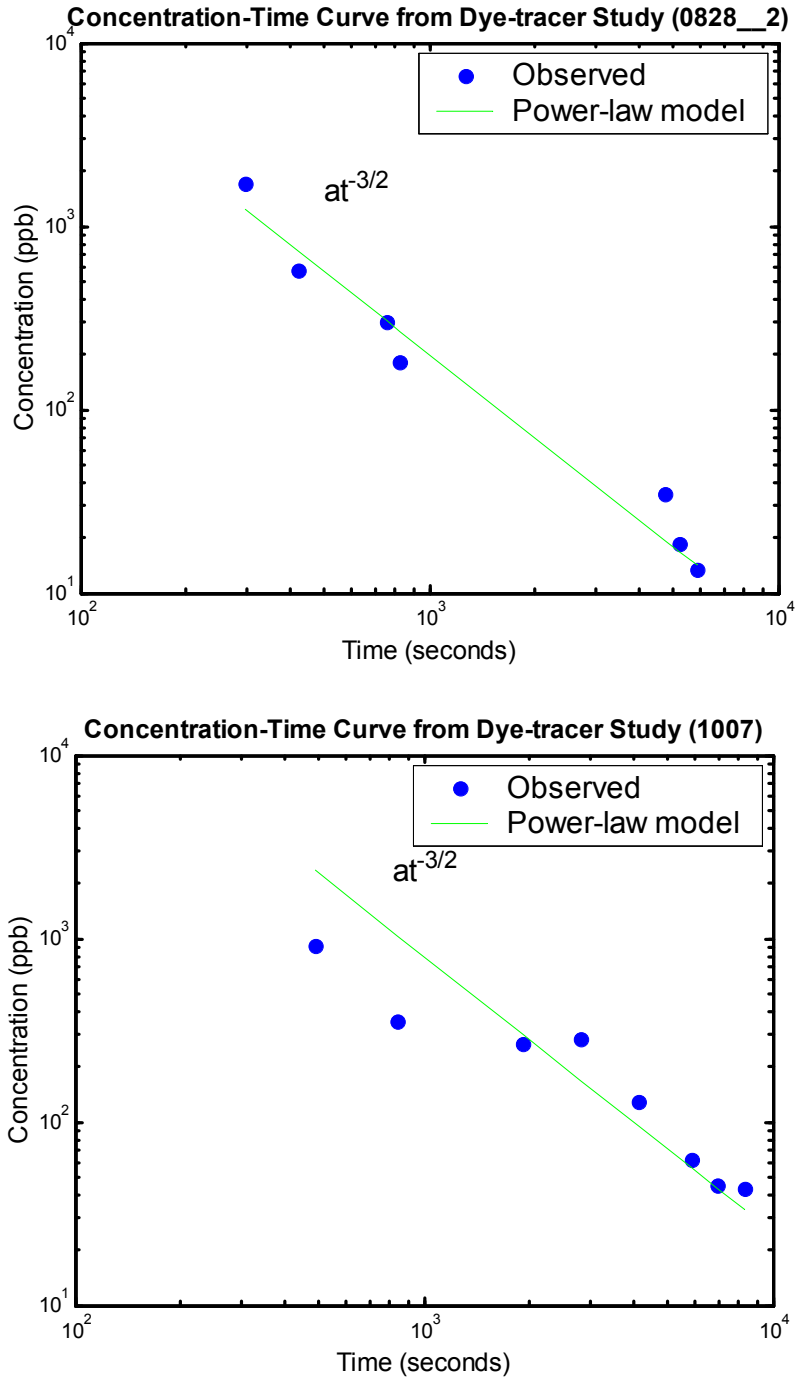

Figure 5.2. Time series of fluorescence values from tracer experiments. Temporally localized peaks show the declining maximum concentration values during each leg of the several crossing made through the dye patch. 2nd order exponential (--*--) curve-fit through the localized peaks.

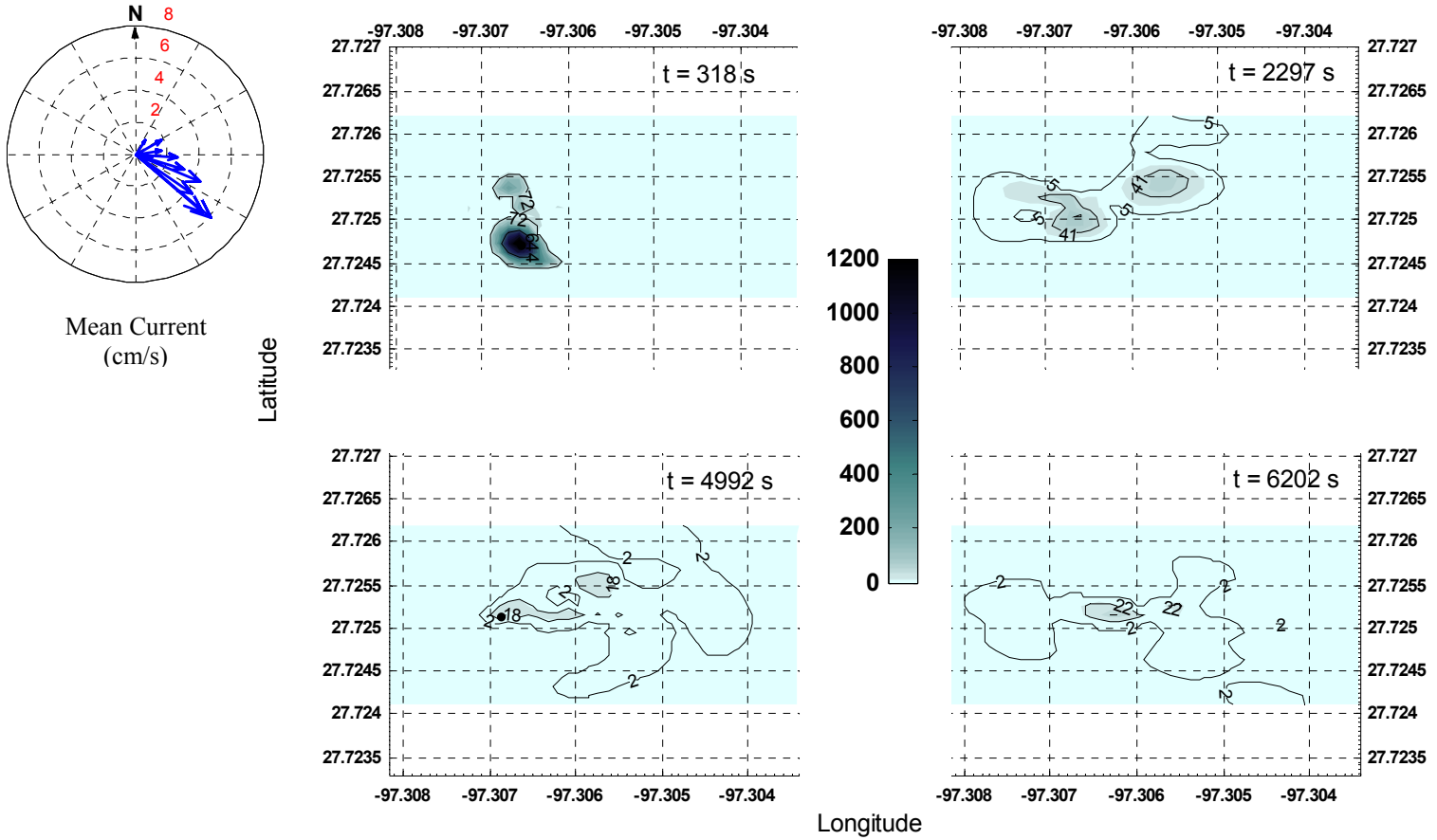

Figure 5.3. Contour plots of reconstructed dye concentration profile at successive time intervals from study 0828_2. The current structure from ADCP measurements is shown upper left.

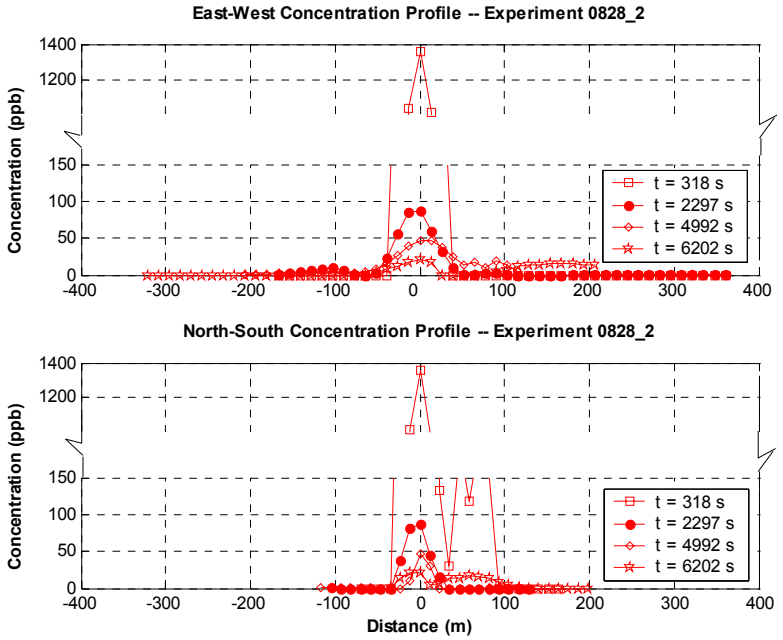

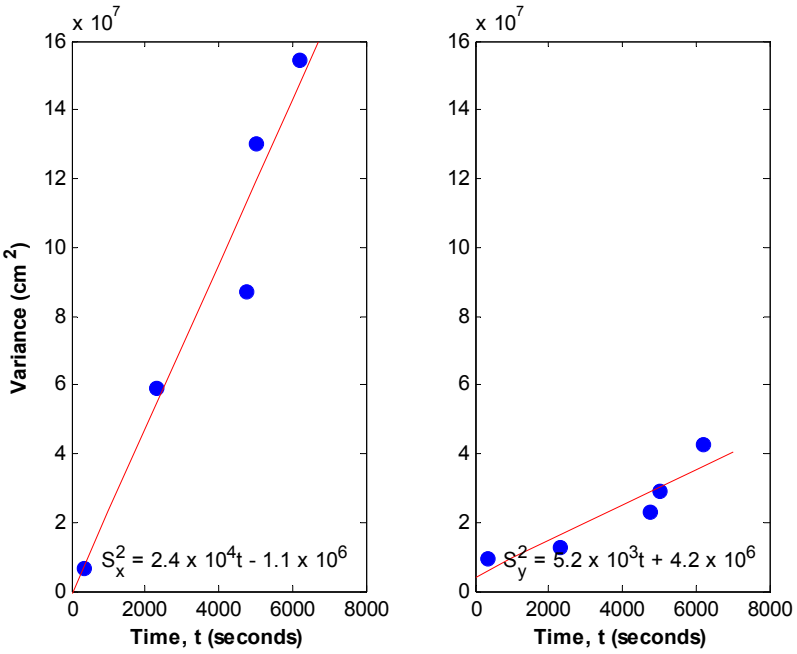

Figure 5.4. Top panel; centerline concentration distribution from study 0828_2. Bottom; variance time plots from concentration profile (S^2_x – east-west, S^2_y – north-south). Regression line fitted to observed data with r^2 = 0.94 and 0.87 respectively.

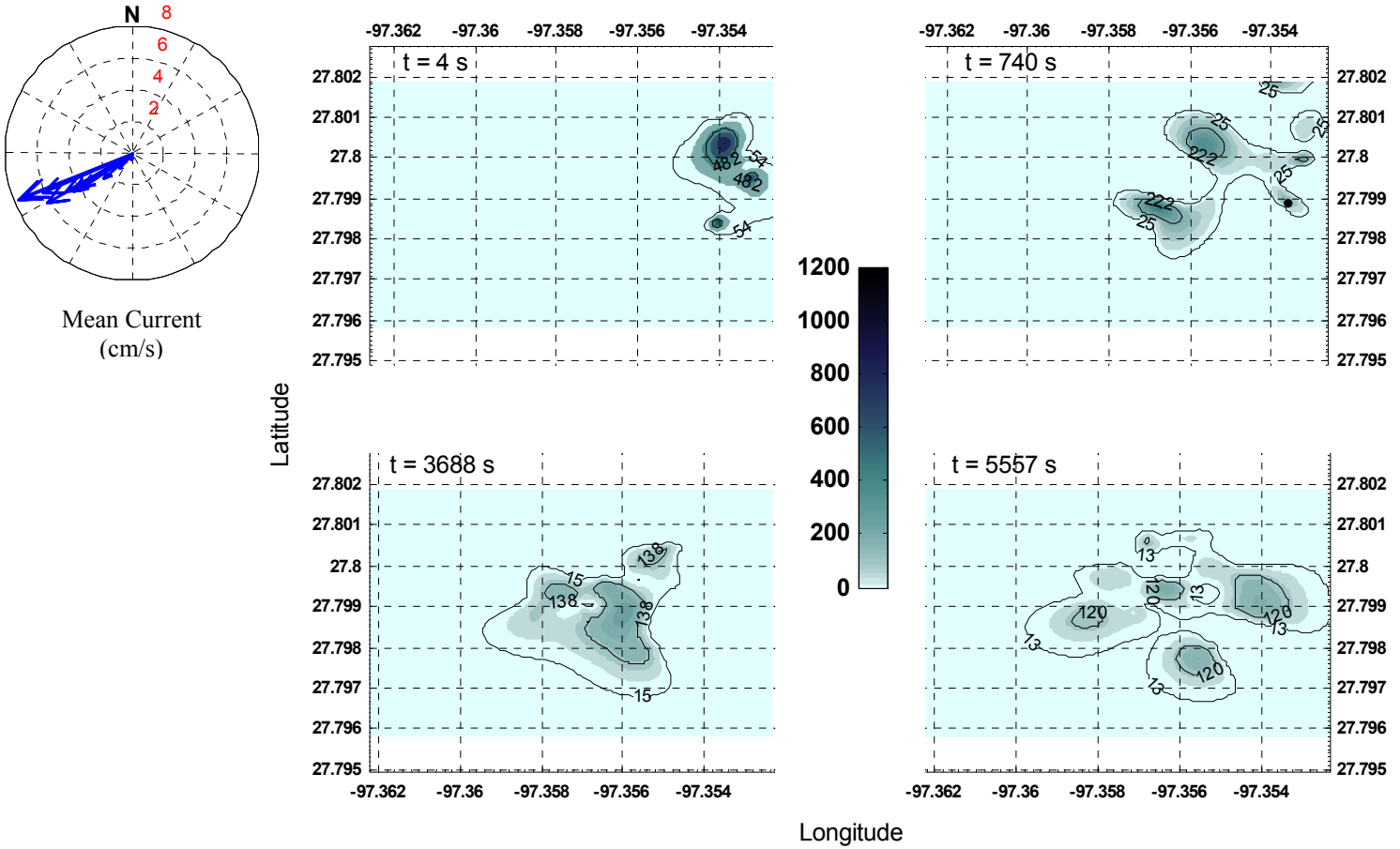

Figure 5.5. Contour plots of reconstructed dye concentration profile at successive time intervals from study 1007. The current structure from ADCP measurements is shown upper left.

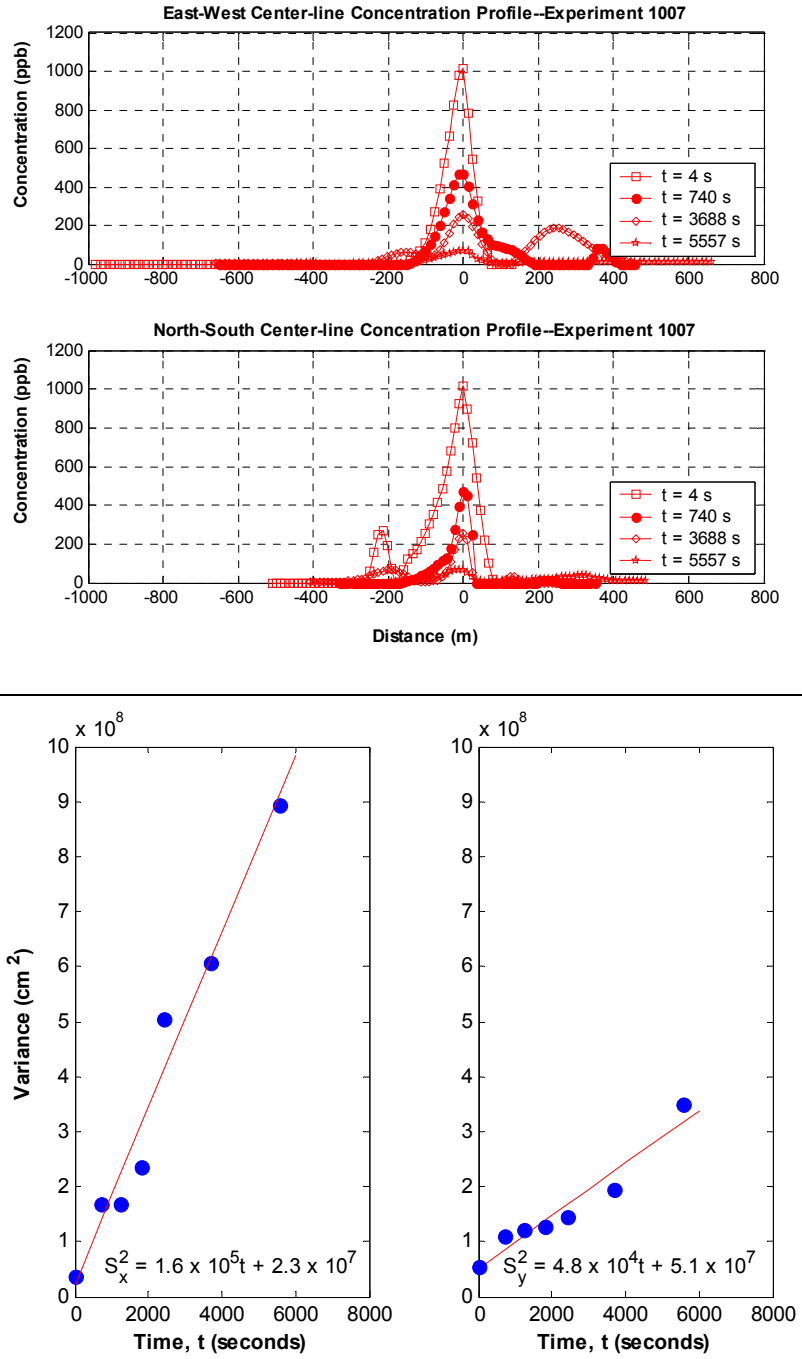

Figure 5.6. Top panel; centerline concentration distribution from study 1007. Bottom; variance time plots from concentration profile (S^2_x – east-west, S^2_y – north-south). Regression line fitted to observed data with r^2 = 0.97 and 0.94 respectively.

Table 5.3. Summary of dye patch characteristics.

Diffusion Time (s)	S^2_x (cm^2) x 10^6	S^2_y (cm^2) x 10^6	Computed Diffusivity x 10^4 (cm^2/s)		Dye Patch		
			K_x	K_y	S^2_r (cm^2) x 10^6	C.G.	
						Lat.	Lon.
318	6.75	9.69			16.44	27.7248	-97.3065
2297	59.05	12.90			71.95	27.7253	-97.3062
4726	87.42	23.39	1.2	0.25	110.81	27.7253	-97.3056
4992	130.09	29.20			159.29	27.7251	-97.3059
6202	154.52	42.82			197.34	27.7251	-97.3057

Variance S_i, at successive time intervals used in the evaluation diffusivity K_i; study 0828_2

Diffusion Time (s)	S^2_x (cm^2) x 10^6	S^2_y (cm^2) x 10^6	Computed Diffusivity x 10^4 (cm^2/s)		Dye Patch		
			K_x	K_y	S^2_r (cm^2) x 10^6	C.G.	
						Lat.	Lon.
4	37.45	55.04			92.49	27.7998	-97.3538
740	167.93	110.78			278.71	27.7996	-97.3556
1227	167.22	119.99			287.21	27.7998	-97.3554
1836	234.92	126.87	8.0	2.4	361.79	27.7996	-97.3560
2436	503.45	145.60			649.05	27.7987	-97.3567
3688	607.62	195.82			803.44	27.7988	-97.3560
5557	892.35	350.71			1243.06	27.7989	-97.3573

Variance S^2_i, at successive time intervals used in the evaluation diffusivity K_i; study 1007

The contour plots in Figures 5.3 and 5.5 were reconstructed from the individual transects through the evolving dye patch. The profiles indicate a northeasterly trajectory for the diffusing dye cloud during study 0828_2 and a southwesterly trajectory can be deduced from study 1007. The contour plots indicate the lack of homogeneity within the dye patches, which may be due to the entrainment of clear water from repeated crossings made by the survey boat. In some cases, bifurcation of the dye patch may result but generally, recovery would occur after a short period.

In Figure 5.2, the plot of peak concentration against time was fitted to a power law plot logarithmic scale. A straight line "best-fit" through the points with slope of –3/2 is suggestive, according to equation (5.11) of constant diffusivities and one would expect to observe linear growth of the variance of a diffusing cloud with time. The diffusivity values so computed using the method of moments as outlined here were found to be $\sim 10^3$ cm^2/s ($r^2 = 0.87$) in the north-south direction and $\sim 10^4$ cm^2/s ($r^2 = 0.94$) in the east-west direction for study 0828_2. These figures were found to be approximately 10 times higher during study 1007 ($r^2 = 0.94$ and 0.97 respectively) but in general, the growth of the dye patch measured by the change in variance over time was indeed found to be linear within the time scale of the experiment during both studies. This would suggest that the diffusion process follows a Fickian model with constant diffusivities.

Discussion

The dye diffusion experiments described in this paper are part of a study aimed at elucidating information on diffusion coefficients in surface waters from hydrodynamic

measurements. Ancillary data provided during the experiments as environmental and oceanographic variables are presented in Figures 1.3 and 1.4 including wind speed, water level and current measurements. In separate but related studies, a set of numerical schemes had been developed for calculating diffusion coefficients based on Taylor's analyses on turbulent and shear flow in pipes and extended to surface waters but these schemes needed to be validated. These dye tracer experiments were conducted at different locations within Corpus Christi Bay and at different times during the tidal cycle and designed to determine the differences in the diffusion process that may result from variability in geomorphological and meteorological conditions.

The diffusivities derived from these tracer experiments, when compared with those obtained using numerical methods and current measurements taken with the ADCP, were found to be in close agreement. Two different diffusion regimes were identified from these experiments, one due to turbulence and the other attributable to shear current. In the presence of vertical shear current structure, the process of turbulence is significantly augmented and the entire diffusion process becomes dominated by shear. This shear-augmentation was observed during study 1007 with the computed diffusivities being approximately one order of magnitude higher along each of the coordinate axes compared with corresponding values determined from the other two studies. This same phenomenon, as observed by other researchers from experiments conducted in different bodies of water has implications regarding the value of the diffusion coefficient being dependent on prevailing meteorological and oceanographic conditions.

In Figure 5.7, the results of these dye-tracer experiments were compared with those obtained by other researchers who had conducted similar experiments in various bodies of water. The plot is a log-log plot of variance against time of an equivalent symmetrical patch represented in equation (5.7a). Okubo's data was fitted to an expression of the form

$$S_r^2 = 0.011t^{2.34} \tag{5.14}$$

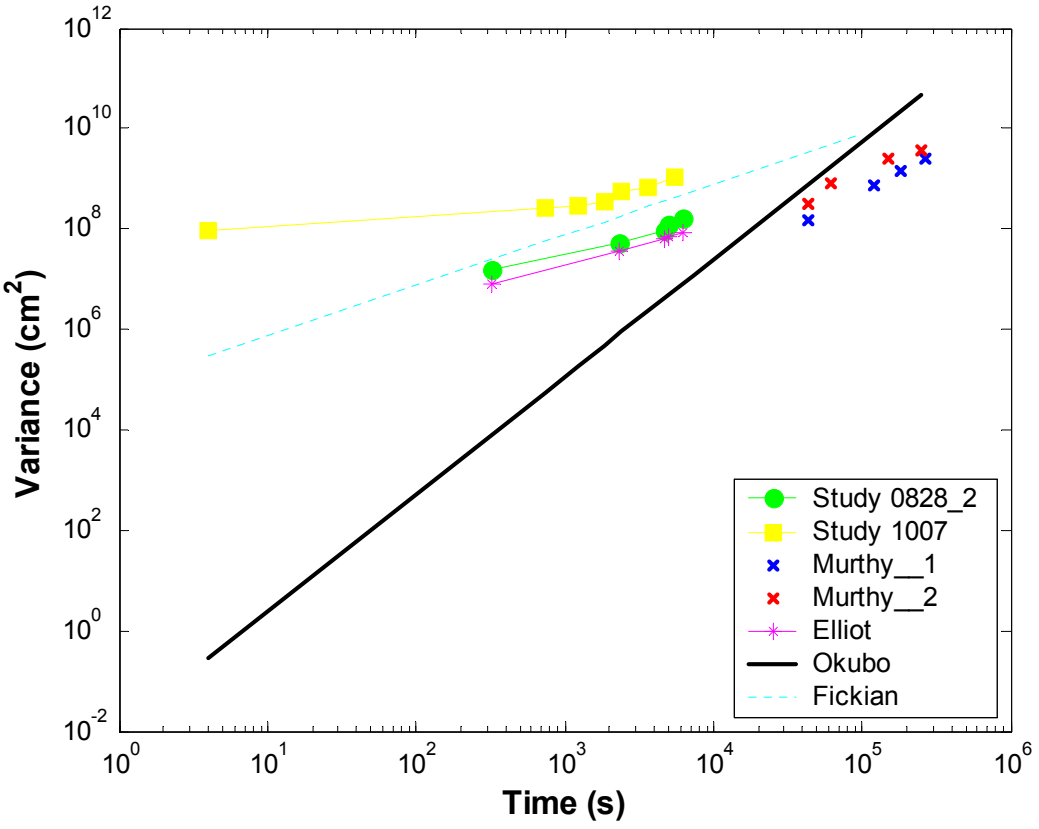

Figure 5.7. Comparison between results of experiments conducted in Corpus Christi Bay and those obtained by Murthy in Lake Ontario and Elliot from coastal waters around Ireland. Okubo's data were from numerous studies conducted from around the world. Fickian diffusion is also presented for comparison.

As shown in Figure 5.7, this underestimates the size of a diffusing cloud at smaller time scales and overestimates the cloud size at longer time scales. The data obtained by Murthy from studies conducted in Lake Ontario, although outside of the temporal scale of the experiments conducted for Corpus Christi Bay, generally follows the same trend in terms of the growth of the cloud. Elliot's data taken from Donegal Harbour in Ireland, a near-shore environment with water depth similar to Corpus Christi Bay shows very good agreement with the data obtained during study 0828_2. Murthy's data was fitted to an expression of the form

$$S_r^2 = 2.4t^{4/3} \tag{5.15}$$

while Elliot's data was fitted to an expression of the form

$$S_r^2 = 7.65t^{4/5} \tag{5.16}$$

Data from studies 0828_2 and 1007 was fitted to an expression of the form

$$S_r^2 \propto t^{3/4} \tag{5.17}$$

the constant of proportionality being 5.4 and 6.1 for study 0828_2 and 1007 respectively. In general, most of the data tend toward the Fickian form ($S_r^2 \propto t$) with linear growth

rate as represented in Figure 5.7, particularly in those early stages of diffusion and at a temporal scale of ~72 hours.

Through these experiments, diffusivity values were determined for Corpus Christi Bay on a temporal scale of 0-2 hours and a corresponding length scale of 10-1000 m hours following an instantaneous discharge of a conservative neutrally buoyant material. Ward's experiments within the vicinity of this water body, although in a shallower part of the bay but on the same temporal scale, showed similar results. The diffusion coefficients he reported were lower than the ones presented in this study but demonstrated similar trends. Thus, this study contributes to existing data on diffusion processes within Corpus Christi Bay and provides supporting data for numerical methods developed for analyzing diffusion coefficients.

In conducting these experiments, the entrainment of unmarked fluid due to numerous crossings of the survey vessel might have contributed to the lack of homogeneity within the dye patch. As the diffusion process progressed, the accuracy of the fluorescence measurements decreased especially against the backdrop of the high background fluorescence encountered and the detection limit of the instrument. Although this had a bearing on the duration of the experiments, the temporal scale of these experiments coincide with the period of sharp gradients following a pulse discharge and may be very important from an ecological standpoint. The data obtained sheds light on the applicability of numerical methods developed for obtaining diffusivities from current measurements viz. the development of operational numerical models for ecological monitoring and emergency response activities. The stability of the

water column as it affects persistence of turbulence and the onset of shear diffusion is generally assumed for the application of turbulence closure schemes in operational circulation models and with the observation made here that shear does not always prevail, may lead to under-prediction of the concentration values for constituents of interest.

This has been a limitation for many of the circulation and transport models that employ the so-called turbulence closure schemes for evaluation of diffusivities in that not enough data exist combining concentration profiles and current measurements. More experiments of the type described here will be required in order to assemble this type of information. With this study and the related numerical schemes developed and reported elsewhere, we have demonstrated the usefulness of 3D current measurements beyond that of oceanographic and/or hydrographic surveys. The tools developed as a result of this study will be very useful within the context of environmental monitoring, allowing the extension of existing or development of new instruments on the basis of these numerical schemes, into applications such as environmental assessments, spill monitoring, emergency response and the likes.

Future Work

It will be necessary to determine the conditions under which shear diffusion dominates over turbulence. The collection of available data on variance with time for various water bodies in the nearshore environment for the generation of a diffusion diagram similar to Okubo's oceanic diffusion diagrams is useful as a first approximation

in predicting diffusion but has limited application. This makes the method of elucidating diffusivities from current measurements particularly attractive since these measurements are routinely made during oceanographic and hydrographic surveys. It is recommended that experiments such as the one described here that combines dye tracer measurements with current data under different meteorological conditions be conducted with a view to developing nomograms that can be applied within the framework of operational numerical schemes for environmental and oceanographic assessments. These charts will be similar to those prescribed for application in the Pasquill-Gifford (Pasquill, 1962) atmospheric dispersion plume model.

CHAPTER VI

SIMULATION OF CONSTITUENT TRANSPORT USING A REDUCED 3D CONSTITUENT TRANSPORT MODEL (CTM) DRIVEN BY HF RADAR: MODEL APPLICATION AND ERROR ANALYSIS

Overview

This chapter discusses a numerical method of estimating diffusion coefficients in anisotropic flow fields and examines, through model error analysis, the effects of using spatially variable coefficients on model predictions. A data-driven constituent transport model (CTM), which relies on surface current measurements from High Frequency (HF) Radar and can be applied within the context of real-time monitoring, nowcasting and emergency response was developed. Error analyses was performed by determining normalized model errors with varying cell Reynolds number, $\boldsymbol{Re} = f(\boldsymbol{u},\boldsymbol{K},\Delta\boldsymbol{x})$ from 0.15-100. Two instantaneous releases were modeled, the model being initialized at two different locations within the domain and there was a marked difference in the predicted spatial extent of the conservative material, this difference being attributable to the spatial variation in diffusivities within the study area. A scheme that allows for the evaluation of the diffusivities (a measure of spread) was developed and incorporated into a data-driven CTM, which was then applied (within the framework of constituent tracking) to Corpus Christi Bay in the Texas Gulf of Mexico region.

Introduction

Mixing processes (turbulence and shear) in surface waters are important as they govern the overall distribution of constituents within the domain of interest, constituents including biogenic and anthropogenic materials. In conjunction with sampling and measurements, constituent transport modeling (CTM) can be a valuable tool for environmental assessments, forming the bedrock of most water quality and pollutant tracking applications in surface waters. A number of these models have been developed for various applications covering a wide range of spatial and temporal scales. These mechanistic models are based on the solution of coupled sets of partial differential equations (PDEs) comprising two distinct modules viz. hydrodynamic and transport modules. The hydrodynamic module is a set of PDEs, the well-known Navier-Stokes equations based on momentum conservation while the transport module is a set of advection-diffusion-reaction PDEs based on mass conservation laws.

The resulting governing equations of transport can be treated with a Fickian diffusive component provided the scale of the phenomenon is larger than the characteristic scale (time or length) of the diffusion process. This derives from the material balance in turbulent flow within an elemental fluid volume accounting for the turbulent fluctuations in the currents field as well as the constituent of interest. The resultant rate of change of solute concentration for conservative materials consists of two additive parts, the advective flux and the diffusive flux. This argument although developed within the context of turbulence can be extended to include other effects that are known to influence diffusive processes such as current shear (Bowden and Howe,

1963; Elliot, 1986). Since the turbulent field in bays exhibits anisotropy, one would expect to find the diffusive process characterized by the diffusivity values also exhibiting spatial-temporal variability (Ojo and Bonner, 2002).

From the foregoing, two sets of coefficients are required in the governing equation of transport; the advection coefficients (velocity) and diffusion coefficients. The former being provided either through direct observations or through direct numerical simulation (DNS) as outlined above while the latter can be estimated using any one of the four methods outlined below, the first three having been applied in a series of related studies within Corpus Christi Bay (Ojo et al., 2004a; Ojo et al., 2004b, c):

a) From the evaluation of the temporal variation of the magnitude and direction of currents (Paul et al., 1989; Taylor, 1920, 1954);

b) Based on the evaluation of the spatial variation of the velocity field (Csanady, 1980 (reprinted); Elder, 1958; Taylor, 1953);

c) Evaluation of the first and second moments of concentration distribution of a diffusing cloud (Murthy, 1975; Okubo, 1971);

d) Inverse problem based on the governing equation of advection-diffusion (Ernest et al., 1991; Lam et al., 1983).

Considering the spatial extent typical of bays and estuaries, the incorporation of velocity information into a transport model defaults to the DNS method, which couples the hydrodynamic module to the transport module. Although a number of turbulence-closure schemes have been developed, there are still uncertainties inherent in their

application especially within shallow wind-driven bodies of water typical of Texas bays. Following recent advances in surface current measurements using HF radar (Kelly et al., 2002; Kelly et al., 2003), it is possible to incorporate near real-time direct measurements of hydrodynamic data into constituent transport and water quality models. By extension, the diffusion coefficients can be derived from the velocity time-series and this method was applied in this study in a data-driven schema, the diffusivities evaluated based on the statistical properties of the turbulent flow field. Since the radar provides surface currents within the domain of interest, the 3D velocity field for the domain of interest was derived through the inclusion of Acoustic Doppler Current Profiler (ADCP) measurements.

The objectives of this study are:

- Estimate diffusion coefficients based on direct observations of hydrodynamic data on spatial scales ~30 km and temporal scales covering several tidal cycles.
- Incorporate direct hydrodynamic observations and derived turbulent diffusivities into a simplified CTM.
- Examine through model error analysis:
    a. The effects on model predictions resulting from errors associated with current measurements.
    b. The results of using spatially averaged values of diffusion coefficients typically obtained from diffusion diagrams or tracer experiments vs. using spatially distributed values obtained through current measurements as outlined above.

- Apply the resulting simplified data-driven CTM to near real-time constituent tracking in Corpus Christi Bay, Texas.

This is important within the framework of spatial characterization of bays and estuaries as well as response to episodic events in surface waters and is part of ongoing research within our laboratory. This effort is aimed at developing an operational environmental and oceanographic assessment system, combining numerical modeling (Ernest et al., 1991; Lee et al., 2000; Sterling et al., 2004a; Sterling et al., 2004b) with real-time measurements (Ojo and Bonner, 2004; Ojo et al., 2003c).

Background Theory

The generalized form of the governing equations that form a coupled set for a CTM is given below where u, v, w are the component velocities, N_x, N_y, N_z are eddy viscosities, K_x, K_y, K_z are diffusivities along each of the coordinate axis, g is the gravitational constant, ρ is the fluid density, R_i is the source/sink term and C_i the concentration of the i^{th} constituent.

Continuity :

$$\frac{\partial u}{\partial x}+\frac{\partial v}{\partial y}+\frac{\partial w}{\partial z}=q$$

Momentum x Direction :

$$\frac{\partial u}{\partial t}=-\frac{\partial(uu)}{\partial x}-\frac{\partial(vu)}{\partial y}-\frac{\partial(wu)}{\partial z}+\frac{\partial}{\partial x}\left[\left(\nu+\frac{N_x}{\rho}\right)\frac{\partial u}{\partial x}\right]+\frac{\partial}{\partial y}\left[\left(\nu+\frac{N_y}{\rho}\right)\frac{\partial u}{\partial y}\right]+$$

$$\frac{\partial}{\partial z}\left[\left(\nu+\frac{N_z}{\rho}\right)\frac{\partial u}{\partial z}\right]+g_x$$

Momentum y Direction :

$$\frac{\partial v}{\partial t}=-\frac{\partial(uv)}{\partial x}-\frac{\partial(vv)}{\partial y}-\frac{\partial(wv)}{\partial z}+\frac{\partial}{\partial x}\left[\left(\nu+\frac{N_x}{\rho}\right)\frac{\partial v}{\partial x}\right]+\frac{\partial}{\partial y}\left[\left(\nu+\frac{N_y}{\rho}\right)\frac{\partial v}{\partial y}\right]+$$

$$\frac{\partial}{\partial z}\left[\left(\nu+\frac{N_z}{\rho}\right)\frac{\partial v}{\partial z}\right]+g_y$$

Momentum z Direction :

$$\frac{\partial w}{\partial t}=-\frac{\partial(uw)}{\partial x}-\frac{\partial(vw)}{\partial y}-\frac{\partial(ww)}{\partial z}+\frac{\partial}{\partial x}\left[\left(\nu+\frac{N_x}{\rho}\right)\frac{\partial w}{\partial x}\right]+\frac{\partial}{\partial y}\left[\left(\nu+\frac{N_y}{\rho}\right)\frac{\partial w}{\partial y}\right]+$$

$$\frac{\partial}{\partial z}\left[\left(\nu+\frac{N_z}{\rho}\right)\frac{\partial w}{\partial z}\right]+g_z$$

} Hydrodynamic

(6.1)

Constituent Transport :

$$\frac{\partial C_i}{\partial t}=-\frac{\partial(uC_i)}{\partial x}-\frac{\partial(vC_i)}{\partial y}-\frac{\partial(wC_i)}{\partial z}+\frac{\partial}{\partial x}\left[K_x\frac{\partial C_i}{\partial x}\right]+\frac{\partial}{\partial y}\left[K_y\frac{\partial C_i}{\partial y}\right]+$$

$$\frac{\partial}{\partial z}\left[K_z\frac{\partial C_i}{\partial z}\right]\pm R(C_i)$$

} Transport Model

Model Coefficients for Simplified CTM

Numerical solutions to these equations can be obtained using any one of a variety of computational techniques (Fletcher, 1991). A simplified set of these equations obtained by uncoupling the momentum equations are given by:

Constituent Transport :

$$\frac{\partial C_i}{\partial t} = -\frac{\partial (uC_i)}{\partial x} - \frac{\partial (vC_i)}{\partial y} - \frac{\partial (wC_i)}{\partial z} + \frac{\partial}{\partial x}\left[K_x \frac{\partial C_i}{\partial x}\right] + \frac{\partial}{\partial y}\left[K_y \frac{\partial C_i}{\partial y}\right] + \frac{\partial}{\partial z}\left[K_z \frac{\partial C_i}{\partial z}\right] \pm R(C_i) \qquad (6.2)$$

(rate = advective flux + diffusive flux ± source/sink)

where the subscript *i* denotes the *i*-th constituent of interest. In the application of equation (6.2) for the simplified CTM, two sets of coefficients are required; one set for the advective flux (coefficients obtained by direct measurements), and the other set for diffusive flux obtained through the auto-correlation functions (ACF) of the velocity time series. The velocity data required for the numerical solution of the resulting advection-diffusion equations are obtained from direct observations of surface current measurements. This includes the components of velocity in the *x*-coordinate direction (east-west) and *y*-coordinate direction (north-south) *u, v* from HF radar and for a full 3D implementation, the vertical component, *w* in the z-coordinate direction obtained from ADCP measurements.

It has been shown (Batchelor, 1953) that turbulent diffusion in a flow field is related to the autocorrelation function (ACF), R_i of the velocity time series ***u****(x,y,z,t)*. Following the work of Taylor (Taylor, 1920, 1953), these coefficients are defined as follows:

$$K_i = \overline{u_i^{'2}} T_i$$

$$T_i = \int_0^t R_i(\tau) d\tau \qquad (6.3)$$

$$R_i(\tau) = \frac{\overline{u_i^{'}(t) u_i^{'}(t+\tau)}}{\overline{u_i^{'}(t)^2}}$$

$0 < R < 1$ for $0 < \tau < \infty$

For a fluid in a turbulent flow, the turbulent velocity field is represented by the time series $u_i(t) = \overline{u_i(t)} + u_i^{'}(t)$ and R_i is the autocorrelation function of the velocity time series, the overbar indicating averaged values over the ensemble of samples and T_i is the characteristic time scale of the process. While several analytical models have been put forward from statistical hydromechanics (e.g. Gaussian, Markov etc.), it is possible to obtain numerical estimates for R_i and this method was used in this study. The values for R_i were obtained directly from the discretized current measurements following which a numerical integration on R_i was performed to obtain the diffusion coefficient K_i. The

above scheme discussed elsewhere in a related study was implemented in MATLAB™, a high-level engineering and scientific programming language.

Model Error Analysis

Two sources of error are identified in the implementation of a typical CTM. Discretization errors or truncation errors are associated with numerically approximating the differencing. The other source of errors is inherent in the application of model coefficients. Two forms of truncation error typically introduced through the discretization are termed as numerical dissipation (artificial diffusion) and numerical dispersion. The latter manifests as a spatial lead or lag while the latter produces a reduction in the concentration levels relative to the analytical results. Both are dependent on the even and odd higher-order spatial derivative approximations respectively and varies with the cell Reynolds number, $Re = u_i \Delta x / K_i$ ($i = x, y, z$) where K_i represents the respective diffusivities and u_i the respective velocities along the coordinate axes.

The truncation errors can be quantified by comparing model results with the closed-form, which for a pulse discharge of mass M_o, is given by equation (6.4) below.

$$c^*(x,y,z,t) = \frac{M_o}{8(\pi)^{3/2}(K_x K_y K_z)^{1/2} t^{3/2}} \exp\left[-\frac{1}{4}\left\{ \frac{(x-u_x t)^2}{K_x t} + \frac{(y-u_y t)^2}{K_y t} + \frac{(z-u_z t)^2}{K_z t} \right\} \right] \quad (6.4)$$

A forward time, centered space (FTCS) finite difference approximation on a spatial [i x j x k] -temporal [x n] grid for equation (6.2) results in a set of discretized algebraic equations (DAE).

$$\frac{\Delta c_{i,j,k}^{n+1}}{\Delta t} = -u_x \frac{c_{i+1,j,k}^{n} - c_{i-1,j,k}^{n}}{2\Delta x} - u_y \frac{c_{i,j+1,k}^{n} - c_{i,j-1,k}^{n}}{2\Delta y} - u_z \frac{c_{i,j,k+1}^{n} - c_{i,j,k-1}^{n}}{2\Delta y}$$
$$+ K_x \frac{c_{i+1,j,k}^{n} - 2c_{i,j,k}^{n} + c_{i-1,j,k}^{n}}{\Delta x^2} + K_y \frac{c_{i,j-1,k}^{n} - 2c_{i,j,k}^{n} + c_{i,j+1,k}^{n}}{\Delta y^2} \qquad (6.5)$$
$$+ K_z \frac{c_{i,j,k-1}^{n} - 2c_{i,j,k}^{n} + c_{i,j,k+1}^{n}}{\Delta z^2}$$

Equation (6.5) can be written in matrix form as follows:

$$\frac{\Delta c_{i,j,k}^{n+1}}{\Delta t} = \begin{bmatrix} \frac{-u_x}{2\Delta x} & \frac{-u_y}{2\Delta y} & \frac{-u_z}{2\Delta z} & \frac{K_x}{\Delta x^2} & \frac{K_y}{\Delta y^2} & \frac{K_z}{\Delta z^2} \end{bmatrix} \begin{bmatrix} c_{i+1,j,k}^{n} - c_{i-1,j,k}^{n} \\ c_{i,j+1,k}^{n} - c_{i,j-1,k}^{n} \\ c_{i,j,k+1}^{n} - c_{i,j,k-1}^{n} \\ c_{i+1,j,k}^{n} - 2c_{i,j,k}^{n} + c_{i-1,j,k}^{n} \\ c_{i,j+1,k}^{n} - 2c_{i,j,k}^{n} + c_{i,j-1,k}^{n} \\ c_{i,j,k+1}^{n} - 2c_{i,j,k}^{n} + c_{i,j,k-1}^{n} \end{bmatrix} \qquad (6.6)$$

This can be written as a set of ordinary differential equations (ODE) by partial discretization writing the LHS as a total derivative ($dc/dt = r$) in terms of spatial differential approximations on the RHS.

$$\boldsymbol{r} = \boldsymbol{SC} \tag{6.7}$$

where $\boldsymbol{r}$ is evaluated as the time rate of change of concentration at a node (i, j, k) on the spatial grid having a concentration, $c_{i,j,k}$ at time-step n; $\boldsymbol{S}$ is a matrix of coefficients and $\boldsymbol{C}$, a matrix of concentration differentials evaluated at surrounding node points. This method-of-lines formulation of an unsteady advection-diffusion transport with appropriate boundary-conditions (B.C.) and forward-stepping in time has a truncation error of $O(\Delta x^2, \Delta y^2, \Delta z^2)$ the initial and boundary conditions being specified appropriately.

Since equation (6.4) is only valid for constant coefficients, solution of equation (6.7) will be analyzed with constant coefficients for comparison against the closed-form. Although Ruan et al. (Ruan et al., 1999) proposed a generalized scheme that allows for spatially distributed coefficients to be used in the evaluation of the numerical accuracy, for the purpose of error analysis in this study, the localized values for u_x, u_y, u_z, K_x, K_y, and K_z will be taken as constant. The accuracy check on the discretization can be performed using the spatially aggregated root-mean-square error, RSME as follows:

$$RMSE = \frac{\Delta x \Delta y \Delta z}{M_o} \sqrt{\left\{ \sum_{i}^{N} \left[c_{i,j,k} - c^*(x,y,z) \right]^2 \right\}} \tag{6.8}$$

where N is the number of nodes in the computational grid. The RSME compares the numerical solution with the analytical. Since the latter has no discretization errors associated with it, the RSME should therefore give a relative indication of the amount of numerical dispersion and dissipation inherent in the discretization. Having quantified the accuracy of the numerical solution, the overall uncertainties in model predictions associated with the model coefficients resulting from errors associated with velocity measurements and errors associated with estimation of diffusion coefficients can be established.

Methods and Materials

This study focuses on intermediate scale mixing processes falling within the temporal scale of 3-10 days or length scale ~10 km. The categorized scale of mixing processes in open waters is as shown below:

- Small Scale -- temporal scale < 24 h, spatial scale between 0-10 km.
- Intermediate Scale -- temporal scale between 1-100 days, spatial scale between 10-300 km.
- Large Scale -- Temporal scale > 100 days, encompassing the ocean basin.

The study area covers a horizontal scale ~25 x 25 km and a vertical scale ~4 m.
Two scenarios were modeled comprising of an instantaneous discharge at two different locations. In both scenarios, the model was initialized with the same concentration of material at the same time within the tidal cycle and the diffusing cloud was then "tracked" over the course of several tidal cycles.

Surface Current Measurements and Vertical Velocity Profile

Surface current required as hydrodynamic input into the model was obtained from HF radar measurements. The Seasonde^{TM} HF Radar equipment manufactured by CODAR Ocean Sensors, which is operated as part of a coastal observatory network maintained by our research group (Kelly et al., 2004) has a range up to 25 km at a grid resolution of 1000 m. Operating on the principle of Bragg Scattering of high frequency (HF) electromagnetic waves incident on surface waves (Barrick et al., 1977), it continuously measures surface currents at 1-hour intervals over the entire study area. Spatial interpolation schemes and temporal filtering routines were written and applied for data pre-processing to account for dropouts and to allow the velocity measurements to be in step with the requirements of the numerical scheme used in evaluation of dispersion coefficients.

The model grid resolution was set at 1000 m in the horizontal and 1 m in the vertical. Hourly surface current measurements were incorporated directly into the model providing the advective flux coefficients. The same dataset was then used in obtaining the diffusive flux coefficients using the autocorrelation function, R_i of the velocity time series. The method and algorithm for estimating the autocorrelation functions are discussed in the next section. Vertical current profiles were obtained using a boat mounted downward looking ADCP during a series of dye-tracer experiments from which a first-order polynomial was found to provide suitable approximation to the vertical profile of current. The linear velocity profile was applied for a 3D implementation of the

computational scheme. This profile was assumed invariant over the computational domain.

Turbulent Diffusivity

Turbulent diffusivity defined in terms of the time variation of the velocity autocorrelation function following Taylor's analysis was used by List et.al in a set of experiments to evaluate diffusion coefficients from velocity time series using Langrangian drifters (List, 1990). Prior to this Okubo had developed a set of oceanic diffusion diagrams based on tracer experiments in surface waters and established a 4/3rds power law between turbulent diffusion coefficients and a diffusion length scale. O'Connor et al. performed assessments in the 106-mile region, a waste disposal site off the coast of New Jersey basing their analysis on the relationship between spatial variance and variance of the velocity field (O'Connor et al., 1985). The dispersion estimates were obtained from the variance-covariance matrix of the velocity time series through a scaling dependence.

In this study, the approach was to numerically analyze the velocity time-series for the evaluation of the time scale of the diffusion process, T_i through the numerically determined autocorrelation function, R_i. Since the scale of the analyses was of the order of several days, the tidal variations in velocity was treated as turbulent fluctuations relative to a mean de-tided velocity, $\bar{u}_i$ ($i = x, y, z$) along the orthogonal coordinate axes. The preprocessed velocity time series was used in conjunction with equation (6.3) to derive the spatially distributed diffusion coefficients. The discretized form of this

equation was used in a numerical scheme in deriving the diffusion coefficients at each node within the computational domain.

Modeling Framework

Since the reduced or simplified model used in this study incorporated direct observations of velocity and diffusion coefficients, the resulting partial differential equation (PDE) was solved in a time-stepping routine using a PDE solver based on the method-of-lines. The velocity coefficients on the surface, which coincides with the top horizontal plane, were provided by radar while sub-surface currents on each of the remaining four horizontal planes were obtained from a linear representation of current profiles from ADCP.

The finite difference 3D computational domain is shown in Figure 6.1 and it covers a spatial extent of 25x25 km on a structured base-grid with 1000 m resolution in the horizontal and 1 m resolution in the vertical plane. The PDE solver VLUGR-3 (Blom and Verwer, 1996), a 3-dimensional vectorizable adaptive grid finite difference scheme accommodates irregular boundaries and the computational grid was made to conform approximately to the outline of the study area. The grid was generated interactively through a graphical interface that allowed for masking of land areas. Five horizontal planes were generated in this implementation having 2030 nodes on the base grid. The solver's adaptive grid scheme allows for on-the-fly grid refinement requiring automatic adjustment to the computational time-step within sections of the computational domain

where sharp gradients may result especially at the start of the simulation and at the boundaries.

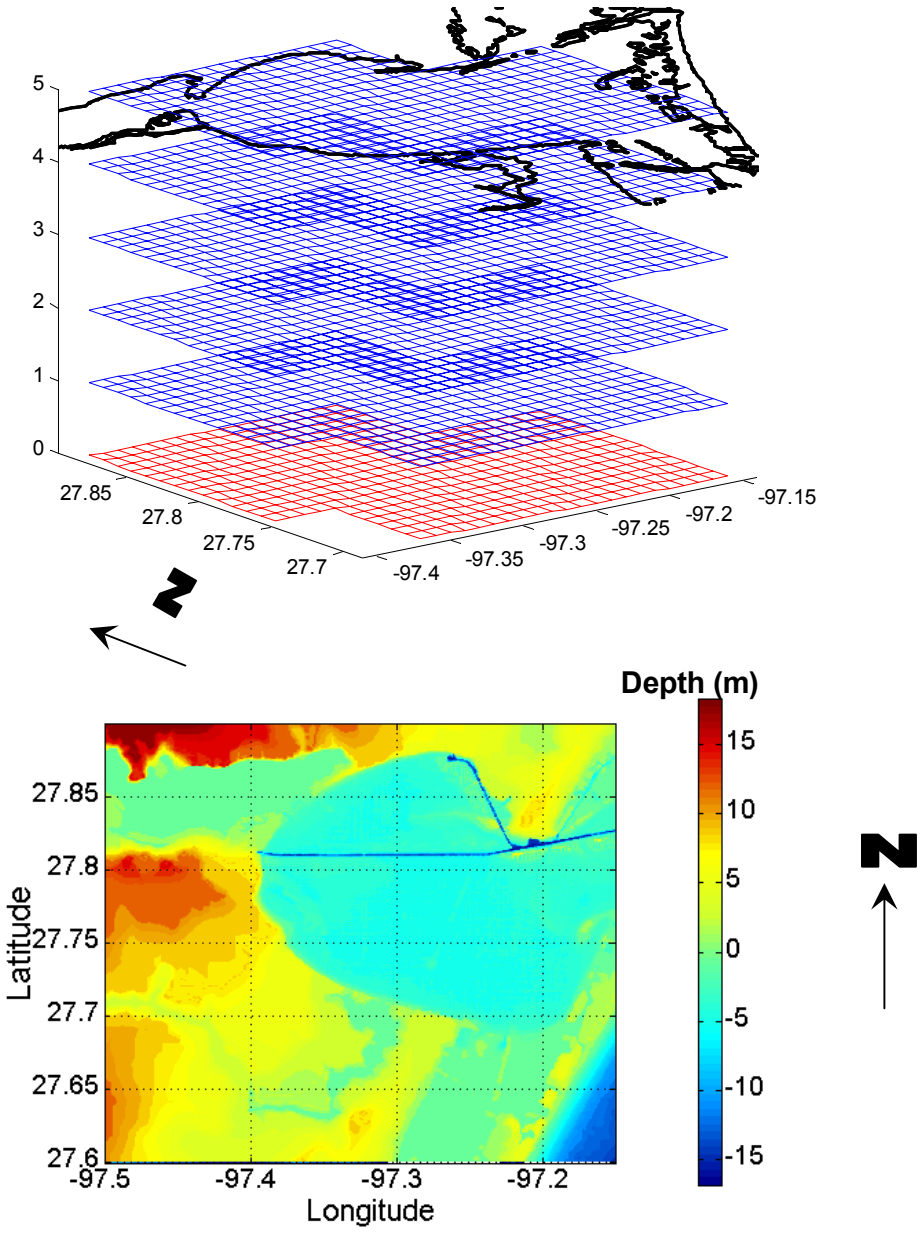

Figure 6.1. Top panel; finite difference computational grid. Bottom pane; bathymetry of the study area, relatively shallow and flat at ~4 m.

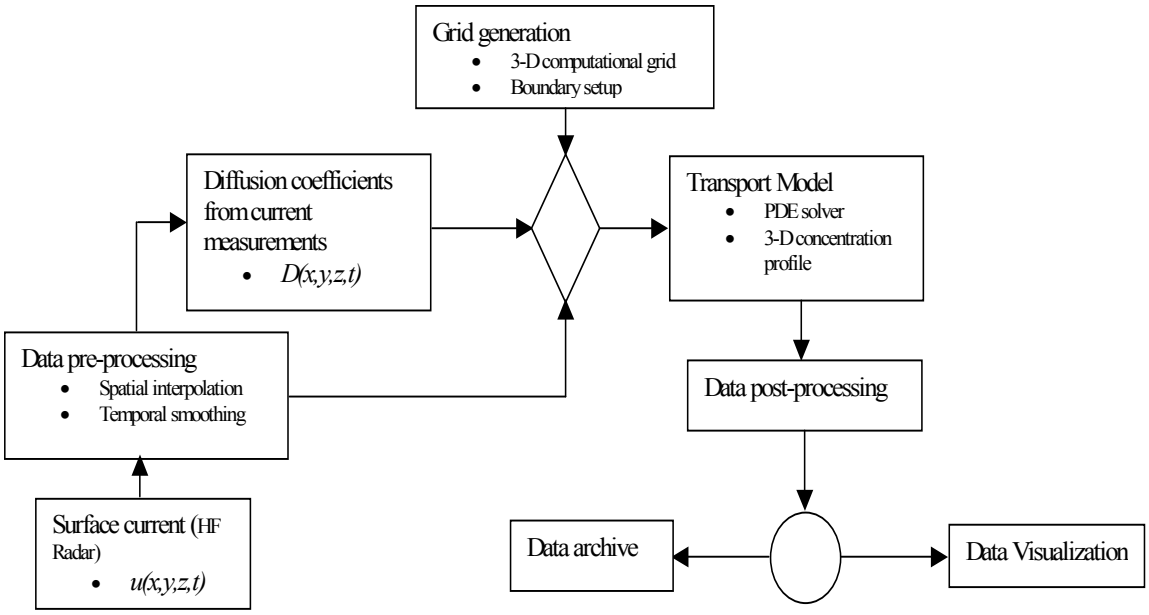

Figure 6.2. Framework for data driven transport model.

Output from the model simulation was written to individual ASCII files every hour for the duration of the computer experiment while MATLAB® based data visualization and analyses routines were applied for data post-processing. Figure 6.2 presents this modeling framework. In each of the simulation runs, initial conditions were established by applying a pulse discharge of material with an initial concentration, C_o = 0.5 ppt at the node on the computational grid corresponding to the coordinates of the two locations used in this study, the material been uniformly mixed to a depth of 1 m. The model simulation was run until maximum concentration dropped below the 1 ppb level and a concentration profile was generated hourly. Neumann (no flux across boundaries) boundary conditions ($\partial C / \partial x = 0$) were set for boundary planes corresponding to the bottom and all sidewalls except at the boundary corresponding to the inlet of the

shipping channel where Dirichlet (fixed concentration) boundary conditions ($C = const.$) was established.

Model Error Analysis

The purpose of the error analysis was to verify the effect of inaccuracies in the model predictions resulting from the discretization of the governing equations. For this part of the study, uniform coefficients (velocity and diffusion) were initially used in the model in order to compare the model results against the analytical solution.

It is imperative that the solver should introduce very little artificial diffusion (which may swamp out physical diffusion) and should accurately locate the center of mass of the concentration profile. In this study, the method of moments was applied to determine the spatial location and extent of the diffusing cloud and therefore the amount of artificial diffusion and numerical dissipation introduced by the model for various values of *Re*. The first moment of the concentration profile given in equation (6.10) locates the center of mass while the second moment given in equation (6.11) evaluates the variance (a measure of dispersion). These values for the center of mass and variance computed from the numerical scheme were compared with those from the exact solution following which the estimate of the error was determined from using equation (6.8).

$$M_o = \int_{-\infty}^{\infty}\int\int c(x,y,z,t)dxdydz \qquad (6.9)$$

$$x_o = \frac{1}{M_o}\int_{-\infty}^{\infty}\int\int xc(x,y,z,t)dxdydz$$

$$y_o = \frac{1}{M_o}\int_{-\infty}^{\infty}\int\int yc(x,y,z,t)dxdydz \tag{6.10}$$

$$S_x^2(t) = \frac{1}{M_o}\int_{-\infty}^{\infty}\int\int (x-x_o)^2 c(x,y,z,t)dxdydz \tag{6.11}$$

$$S_y^2(t) = \frac{1}{M_o}\int_{-\infty}^{\infty}\int\int (y-y_o)^2 c(x,y,z,t)dxdydz$$

Having established the numerical accuracy of the model, spatially varying coefficients were applied in the advection-diffusion model. The scheme used for generating these coefficients was described earlier. The computational domain was initially divided into a 26x26x5 grid and a level-4 grid refinement specified for the solver. Each level of grid refinement results in halving of the grid spacing in the areas where sharp gradients were found to occur during computation. Two scenarios were modeled in this study with the same amount of instantaneous tracer release.

Results

First, the results of the accuracy check are presented in Tables 6.1-6.3 using spatially uniform coefficients (velocity and dispersion) in both the analytical solution and numerical solution, and then the results of the two model scenarios are presented.

Table 6.1. Variance and spatial location estimates of a dye patch from an instantaneous point discharge for different values of Re (constant velocities).

	Distance of center of mass relative to origin, (m)		**Computed variance, (m^2)**		**Cell Reynolds Number, Re**		**Velocity, (cm/s)**		**Diffusion Coefficient, (cm^2/s)**	
	x-coordinate	y-coordinate	x-dir	y-dir	x-dir	y-dir	u	v	K_x	K_y
Actual	540	1620	1.08×10^4	1.08×10^5	100	30	10	30	1×10^4	1×10^5
Numeric	273	914	2.78×10^5	9.11×10^5						
Actual	540	1620	1.08×10^5	1.08×10^6	10	3	10	30	1×10^5	1×10^6
Numeric	323	1380	3.25×10^5	1.35×10^6						
Actual	540	1620	1.08×10^6	1.08×10^7	1	0.3	10	30	1×10^6	1×10^7
Numeric	534	1595	1.07×10^6	1.06×10^7						

Grid Res = 1000 x 1000 x 1; Number of nodes = 4056; Time elapsed = 3 x 1800 s

	Distance of center of mass relative to origin, (m)		**Computed variance, (m^2)**		**Cell Reynolds Number, Re**		**Velocity, (cm/s)**		**Diffusion Coefficient, (cm^2/s)**	
	x-coordinate	y-coordinate	x-dir	y-dir	x-dir	y-dir	u	v	K_x	K_y
Actual	346	1037	6.91×10^3	6.91×10^4	50	15	10	30	1×10^4	1×10^5
Numeric	180	646	9.23×10^4	3.13×10^5						
Actual	346	1037	6.91×10^4	6.91×10^5	5	1.5	10	30	1×10^5	1×10^6
Numeric	244	1034	1.22×10^5	6.86×10^5						
Actual	346	1037	6.91×10^5	6.91×10^6	0.5	0.15	10	30	1×10^6	1×10^7
Numeric	343	1020	6.85×10^5	6.80×10^6						

Grid Res = 500 x 500 x 1; Number of nodes = 15606; Time elapsed = 3 x 1152 s (6 x 900 s)

Table 6.2. Variance and spatial location estimates of a dye patch from an instantaneous point discharge for different values of Re (constant diffusivities).

	Distance of center of mass relative to origin, (m)		**Computed variance, (m^2)**		**Cell Reynolds Number, Re**		**Velocity, (cm/s)**		**Diffusion Coefficient, (cm^2/s)**	
	x-coordinate	y-coordinate	x-dir	y-dir	x-dir	y-dir	u	v	K_x	K_y
Actual	360	1080	7.20×10^5	7.20×10^6	1.0	0.3	10	30	1×10^6	1×10^7
Numeric	316	966	6.30×10^5	6.44×10^6						
Actual	720	2160	7.20×10^5	7.20×10^6	2.0	0.6	20	60	1×10^6	1×10^7
Numeric	558	1863	1.53×10^6	7.14×10^6						
Actual	1080	3240	7.20×10^5	7.20×10^6	3.0	0.9	30	90	1×10^6	1×10^7
Numeric	799	2887	7.86×10^5	6.22×10^6						

Grid Res = 1000 x 1000 x 1; Number of nodes = 15606; Time elapsed = 4 x 900 =3600 s.

	Distance of center of mass relative to origin, (m)		**Computed variance, (m^2)**		**Cell Reynolds Number, Re**		**Velocity, (cm/s)**		**Diffusion Coefficient, (cm^2/s)**	
	x-coordinate	y-coordinate	x-dir	y-dir	x-dir	y-dir	u	v	K_x	K_y
Actual	360	1080	7.20×10^5	7.20×10^6	0.5	0.15	10	30	1×10^6	1×10^7
Numeric	318	963	6.33×10^5	6.40×10^6						
Actual	720	2160	7.20×10^5	7.20×10^6	1.0	0.3	20	60	1×10^6	1×10^7
Numeric	633	1926	6.25×10^5	6.32×10^6						
Actual	1080	3240	7.20×10^5	7.20×10^6	1.5	0.45	30	90	1×10^6	1×10^7
Numeric	953	2893	6.18×10^5	6.19×10^6						

Grid Res = 500 x 500 x 1; Number of nodes = 15606; Time elapsed = 4 x 900 =3600 s.

Table 6.3. Normalized error from numerical estimates of variance and spatial location in comparison with exact solution for different values of Re.

Normalized error; variable dispersion, constant velocities			Normalized error; constant dispersion, variable velocities		
Cell Reynolds number, Re	**Error**		**Cell Reynolds number, Re**	**Error**	
	Variance estimates	Spatial location		Variance estimates	Spatial location
100	-24.7	0.49	1	0.13	0.12
10	-2.01	0.40	2	-1.13	0.23
1	9.26×10^{-3}	1.11×10^{-2}	3	-9.17×10^{-2}	0.26
50	-12.4	0.48×10^{-1}	0.3	0.12	0.12
5	-0.77	2.95×10^{-1}	0.6	0.13	0.12
0.5	8.68×10^{-3}	8.67×10^{-3}	0.9	0.14	0.12
30	-7.44	4.36×10^{-1}	0.5	0.11	0.11
3	-0.25	1.48×10^{-1}	1.0	8.33×10^{-3}	0.14
0.3	1.85×10^{-2}	1.54×10^{-2}	1.5	0.14	0.11
15	-3.53	0.38	0.15	0.11	0.11
0.5	7.24×10^{-3}	2.89×10^{-3}	0.3	0.12	0.11
0.15	1.59×10^{-2}	1.64×10^{-2}	0.45	0.14	0.11

Turbulent Diffusivity

The velocity time series used for the eventual computer experiments were obtained over a 10-day period between 1700 hrs on 03/17/03 and 1800 hrs on 03/27/03 for each of the coordinate axes on the horizontal plane. These surface current measurements represented in Figure 6.3 (as a time series at a location within the computational domain) and as current vectors in Figure 6.4 (at four successive times over the entire domain) were combined with a linear velocity profile in the vertical coordinate direction to obtain a 3D velocity field for the simulation run. The de-tided time series is shown by the broken lines in Figure 6.3 revealing the tidal variations in velocity on the given temporal scale (~10 days) as turbulent fluctuations, a necessary condition for evaluating diffusivity values in accordance with equation (6.3).

Following the application of equations (6.3), the distribution density function for diffusivity is shown in Figure 6.5 while the spatially distributed diffusivity values obtained are shown in Figure 6.6. The diffusivity values are seen to fall within the range $8.62 \pm 4.98 \times 10^5$ cm^2/s in the *x*-coordinate direction and $1.01 \pm 0.58 \times 10^6$ cm^2/s in the *y*-coordinate.

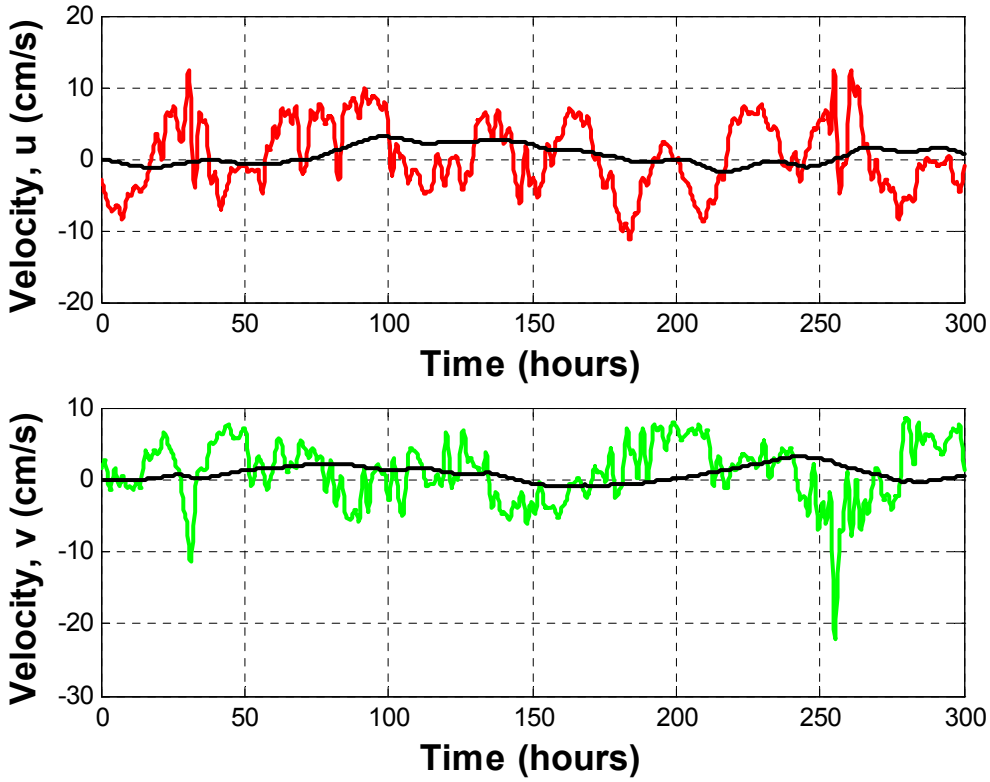

Figure 6.3. Typical velocity time series from surface current measurements at one location in the computational grid, shown as a time series (solid line) and the de-tided signal (dotted line) for east-west (top panel) and north-south (lower panel) coordinate axes.

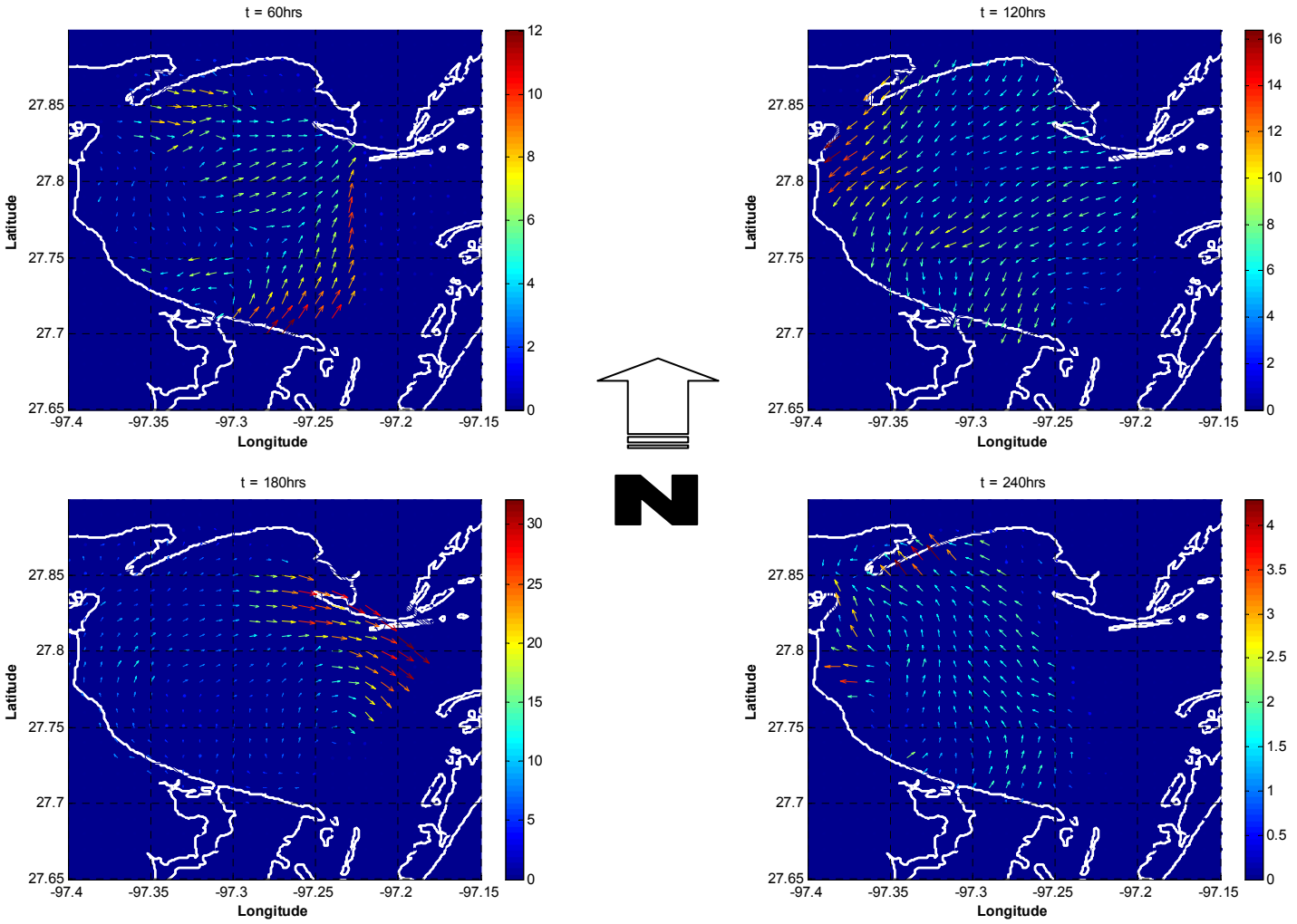

Figure 6.4. From top left to bottom right, the spatial distribution of current vector, colored arrows scaled by current magnitude (cm/s) at successive times: time t = 60, 120, 180 and 240 hrs.

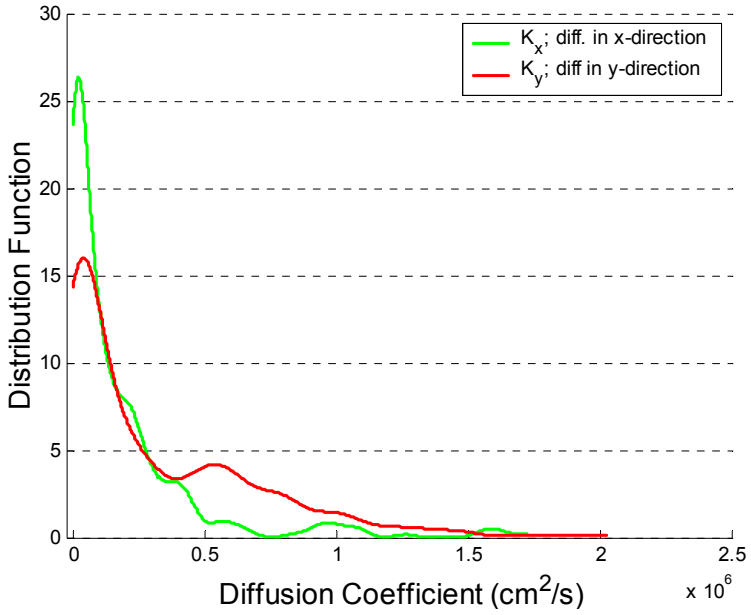

Figure 6.5. Distribution density for turbulent diffusivity along the coordinate axes.

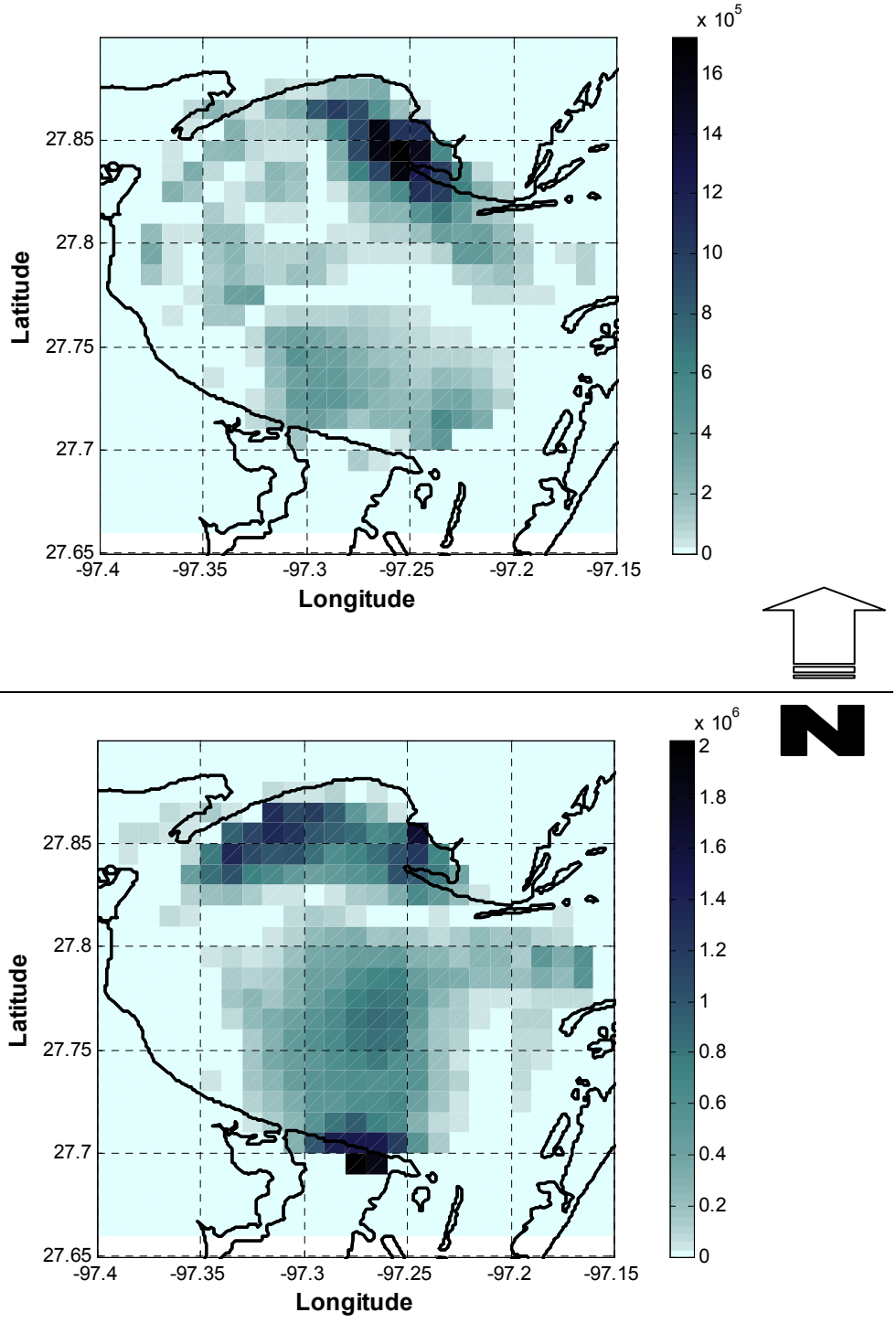

Figure 6.6. Spatial distribution of turbulent diffusivity; top panel, diffusivity K_x in x-direction (modal value = 2.1 x 10^4 cm^2/s; bottom panel, diffusivity K_y in y-direction (modal value = 4.0 x 10^4 cm^2/s).

Error Analyses

Figures 6.7 and 6.8 indicates that the error in the spread of the plume increases with increasing Re (the largest errors occurring at Re > 2) associated with changing diffusivity values, going up to as much as a 25-fold difference in variance estimates at Re = 100. Very little effect on variance estimates due to changing velocity values can be observed even at Re > 2. It is therefore apparent (from the data represented in Figures 6.7 and 6.8, which is also presented in Tables 6.1-6.3) that order of magnitude errors in diffusivity makes the numerical scheme more error prone. Since diffusivities can be off by at least one order of magnitude and going by the spatial distribution of diffusivity, it becomes imperative that the model predictions will be significantly affected from the wrongful application of diffusivity values, less so directly from current measurements.

Given the distribution of diffusivity values as shown in Figure 6.5, the target for the model error analysis was ~1 x 10^4 -10^5 cm^2/s. The model was run for comparison with the analytical solution using values within the target range as well as values of diffusivity in the range 1 x 10^5- 10^6 cm^2/s. These concentration profiles are shown in Figure 6.9 in comparison with the analytical form. The agreement between the numerical results and the exact solution is quite good indicating that the model does not appear to introduce any significant amount of numerical dissipation and dispersion with the base grid of 1000 x 1000 x 1 m and computational time step of 1 s.

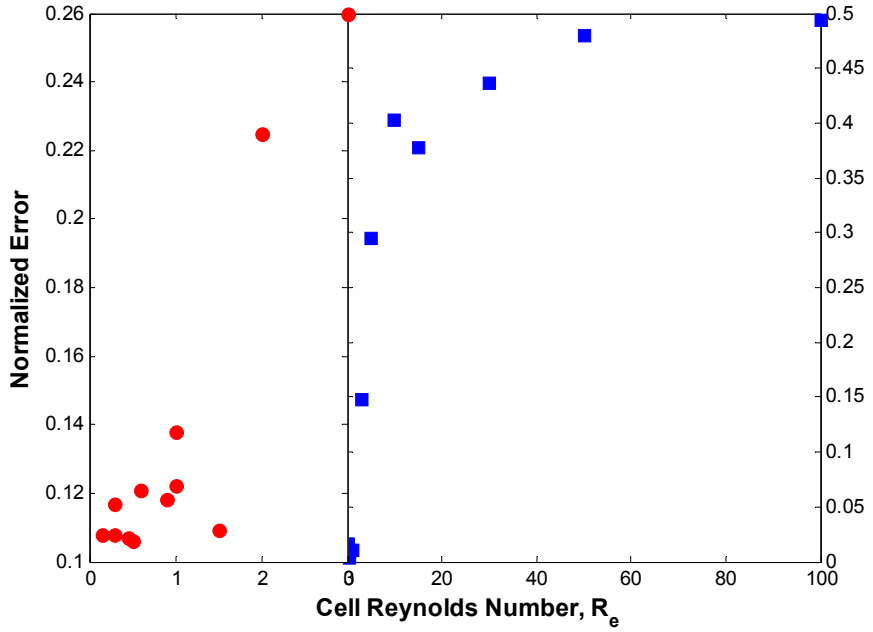

Figure 6.7. Normalized error from model simulation for spatial location of plume with varying Re; -●-, constant diffusivity, varying velocity; -■-, varying diffusivity, constant velocity.

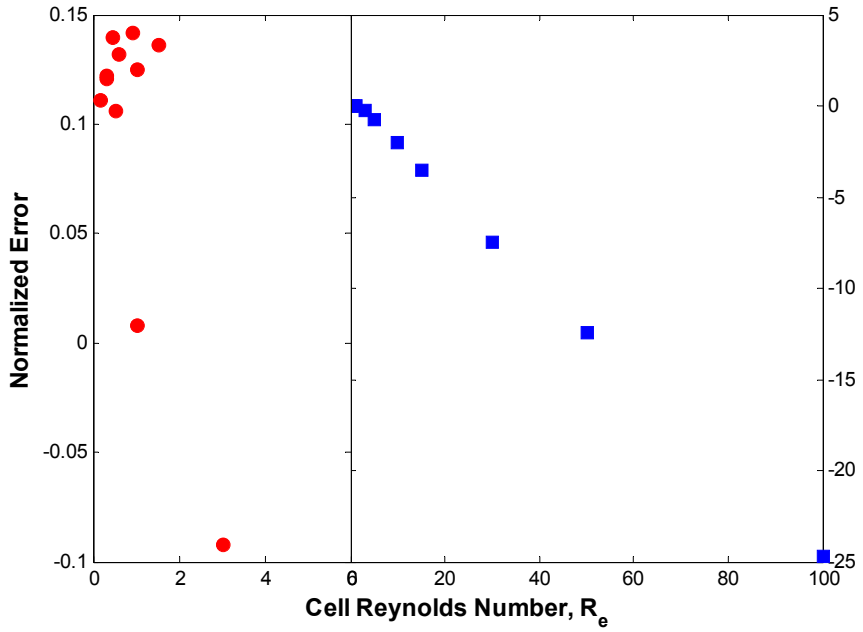

Figure 6.8. Normalized error from model simulation for variance of concentration distribution with varying Re; -●-, constant diffusivity, varying velocity; -■-, varying diffusivity, constant velocity.

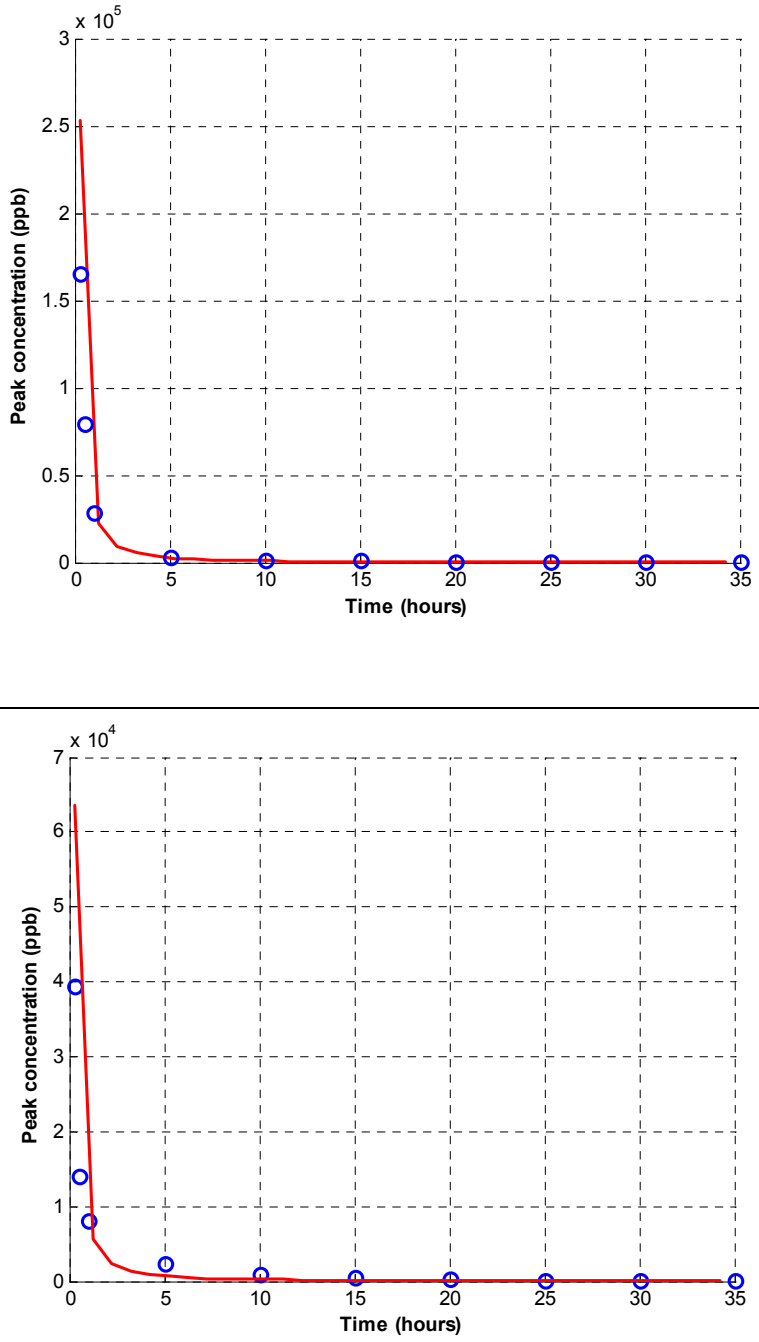

Figure 6.9. Plot of peak concentration against time; top panel, $K_x = 1 \times 10^4$, $K_y = 1 \times 10^5$; bottom panel, $K_x = 1 \times 10^5$, $K_y = 1 \times 10^6$. Solid line, exact solution, open circle, results from model simulation.

Model Results

Results from the two scenarios modeled results indicate the difference, particularly in the variance estimates obtained after 90 hours of tracking an instantaneous pulse discharge. The difference in variance of the concentration profile along each of the coordinate axis can be seen in Figure 6.10, the slope of the variance-time plots being remarkably different, a direct consequence of the differences in diffusivities with respect to location. Concentration profiles are displayed in Figure 6.11, a plot of peak concentration vs. time. The difference in peak values particularly between 5 and 25 hours following the introduction of the conservative, neutrally buoyant material into the body of water can be observed. Therefore, we observe differences in both spatial extent as well as peak concentration values of the diffusing material, differences that can be readily attributed to the spatial variation in observed diffusivities, the mixing process being stronger in some parts of the bay compared to others.

In addition, the diffusing material would be seen to grow at a faster rate in one scenario compared to the other, the computed variance in the y-coordinate direction being remarkably different between the two scenarios modeled. In both scenarios, the growth along the y-coordinate direction was higher than the growth along the x-coordinate direction. This observation would not have manifested had the simulation employed spatially uniform diffusivities, which would be the case if diffusivity values were obtained using diffusion diagrams or if they were based in results from tracer experiments.

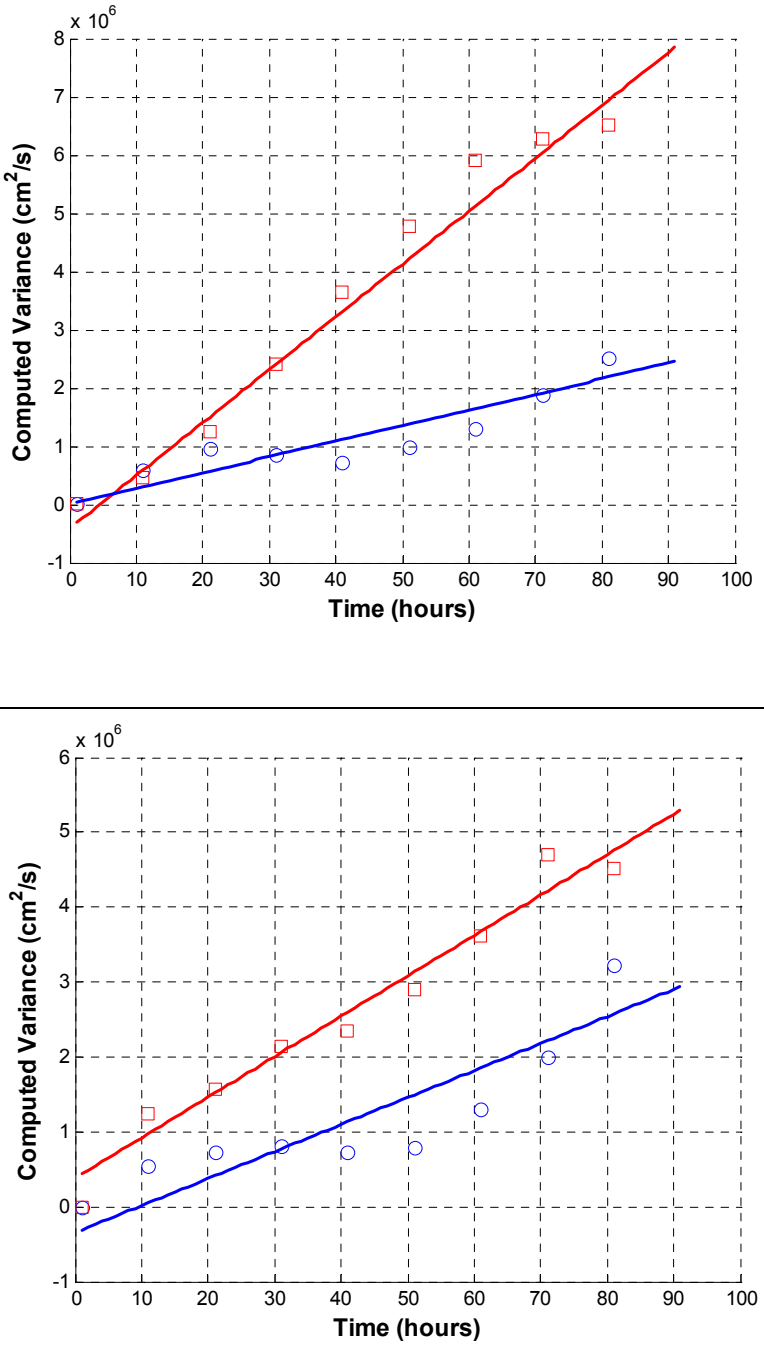

Figure 6.10. Plot of variance of concentration for pulse discharge initialized at two different locations within the computational domain. The difference in variance attributable to the difference in diffusivity values dependent on spatial location.

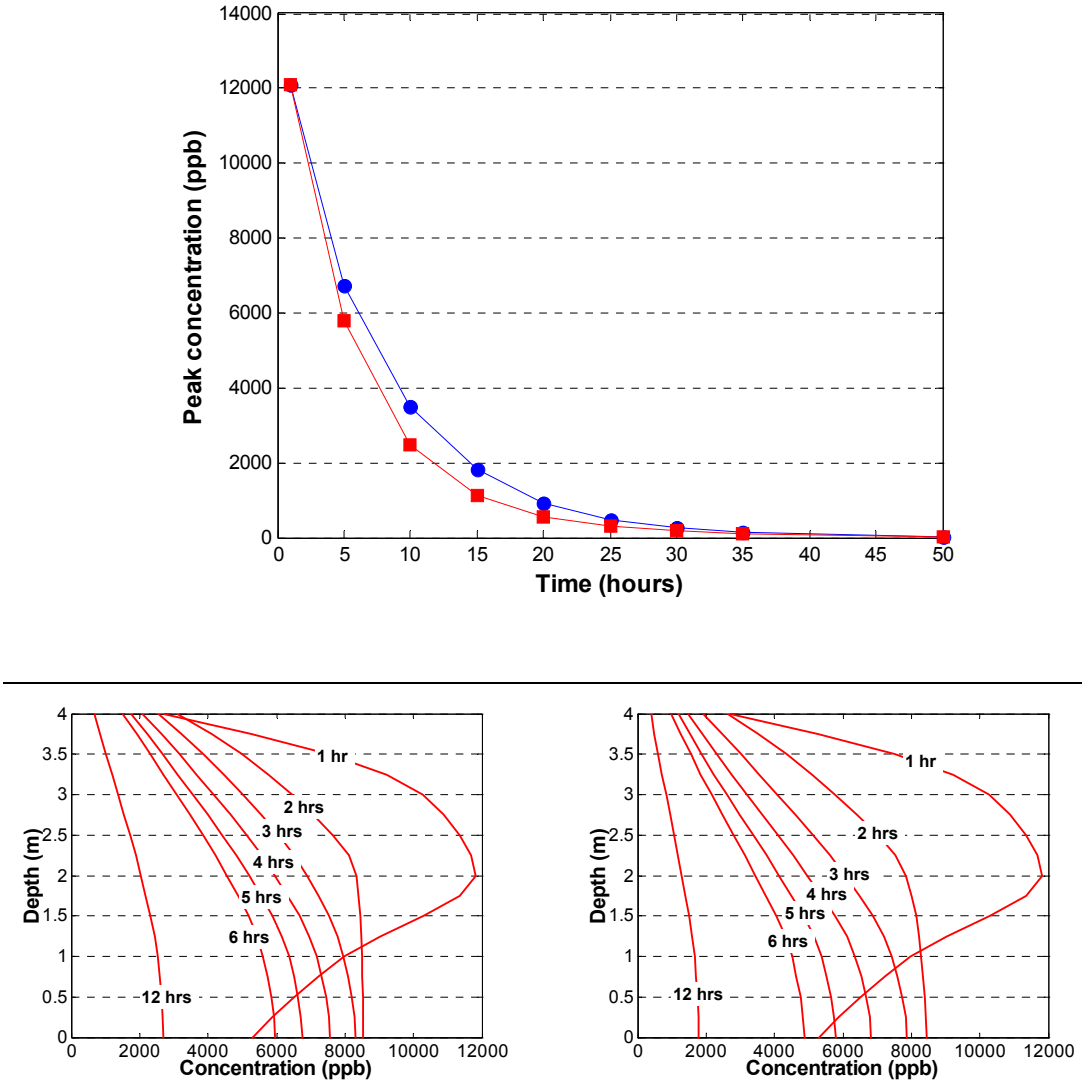

Figure 6.11. Top panel; peak concentration vs. time for scenario 1 (-●-) and scenario 2 (-■-). Bottom left panel; vertical profile from run #1. Bottom right panel; vertical profile from run #2.

Whereas a number of turbulence closure schemes exist, which might capture the dynamics of the water body in terms of the mixing coefficients, these schemes are difficult to implement and lack sufficient data to support their applicability. The scheme presented here is relatively simple and has been validated with data from a related study combining current measurements with data from the evolution of a dye patch (Ojo et al., 2004a).

Tables 6.4 and 6.5 summarize the results displayed in Figures 6.10 and 6.11. Concentration profiles of the material at six successive times for each of the two scenarios are displayed in Figures 6.12 and 6.13 showing the evolution of the material with time with the currents overlayed. This model output is also produced as an animated sequence over the entire 90-hour period in *avi format viewable in Windows Media Player™. From the vertical profiles of the peak concentration presented in Figure 6.11, it can be observed that in this shallow body of water the conservative neutrally buoyant constituent becomes fully mixed into the water column about 12 hours following release. It is instructive to note that the profile is similar to what one would obtain from an elevated source release in atmospheric applications.

Table 6.4. Peak concentration at successive time intervals for modeled scenarios.

Time Elapsed (hours)	Peak Concentration (ppb)	
	Scenario 1	Scenario 2
1	12100	12100
5	6750	5780
10	3510	2470
15	1820	1110
20	926	537
25	468	295
30	273	167
35	162	96
50	29	19

Table 6.5. Variance-time summary for modeled scenarios.

Elapsed Time (hours)	Scenario 1		Scenario 2	
	Variance in x-direction (cm^2/s x 10^6)	Variance in y-direction (cm^2/s x 10^6)	Variance in x-direction (cm^2/s x 10^6)	Variance in y-direction (cm^2/s x 10^6)
1	-	-	-	-
10	0.56	0.43	0.50	1.17
20	0.94	1.18	0.69	1.53
30	0.90	2.23	0.79	2.21
40	0.68	3.53	0.74	2.28
50	0.95	4.78	0.77	2.90
60	1.25	5.76	1.27	3.68
70	1.84	6.25	1.87	4.80
80	2.43	6.58	3.09	4.43
90	3.03	6.94	4.00	5.37

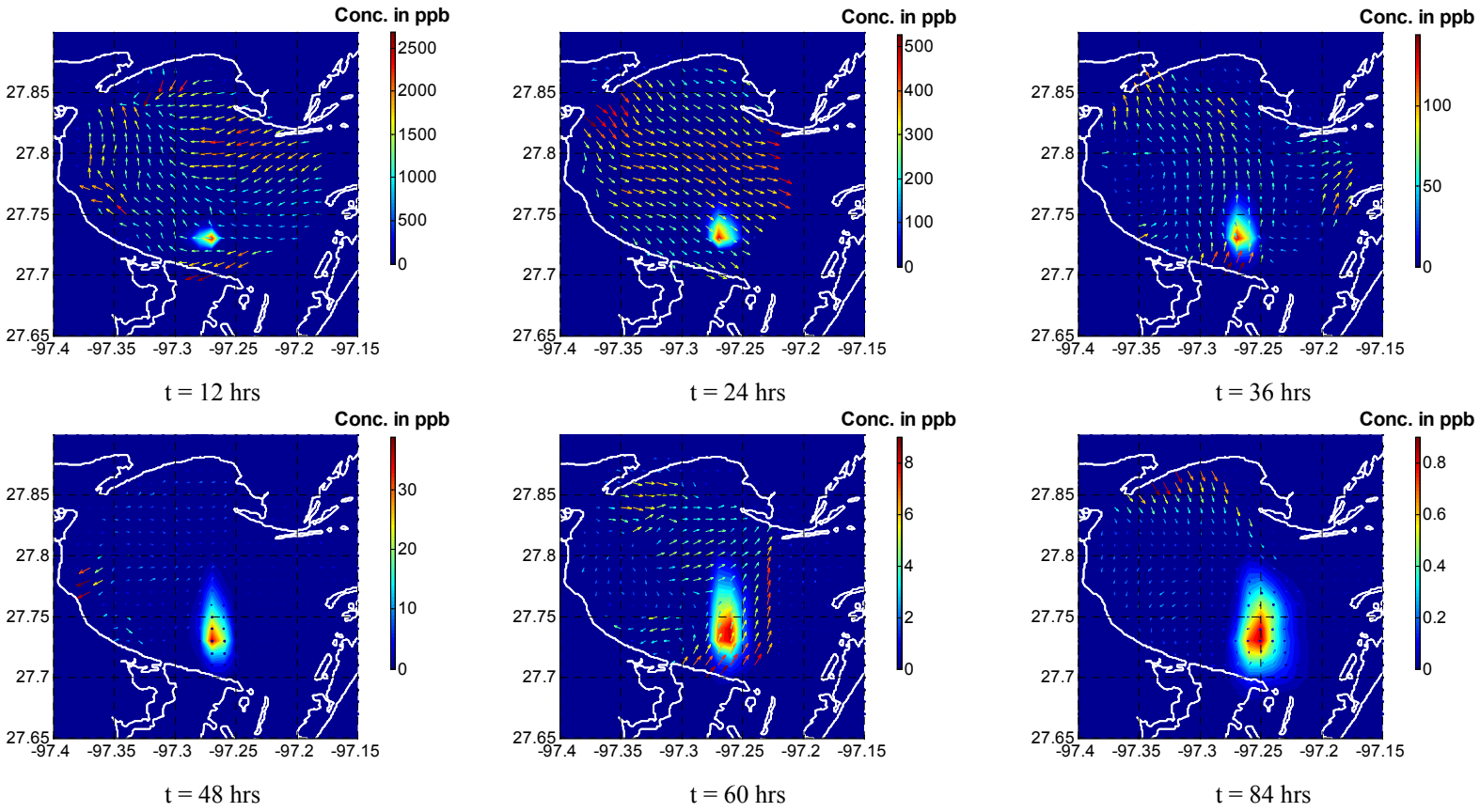

Figure 6.12. Evolution of diffusing conservative material over three tidal cycles; run #1. The arrows representing the current vectors are colored for relative strength from blue to red on a scale of 0-150 cm/s.

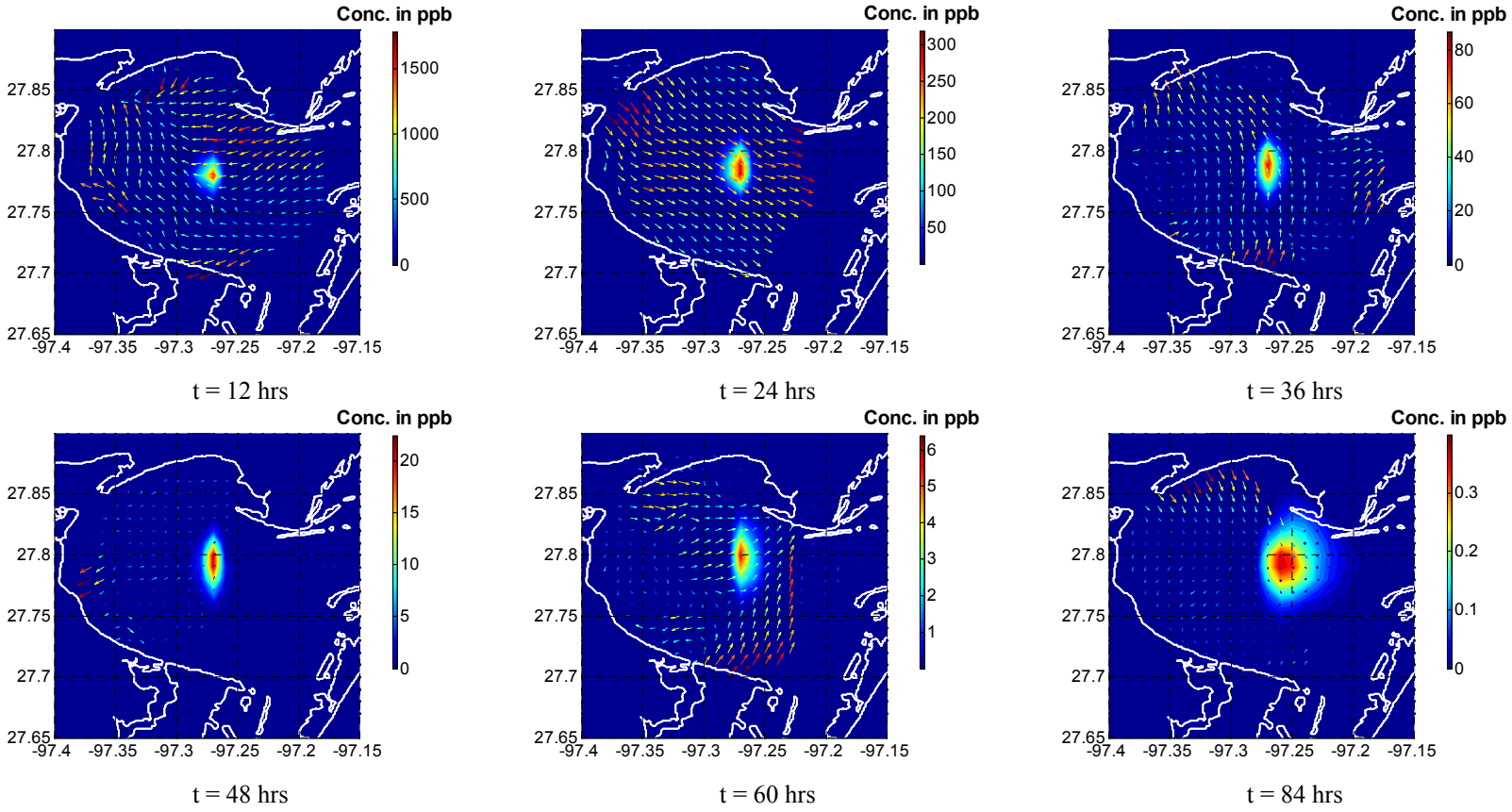

Figure 6.13. Evolution of diffusing conservative material over three tidal cycles; run #2. The arrows representing the current vectors are colored for relative strength from blue to red on a scale of 0-150 cm/s.

Discussion

The computer experiments performed in the study show that by taking into account the heterogeneous nature of the turbulent field in a bay with the geomorphology of Corpus Christi Bay, better accuracy could be achieved in the results of model predictions. Using surface current measurements from HF radar, we developed a simplified model for 3D constituent transport and plume trajectory tracking driven by direct hydrodynamic observations with spatially distributed diffusivities applied within the model framework. The accuracy of the model predictions was subsequently tested against analytical solutions and two instantaneous applications of conservative material were successfully modeled using this simplified CTM.

Traditionally the diffusivities, K_x, K_y, K_z would be taken to be constant over the domain of interest, and these coefficients being determined from tracer experiments or taken from diffusion diagrams may not adequately account for the anisotropic characteristic observed in this study. Although models that couple hydrodynamic modules and employing turbulence closure schemes may capture this property of the turbulent field, they are difficult to implement and deploy within the context of emergency response. A paradigm shift for transport modeling in surface waters through this simplified data-driven model is proposed. The advective flux coefficients (u, v, w) are obtained directly from radar while the diffusive flux coefficients (K_x, K_y, K_z) are obtained through the resulting velocity time series. Although as seen from the results that model error in terms of peak concentration and spatial location may not be so significant (Figures 6.7-6.11), the error in terms of spatial extent may be significant. The

ramification from a response perspective is that the worst performing model might be able to locate an evolving patch but be considerably impacted in its ability to determine where or when it makes landfall. In light of the allocation of resources for countermeasures viz. Emergency Response and Homeland Security, an operational real-time environmental and oceanographic assessments system in surface waters provides a very valuable tool and it becomes very important to be able to reduce uncertainties inherent in the parameterization of the associated numerical models. The data-driven scheme developed here which was applied to Corpus Christi Bay would afford us this capability.

In this study, we employed a 26x26x5 uniform grid for the 3D transport model. Since data from HF Radar is essentially 2D, we used a linear (vertical) velocity profile to obtain currents along the remaining horizontal planes below the surface although, the vertical component of velocity, w as well as K_z were assumed to be uniform. Using this scheme, we were able to 1) decouple hydrodynamics from the overall transport within the modeling framework and 2) capture the dynamics of the transport and mixing process inherent in both advection and turbulent diffusion. This simplified model results in improved accuracy for predicting concentration profiles of constituents of interest, and would provide for better tracking of plumes in surface waters. Model calibration would be performed on-the-fly and the implication for modelers, responders as well as decision makers is a near real-time contaminant transport and monitoring system that can be deployed rapidly in any body of water where surface current mapping can be applied.

Some general comments about the behavior of the patch are given here. In both runs, the release occurred towards the end of the ebb tide and about the beginning of flood. The patch would be observed to orient itself in an east-west direction after a few hours into the run and at approximately 24 hours following release, begins to orient itself in a north-south direction eventually becoming elongated in this direction. The patch did not exit the computational domain during both runs but during run #1, it makes contact at the southernmost edge with land after approximately 48 hours while it begins to move towards the Laguna Madre located on the eastern boundary. In run #2, contact was made with land on the northernmost tip of the patch after approximately 60 hours, while moving towards the shipping channel entrance. In both runs, the constituent impacts the bottom long before it makes contact with any land boundaries and in this shallow bay, this may be the most important consideration especially if one were interested in the effect of a pollutant on the benthos. This of course would be influenced by other factors including the properties of the constituent of interest and its interactions with other constituents within the water column hence the result obtained here for a conservative neutrally buoyant material may be of an extreme nature.

Future Work

As can be seen in the current mapping created by HF radar, there remains work to be done in ensuring that gaps are removed from the dataset particularly with respect to the spatial coverage. One way of doing this is to develop data assimilation techniques or spatial interpolation techniques that would allow for a better representation of the

surface currents during those times that the dataset from radar may suffer degradation. In this study, simple spatial interpolation methods were used and may not be robust enough but would suffice within this conceptual framework. An operational model will need to consider these limitations in addition to the need to couple bio-geochemical interactions, which is the subject of ongoing research within our laboratory.

Conclusion

The modeling framework presented here addresses the physical and hydrodynamic component of the transport phenomena in surface waters. The model developed is simple to deploy and easy to configure and would be very useful for emergency response activities as it takes actual hydrodynamic observations as input thereby capturing the variability that is characteristic of shallow wind-driven bays in particular, Corpus Christi Bay, TX.

CHAPTER VII

SUMMARY AND CONCLUSION

These studies provide new insight into the turbulent and shear diffusion processes within a wind-driven bay such as Corpus Christi Bay and methods were developed that allows for the evaluation of coefficients that characterize the diffusion process for use within a constituent transport scheme. This will extend the use of instruments and sensors developed for current measurements in surface waters into other areas such as response to episodic events or even routine environmental and oceanographic assessments. The scheme couples real-time measurements with a computational model, which takes as input current measurements in a data-driven implementation of constituent transport modeling. The scheme includes hardware and software tools and in conjunction with the simplified transport model, provides a rapid deployment emergency response tool for nearshore and coastal environments.

During emergency response situations in coastal environments especially relating to clean-up operations, search and rescue, we often rely on visual tracking of the plume in terms of location and extent or even debris scatter. This is usually achieved through aerial reconnaissance, a method that becomes severely impaired under conditions of poor visibility such as nighttime operations, bad weather among others. In addition, some constituents of interest do not lend themselves readily to such visual techniques. To enable emergency operations under such conditions, enhanced surface reconnaissance is proposed for constituent tracking which will be operable even under

poor visibility conditions. Using a geo-referenced mobile instrument and sensing platform equipped with real-time data visualization tools developed for characterizing and mapping bays, estuaries and coastal environments.

This will be centered on the numerical scheme generating plume trajectory and extent coupled with real-time measurements employing correlative visualization between disparate data sets as an interpretative tool. The mobile platform equipped with wireless data telemetry will form a node within a data network that includes a shore-based data archival, post-processing and visualization system. The overall system can be implemented within an Incident Command System (ICS) structure during emergency response efforts and has been independently assessed through simulated spill exercises within Corpus Christi and Galveston Bay as to efficacy.

Augmented by vessel navigation and guidance system, this tool will be available for monitoring water quality parameters within the sensitive marine ecosystems such as bays and estuaries and has been used for dye tracer experiments and routine oceanographic and environmental assessments within Corpus Christi Bay. The system developed in this research project is important as it will enhance the ICS in emergency response situations in nearshore and coastal environments by providing a near real-time contaminant plume tracking system. Several oceanographic and environmental data processing and visualization schemes were developed as part of this project. These are listed below in Table 7.1 and the routines are accessible through the companion disk.

Algorithms and Software Modules Developed

Table 7.1. Listing of routines developed and their respective applications.

Module	Components
Grid Generator	Number Plot Points Extractor Grid Trim (Vertical and Horizontal)
Current Measurements	Spectral Analysis Filtering Spatial Interpolation and Regridding
Diffusion Coefficients Generator	Autocorrelation Function Length/Time scale of diffusion Diffusion Coefficients (lateral, longitudinal and vertical)
Numerical Model	Finite difference, adaptive grid
Computing Infrastructure	IDACC Submersible device server MPIACS Web server Data telemetry, broadband wireless Ethernet
Visualization	Plume Tracker Animation Generator Contouring Scheme Vector Plots
Tracker	Geo-referenced instrument platform Waypoints Generator

Future Work

Work performed here is a prototype and needs to be fully implemented within the framework of Emergency Response and Homeland Security. Future work will include developing the computing infrastructure for distributed applications with real-time information exchange. A web-based unified interface will be required that can be used by operators to run the individual modules that make up the IEOAS tied as a node into

the extended computing network for central administration and maintenance. Also it will be necessary to ensure that the mobile instrument platform is equipped with an autopilot which accepts as input, the NMEA 2.0 sentences from the plume tracking module for vessel guidance and navigation. Finally to integrate and deploy the numerical model in the field incorporating particle aggregation kinetics developed as part of our research efforts.

REFERENCES

Agrawal, Y. C., & Pottsmith, H. C. 2000 Instruments for particle size and settling velocity observations in sediment transport. *Marine Geology* **168**, 89-114.

Altinsoy, N., & Tugrul, A. B. 2002 A new proposal for Lagrangian correlation coefficient. *International Journal of Heat and Fluid Flow* **23**, 766-768.

Austin, T. C., Edson, J. B., McGillis, W. R., Purcell, M., Petitt, R. A., McElroy, M. K., Grant, C. W., Ware, J., & Hurst, S. K. 2002 A network-based telemetry architecture developed for the Martha's Vineyard Coastal Observatory. *IEEE Journal of Oceanic Engineering* **27**, 228-234.

Barrick, D. E., Headrick, J. M., Bogle, R. W., & Crombie, D. D. 1977 Ocean surface currents mapped by radar. *Science* **198**, 138-144.

Batchelor, G. K. 1950 The applications of the similarity theory of turbulence to atmospheric diffusion. *Journal of Royal Meteorological Society* **76**, 328-353.

Blom, J. G., & Verwer, J. G. 1996 Algorithm 759: VLUGR3: A vectorizable adaptive-grid solver for PDEs in 3D—Part II. Code description. *ACM Transactions on Mathematical Software,* **22**, 329–347.

Bowden, K. F. 1965 Horizontal mixing in the sea due to a shearing current. *Journal of Fluid Mechanics* **21**, 83-95.

Bowden, K. F., & Fairbairn, L. A. 1952 Further observations of the turbulent fluctuations in a tidal current. *Philosophical Transactions of the Royal Society of London. Series A, Mathematical and Physical Sciences* **244**, 335-356.

Bowden, K. F., & Howe, M. R. 1963 Observations of turbulence in a tidal current. *Journal of Fluid Mechanics* **17**, 271-284.

Brando, T. J., 1995 Comparing DCE and CORBA. *MITRE Document MP 95B-93*, http://www.mitre.org/tech/domis/reports/DCEvCORBA.html, March 25, 2003.

Burton, D., West, J., & Horsington, R. 1995 Modeling transport processes in the Ribble Estuary. *Environment International* **21**, 131-141.

Clark, J. F., Schlosser, P., Stute, M., & Simpson, J. H. 1996 SF6-3He Tracer release experiment: A new method of determining longitudinal dispersion coefficients in large rivers. *Environmental Science and Technology* **30**, 1527-1532.

Cracknell, A. P. 1999 Remote sensing techniques in estuaries and coastal zones -- an update. *International Journal of Remote Sensing* **19**, 485-496.

Csanady, G. T. 1966 Accelerated diffusion in the skewed shear flow of lake current. *Journal of Geophysical Research* **71**, 411-420.

Csanady, G. T. 1980 *Turbulent Diffusion in the Environment.* D. Reidel Publishing Co., London.

Davies, J. T. 1972 *Turbulence Phenomena.* Academic Press, New York.

Elder, J. W. 1958 The dispersion of marked fluid in turbulent shear flow. *Journal of Fluid Mechanics* **8**, 33-40.

Elliot, A. J. 1986 Shear diffusion and the spread of oil in the surface layers of the North Sea. *Deutsche Hydrographische Zeitschrift.* **39**, 114-137.

Elliot, A. J., Barr, A. G., & Kennan, D. 1997 Diffusion in Irish coastal waters. *Estuarine, Coastal and Shelf Science* **44**, 15-23.

Ernest, A. N., Bonner, J. S., & Autenrieth, R. L. 1991 Model parameter-estimation for particle-transport. *Journal of Environmental Engineering-ASCE* **117**, 573-594.

Fischer, H. B. 1973 Longitudinal dispersion and turbulent mixing in open-channel flow. *Annual Reviews*.

Fischer, H. B., List, E. J., Koh, R. C. Y., Imberger, J., & Brooks, N. H. 1979 *Mixing in Inland and Coastal Waters.* Academic Press, Inc., San Diego.

Fletcher, C. A. J., ed., 1991 *Computational Techniques for Fluid Dynamics*. (Springer Series in Computational Physics), 1, Springer, New York.

Frenkiel, F. N., 1953 Turbulent diffusion: mean concentration distribution in a flow field of homogeneous turbulence. In *Advanced Applied Mechanics*, 3, (Miles, R.V. & Karman, T.V., eds). Academic Press, New York, pp. 61-107.

Hanson, K. H., 2000 A new *in situ* chemical analyzer for mapping coastal nutrient distributions in real time. In *Proceedings of the MTS/IEEE Oceans 2000 Conference*, pp. 1975-1982.

Harleman, D. R. F., 1964 The significance of longitudinal dispersion in the analysis of pollution in estuaries. In *Proceedings of the 2nd International Conference on Water Pollution Research*, pp. 171-182.

Hashimoto, H., Ito, T., & Yamaura, T., 1996 Distributed file access manager -- functional specification. *Open Software Foundation RFC 96.0*, http://www.opengroup.org/tech/rfc/rfc96.0.html, March 25, 2003.

Hay, J. S., & Pasquill, F. 1959 Diffusion from a continous source in relation to the spectrum and scale of turbulence. *Advances in Geophysics* **6**, 345.

He, C., & Hamblin, P. F. 2000 Visualization of model results and field observations in irregular coastal regions. *Estuarine Coastal and Shelf Science* **50**, 73-80.

Ippen, A. T. 1966 *Estuary and Coastline Hydrodynamics.* McGraw Hill Book Company, Inc., New York.

Kelly, F. J., Bonner, J. S., Ojo, T. O., & Durel, A., 2004 Port Freeport's "FlowInfo": an example of an integrated port navigation and environmental data system (IPNEDS). In *Proceedings of the ASCE Ports 2004 Conference*, pp. 155-160.

Kelly, F. J., Bonner, J. S., Perez, J. C., Adams, J. S., Prouty, D. B., Trujillo, D., Weisberg, R. H., Luther, M. E., He, R., Cole, R., Donovan, J., & Merz, C. R., 2002 An HF radar test deployment amidst an ADCP array on the West Florida Shelf. In *Proceedings of the Sixth Working Conference on Current Measurement Technology*, pp. 692-698.

Kelly, F. J., Bonner, J. S., Perez, J. C., Trujillo, D., Weisberg, R. H., Luther, M. E., & He, R., 2003 A comparison of near-surface current measurements by ADCP and HF radar on the West Florida Shelf. In *Proceedings of the Seventh Working Conference on Current Measurement Technology*, pp. 70-74.

Lam, D. C., Murthy, C. R., & Simpson, R. B. 1983 *Effluent Transport and Diffusion Models for the Coastal Zone.* Springer-Verlag, New York.

Ledwell, J. R. 1991 The Santa Monica tracer experiment: a study of diapycnal and isopycnal mixing. *Journal of Geophysical Research* **96**, 8695-8718.

Lee, D. G., Bonner, J. S., Garton, L. S., Ernest, A. N., & Autenrieth, R. L. 2000 Modeling coagulation kinetics incorporating fractal theories: a fractal rectilinear approach. *Water Research* **37**, 1987-2000.

List, J., Gartrell, G., & Winant, C. 1990 Diffusion and dispersion in coastal waters. *Journal of Hydraulic Engineering* **116**, 1158-1179.

Manomaiphiboon, K., & Russell, A. G. 2003 Evaluation of some proposed forms of Lagrangian velocity correlation coefficient. *International Journal of Heat and Fluid Flow* **24**, 709-712.

Mellor, G. L., & Yamada, T. 1982 Development of a turbulence closure model for geophysical fluid problems. *Reviews of Geophysics and Space Physics* **20**, 851-875.

Murthy, C. R., 1970 An experimental study of horizontal diffusion in Lake Ontario. In *Proceedings of the 13th Conference of Great Lakes Research*, pp. 477-489.

Murthy, C. R. 1975 Horizontal diffusion characteristics in Lake Ontario. *Journal of Geophysical Research* **6**, 76-84.

Ocker, J. 2002 RD Instruments: leading edge technology, age-old principle. *Sea Technology* **43**, 29-40.

O'Connor, T. P., Walker, H. A., Paul, J. F., & Victor J. Bierman, J. 1985 A strategy for monitoring of contaminant distributions resulting from proposed sewage sludge disposal at the 106-mile ocean disposal site. *Marine Environmental Research* **16**, 127-150.

Ojo, T., & Bonner, J., 2002 3-dimensional self-calibrating coastal oil spill trajectory tracking and contaminant transport using HF radar. In *Proceedings of the Twenty-Fifth Arctic and Marine Oilspill Progam (AMOP) Technical Seminar*, pp. 215-226.

Ojo, T., Bonner, J., Fuller, C., Kelly, F., Page, C., & Sterling, M. J., 2003a Field simulation of aerial dispersant application for spill of opportunity. In *Proceedings of the Twenty-Sixth Arctic and Marine Oilspill Progam (AMOP) Technical Seminar,* pp. 813-824.

Ojo, T., Sterling, M. C. J., Bonner, J. S., Fuller, C. B., Kelly, F., & Page, C. A., 2003b Multi-parameter instrument array and control system (MPIACS): a software interface implementation of real-time data acquisition and visualization for environmental monitoring. In *Proceedings of the MTS/IEEE Oceans 2003 Conference*, pp. 2875-2879.

Ojo, T. O., & Bonner, J. S. 2004 Implementation of a rapid deployment integrated environmental and oceanographic assessment system (IEOAS) for coastal waters and nearshore environments. *Marine Pollution Bulletin* Submitted.

Ojo, T. O., Bonner, J. S., Fuller, C. B., & Page, C. A. 2004a Diffusion and mixing experiments in Corpus Christi Bay, TX: dye-tracer study to determine diffusivity values. *Estuarine Coastal and Shelf Science* Submitted.

Ojo, T. O., Bonner, J. S., Kelly, F. J., Page, C. A., Perez, J. C., Fuller, C. B., & Sterling, M. J., 2002 Adaptive sampling for coastal environmental monitoring using a georeferenced mobile instrument platform and correlative data visualization. In

Building the European Capacity in Operational Oceanography - Third International Conference on EuroGOOS. pp. 601-604.

Ojo, T. O., Bonner, J. S., & Page, C. A. 2004b Observations of shear-augmented diffusion processes and evaluation of effective diffusivity from current measurements in Corpus Christi Bay. *Continental Shelf Research* Submitted.

Ojo, T. O., Bonner, J. S., & Page, C. A. 2004c Studies on turbulent diffusion processes and evaluation of diffusivity values from hydrodynamic observations in Corpus Christi Bay using an ADCP. *Continental Shelf Research* Submitted.

Ojo, T. O., Bonner, J. S., Sterling, M. C., Fuller, C. B., Page, C. A., & Autenrieth, R. L., 2003c Implementation of distributed computing system for emergency response and contaminant spill monitoring. In *Proceedings of the Twenty-Sixth Arctic and Marine Oilspill Program (AMOP) Technical Seminar*, pp. 287-297.

Okubo, A. 1971 Oceanic diffusion diagrams. *Deep-Sea Research* **18**, 789-802.

Okubo, A., & Carter, H. H. 1966 An extremely simplified model of the 'Shear Effect' on horizontal mixing in a bounded sea. *Journal of Geophysical Research* **71**, 5267-5270.

Pasquill, F. 1962 *Atmospheric Diffusion* D. Van Nostrand Co., New York.

Paul, J. F., Victor J. Bierman, J., Walker, H. A., & Gentle, J. H., eds., 1989 *Application of a Hazard-Assessment Research Strategy for Waste Disposal at 106-Mile Ocean Disposal Site: Oceanic Processes in Marine Pollution*, 4: Robert E. Krieger Publishing Company, Malabar, FL.

Pernetta, J. C., & Milliman, J. D., 1995 Land-ocean interactions in the coastal zone. Implementation plan. Global Change Report no. 33, IGBP, Stockholm.

Pope, S. B. 2000 *Turbulent Flows.* Cambridge University Press, Cambridge.

Rew, R., & Davis, G. 1990 NetCDF - an interface for scientific-data access. *IEEE Computer Graphics and Applications* **10**, 76-82.

Riddle, A. M., & Lewis, R. E. 2000 Dispersion experiments in U.K. coastal waters. *Estuarine, Coastal and Shelf Science* **51**, 243-254.

Ruan, F., McLaughlin, D., & Li, S. 1999 A general technique for assessing the numerical accuracy of solute transport models. *Water Resources Research* **35**, 3961-3966.

Schofield, O., Bergmann, T., Bissett, P., Grassle, J. F., Haidvogel, D. B., Kohut, J., Moline, M., & Glenn, S. M. 2002 The long-term ecosystem observatory: an integrated coastal observatory. *IEEE Journal of Oceanic Engineering* **27**, 146-154.

Schott, F. 1978 Langrangian and Eulerian measurements of horizontal mixing in the Baltic. *Tellus* **31**, 139-143.

Stein, A., & Ettema, C. 2003 An overview of spatial sampling procedures and experimental design of spatial studies for ecosystem comparisons. *Agriculture Ecosystems & Environment* **94**, 31-47.

Sterling, J., Michael C., Bonner, J. S., Ernest, A. N. S., Page, C. A., & Autenrieth, R. L. 2004a Characterizing aquatic sediment-oil aggregates using *in situ* instruments. *Marine Pollution Bulletin* **48**, 533-542.

Sterling, M. C., Jr., Bonner, J. S., Page, C. A., Fuller, C. B., Ernest, A. N., & Autenrieth, R. L. 2004b Modeling crude oil droplet-sediment aggregation in nearshore waters. *Environmental Science and Technology* **38**, 4627-4634.

Stummel, H. 1949 Horizontal diffusion due to oceanic turbulence. *Journal of Marine Research* **8**, 199-225.

Taylor, G. I. 1920 Diffusion by continuous movements. *Proceedings of the London Mathematical Society* **20**, 196-211.

Taylor, G. I. 1953 Dispersion of soluble matter in solvent flowing slowly through a tube. *Proceedings of the Royal Society of London. Series A, Mathematical and Physical Sciences* **219**, 186-203.

Taylor, G. I. 1954 The dispersion of matter in turbulent flow through a pipe. *Proceedings of the Royal Society of London. Series A*, *Mathematical and Physical Sciences* **223**, 446-467.

Tchobanoglous, G., & Schroeder, E. D. 1985 *Water Quality (Characterisitcs, Modeling, Modification).* Addison-Wesley Publishing Company, Reading, MA.

Thau, R. 1996 Design considerations for the Apache server API. *Computer Networks and ISDN Systems* **28**, 1113-1122.

Thompson, S. K., & Seber, G. A. F. 1996 *Adaptive Sampling.* Wiley, New York.

Treinish, L. A., & Goettsche, C. 1991 Correlative visualization techniques for multidimensional data. *IBM Journal of Research and Development* **35**, 184-204.

Vinoski, S. 1997 CORBA: Integrating diverse applications within distributed heterogeneous environments. *IEEE Communications Magazine* **35**, 46-55.

Volpe, A. M., & Esser, B. K. 2002 Real-time ocean chemistry for improved biogeochemical observation in dynamic coastal environments. *Journal of Marine Systems* **36**, 51-74.

Ward, G. H. 1985 Dye diffusion experience in the Texas Bays; low-wave conditions. *Journal of Geophysical Research* **90**, 4959-4968.

Wiebe, P. H., Stanton, T. K., Greene, C. H., Benfield, M. C., Sosik, H. M., Austin, T. C., Warren, J. D., & Hammar, T. 2002 BIOMAPER-II: an integrated instrument platform for coupled biological and physical measurements in coastal and oceanic regimes. *IEEE Journal of Oceanic Engineering* **27**, 700-716.

VITA

Name:	Temitope O. Ojo
Address:	Civil Engineering Department Environmental and Water Resources Division 205T Wisenbaker Engineering Research Center Texas A&M University College Station, TX 77843-3136
Education:	Bachelor of Science 1984 Mechanical Engineering University of Ife, Ile-Ife, Nigeria
	Master of Engineering 2000 Civil Engineering Texas A&M University College Station, TX
	Doctor of Philosophy 2005 Civil Engineering Texas A&M University College Station, TX